



**Variations in conformational stability and thermodynamics of the
28-kDa and a pseudo-26-kDa glutathione transferases from
*Schistosoma haematobium***

By

Malefo Tshepiso Seeletse (1363639)

A dissertation

Submitted in fulfilment of the requirements for the degree of

Master of Science

in

Molecular and Cell Biology

**In the Faculty of Science, University of the Witwatersrand, Johannesburg,
South Africa**

Supervisor: Dr Ikechukwu A. Achilonu

June 2023

DECLARATION

I, **Malefo Tshepiso Seeletse (1363639)**, am a student registered for a Master of Science in biochemistry and cell biology by dissertation in the academic year 2022. I hereby declare the following:

- I am aware that plagiarism (the use of someone else's work without their permission and/or without acknowledging the source) is wrong.
- I confirm that the work submitted for assessment for the above degree is my unaided work except where explicitly indicated otherwise.
- I have not submitted this work before for any other degree or examination at this or any other University.
- I have followed the required conventions in referencing the thoughts and ideas of others.
- I understand that the University of the Witwatersrand may take disciplinary action against me if there is a belief that this is not my unaided work or that I have failed to acknowledge the source of the ideas or words in my writing.

Signature



Date

11th of June 2023

ABSTRACT

Schistosomiasis is a neglected tropical disease caused by blood flukes of the genus *Schistosoma*, affecting over 240 million individuals worldwide. The key detoxification enzymes of the parasite, glutathione-S-transferases (GSTs), play a crucial role in its survival by helping it evade the host immune system. Two isozymes, the *Schistosoma haematobium* 28-kDa glutathione transferase and the *Schistosoma bovis/haematobium* 26-kDa glutathione transferase are expressed during the parasite's life cycle, and the reason for encoding two similar enzymes within the genome is not fully understood. This study aims to comprehensively investigate and reveal the conformational stability and thermodynamics variations of the 28-kDa and a pseudo-26-kDa glutathione transferases from *Schistosoma haematobium*. Recombinant *Sh28GST* and *Sbh26GST* were overexpressed in *Escherichia coli* T7 cells and purified using immobilised metal affinity chromatography. The specific activity of the enzymes was determined using glutathione-1-chloro-2,4-dinitrobenzene (GSH-CDNB) assay, which was subsequently employed for Michaelis Menten kinetics of the two GSTs. The secondary structure of each enzyme was evaluated using far-ultraviolet (UV) Circular Dichroism (CD) and the tertiary structure using intrinsic tryptophan and extrinsic ANS fluorescence, in the presence and absence of urea. The conformational stability of the two GSTs was assessed under two different denaturing conditions: chemically induced denaturation using urea and far-UV CD, as well as heat-denaturing studies using Differential Scanning Calorimetry. Both proteins were successfully overexpressed, and high yields of purity were achieved. The secondary structural content of both proteins was predominantly alpha-helical. The tertiary structure showed that both proteins had most of their tryptophan residues exposed to the polar environment, and fluorescence spectra resulted in minor intensity changes from native to denatured protein. The specific activity of each enzyme was determined to be 40 $\mu\text{mol}/\text{min}/\text{mg}$ for *Sbh26GST* and 67 $\mu\text{mol}/\text{min}/\text{mg}$ for *Sh28GST*, indicating that *Sh28GST* had the higher specific activity among the two enzymes. Furthermore, when comparing their overall catalytic efficiency, *Sbh26GST* exhibited a higher value of 200 $\text{mM}^{-1}\text{min}^{-1}$, whereas *Sh28GST* showed a lower catalytic efficiency of $\text{mM}^{-1}\text{min}^{-1}$. Conformational stability and thermodynamics studies revealed interesting findings: *Sbh26GST* was more stable in the presence of urea, while *Sh28GST* was more stable in the presence of heat. Our collective findings led us to conclude that greater chemical denaturant stability observed in a protein does not always correlate with its stability in the presence of heat. These findings were attributed to the number and location of tryptophan residues found in each GST.

“I will go before you and will level the mountains; I will break down gates of bronze and cut through bars of iron. I will give you the treasures of darkness, riches stored in secret places, so that you may know that I am the LORD, the GOD of Israel, who summons you by name.”-

Isaiah 45:2-6.

ACKNOWLEDGEMENTS

Dear Heavenly Father, Son Jesus Christ, and Holy Spirit, I humbly offer my utmost gratitude to You for the privilege of being chosen and guided throughout this journey. Your divine hand has enabled me to connect with nature and fulfil my calling, and it has been an exceptional honor to have You by my side always. This life-changing experience will forever be cherished and appreciated.

To my beautiful mother, Mrs Boitumelo Doreen Seeletsa, the sweetest and most loving person I know, I thank the Almighty for you, my Queen. You have been instrumental in helping me discover this precious gift, accepting and embracing it. Your unwavering support, prayers, guidance, advice, and motivation have been the cornerstone of my success. You are a God-sent angel on earth.

To Dr Ikechukwu Anthony Achilonu, I am deeply grateful for this opportunity. Your acceptance, mentorship, trust, respect, and kindness are beyond words. Entrusting me with your lab and project was an honor, and your expertise has been invaluable.

To my siblings, grandmother, and father; your patience, support, love, and prayers have been immeasurable. You are all precious and amazing to me.

To Mr Mohale, your unwavering support, prayers, advice, motivation, and love have been priceless. I consider you one of my greatest blessings and will forever cherish you. Thank you for being part of my journey.

To my extended family and friends, I extend my sincerest gratitude for everything.

To Dr Nishal and UNISA, I am truly grateful for the opportunity to work in your lab. Thank you for allowing me to do DSC and for your support.

To the PSFRU and the University of the Witwatersrand, being part of your community has been a rewarding experience. Your teachings of perseverance, patience, and hard work will remain with me always.

Last but certainly not least, to Bahumi/Kehumile, I did it, my angel. I hope that you will take my milestone as motivation and recognize that if I could achieve it, so can you. You are an extraordinary gem, possessing incredible capabilities with royal favor. Never, under any circumstances, forget this truth. My love for you is everlasting and unwavering.

CONTENTS

DECLARATION.....	2
ABSTRACT.....	3
ACKNOWLEDGEMENTS.....	5
LIST OF FIGURES.	8
LIST OF TABLES.....	10
LIST OF ABBREVIATIONS.....	11
Chapter 1.....	13
1.1 Introduction.....	13
1.2 Problem statement.....	13
1.3 Rationale and research question.....	14
1.4 Aims and Objectives.....	15
Chapter 2.....	17
Literature Review.....	17
2.1 The History of Schistosomiasis.....	17
2.2 The life cycle of Schistosomiasis.....	19
2.3 The clinical manifestation of Schistosomiasis.....	20
2.4 Recent advances in anthelmintic drug discovery.....	22
2.5 Redox and detoxification pathways of the Schistosoma parasite.....	27
2.6 Schistosoma glutathione transferases.....	28
2.7 Protein stability and protein folding studies.....	29
Chapter 3.....	33
Recombinant <i>Sh28GST</i> and <i>Sbh26GST</i> overexpression and purification studies.....	33
3.1 Introduction.....	33
3.2 Materials.....	33
3.3 Methods.....	34
3.3.1 Adaptation of the recently constructed gene of <i>Sbh26GST</i>	34
3.3.2 Vector construction of <i>Sh28GST</i> and <i>Sbh26GST</i>	34
3.3.3 Competent <i>E. coli</i> T7 cells transformation with designed constructs of <i>Sh28GST</i> and <i>Sbh26GST</i>	36
3.3.4 Overexpression of <i>Sh28GST</i> and <i>Sbh26GST</i>	37
3.3.5 Purification of <i>Sh28GST</i> and <i>Sbh26GST</i>	38
3.3.6 Qualitative analysis of <i>Sh28GST</i> and <i>Sbh26GST</i> using SDS-PAGE and UV-vis spectroscopy.....	39

3.4 Results.....	41
3.5 Discussion.....	45
Chapter 4.....	48
Comprehensive analysis of the structural and functional properties of <i>Sh28GST</i> and <i>Sbh26GST</i>	48
4.1 Introduction.....	48
4.2 Materials.....	48
4.3 Methods.....	48
4.3.1 Enzyme activity studies of <i>Sh28GST</i> and <i>Sbh26GST</i>	48
4.3.2 Michaelis-Menten enzyme kinetics of <i>Sh28GST</i> and <i>Sbh26GST</i>	50
4.3.3 Secondary structure prediction of <i>Sh28GST</i> and <i>Sbh26GST</i> using far-UV CD.....	52
4.3.4 Tertiary structure analysis of <i>Sh28GST</i> and <i>Sbh26GST</i> using fluorescence spectroscopy.....	53
4.4 Results.....	55
4.5 Discussion.....	61
Chapter 5.....	66
Stability studies of <i>Sbh26GST</i> and <i>Sh28GST</i>	66
5.1 Introduction.....	66
5.2 Materials.....	66
5.3 Methods.....	67
5.3.1 Establishing reversibility of urea-induced unfolding of <i>Sh28GST</i> and <i>Sbh26GST</i>	67
5.3.2 Urea-induced unfolding of <i>Sh28GST</i> and <i>Sbh26GST</i>	69
5.3.3 Differential scanning calorimetry <i>Sh28GST</i> and <i>Sbh26GST</i>	70
5.4 Results.....	71
5.5 Discussion.....	75
Chapter 6.....	79
Conclusion and possible future prospects.....	79
References.....	81
Appendix.....	88

LIST OF FIGURES

Figure 2.1. Geographical distribution of different types of <i>Schistosoma</i> species spread across the sub-tropical regions of the world.....	18
Figure 2.2. The Life Cycle of the Schistosome.....	20
Figure 2.3. Main clinical manifestations of acute versus chronic schistosomiasis.....	21
Figure 2.4. Four prominent structures of proteins.....	29
Figure 2.5. Globular protein stability under the influence of various interactions.....	32
Figure 3.1. Schematic representation of pET-11a vector that was engineered to incorporate recombinant <i>Sh28GST</i>	35
Figure 3.2. Schematic representation of pET-28a vector that was engineered to incorporate recombinant <i>Sbh26GST</i>	36
Figure 3.3. SDS-PAGE overexpression results of recombinant <i>Sh28GST</i> and <i>Sbh26GST</i> for induced versus uninduced culture.....	42
Figure 3.4. SDS-PAGE analysis showing the purification profiles of <i>Sh28GST</i> and <i>Sbh26GST</i> from <i>Schistosoma haematobium</i>	43
Figure 3.5. UV absorption spectra <i>Sh28GST</i> and <i>Sbh26GST</i>	44
Figure 3.6. Absorbance against dilution plot for concentration determination of <i>Sh28GST</i> and <i>Sbh26GST</i>	45
Figure 4.1. Schematic illustration of the GSH-CDNB conjugation assay.....	49
Figure 4.2. Schematic illustration of reaction rate versus substrate concentration described using Michaelis-Menten kinetics.....	51
Figure 4.3. Enzyme specific activity analysis of <i>Sh28GST</i> and <i>Sbh26GST</i> using GSH-CDNB conjugation assay.....	56
Figure 4.4. Michaelis-Menten plot of velocity versus GSH concentration for <i>Sh28GST</i> (A) and <i>Sbh26GST</i> (B).....	57
Figure 4.5. Far UV-CD spectra of <i>Sh28GST</i> and <i>Sbh26GST</i> for secondary structure prediction.....	58
Figure 4.6. Intrinsic tryptophan fluorescence emission spectra of two glutathione S-transferase proteins, <i>Sh28GST</i> (A) and <i>Sbh26GST</i> (B), in the presence (depicted in orange) and absence (depicted in blue) of 8 M urea with a corresponding structure showing exposed tryptophan (depicted as yellow spheres) residues.....	60
Figure 4.7. Extrinsic ANS fluorescence emission spectra of <i>Sh28GST</i> (A) and <i>Sbh26GST</i> (B), in the presence (depicted in orange) and absence (depicted in blue) of 8 M urea.....	61
Figure 5.1. Schematic illustration of the experimental setup of a DSC experiment.....	71
Figure 5.2. Detecting the equilibrium pathway by following unfolding and refolding curves of <i>Sh28GST</i> (A) and <i>Sbh26GST</i> (B) using far-UV CD.....	72
Figure 5.3. Global fitted urea unfolding curves of <i>Sh28GST</i> (red) and <i>Sbh26GST</i> (blue) using far-UV CD.....	73
Figure 5.4. Heat capacity against temperature curve of <i>Sh28GST</i>	74

Figure 5.5. Heat capacity against temperature curve of *Sbh26GST*.....74

Figure S1. Multiple sequence alignment of *Schistosoma bovis* (*Sb*) 26-kDa glutathione transferase (EBI ID RTG84353) with the *Schistosoma haematobium* (*Sh*) 26-kDa glutathione transferase (EBI ID KAF1314627) acquired from Clustal Omega Program..... 88

LIST OF TABLES

Table 3.1. Glycine gel protocol for producing a high-resolution gel.....	40
Table 4.1. Kinetic parameters of <i>Sh28GST</i> and <i>Sbh26GST</i> determined by Michaelis-Menten plotting using the GSH-CDNB assay with varied GSH concentrations and constant GST concentrations.....	57
Table 4.2. Secondary structure prediction of <i>Sh28GST</i> and <i>Sbh26GST</i> determined using DichroWeb software.....	58
Table 5.1. Thermodynamic parameters obtained from urea unfolding curves of <i>Sh28GST</i> and <i>Sbh26GST</i>	73
Table 5.2. Thermodynamic parameters obtained from thermal heat curves of <i>Sh28GST</i> and <i>Sbh26GST</i> using Differential Scanning Calorimetry.....	75

ABBREVIATIONS LIST

A280	Absorbance observed at 280 nm
ANS	8-anilino-1-naphthalenesulfonate
CDNB	1-chloro-2,4-dinitrobenzene
DTT	Dithiothreitol
DSC	Differential Scanning Calorimetry
EC	Enzyme class
ΔH	Enthalpy change
ΔS	Entropy change
ΔG_{H2O}	Gibbs free energy (water)
GSH	Reduced L-glutathione
GST	Glutathione S-transferase
IPTG	Isopropyl- β -D-thiogalactopyranoside
k_{cat}	Turnover number
k_{cat}/K_M	Catalytic efficiency
kDa	Kilodalton
kd	Dissociation constant
K_M	Michaelis-Menten constant
kJ/mol	kilojoules per mole
mdeg	Millidegrees
MW	Molecular weight
μL	Microlitre
μm	Micrometre
μM	Micromolar
nm	Nanometre
nM	Nanomolar
ϵ	Molar extinction coefficient
$[\theta]$	Mean residue ellipticity
OD	optical density
RMSD	Root mean square deviation
rpm	revolution per minute
Sb26GST	<i>Schistosoma bovis</i> 26-kDa glutathione transferase

Sbh26GST	<i>Schistosoma bovis/haematobium</i> 26-kDa glutathione transferase
Sj26GST	<i>Schistosoma japonicum</i> 26-kDa glutathione transferase
Sh28GST	<i>Schistosoma haematobium</i> 28-kDa glutathione transferase
SDS-PAGE	Sodium dodecyl sulfate polyacrylamide gel electrophoresis
TEMED	N, N, N', N' tetramethylethylenediamine
v/v	Volume per volume
w/v	Weight per volume

The IUPAC-IUBMB one and three letters code for amino acids are used.

Chapter 1

Introduction

1.1 Introducing the study

This study focuses on exploring the variations in conformational stability and thermodynamics of two key glutathione transferases derived from *Schistosoma haematobium*. These enzymes, namely the 28-kDa isoform and a pseudo-26-kDa isoform, play crucial roles in the parasitic flatworm's biology and pathogenesis. By investigating their conformational dynamics and thermodynamic properties, this research aims to gain insights into the distinct characteristics and functional implications of these isoforms. The findings will contribute to our understanding of the parasite's molecular mechanisms and potentially inform the development of targeted interventions against schistosomiasis.

1.2 Problem statement

Schistosomiasis emerges from the parasitic blood flukes of the *Schistosoma* genus, exerting its pernicious impact on over 240 million individuals worldwide, predominantly in the tropical and sub-tropical regions of sub-Saharan Africa (WHO, 2022; Adenowo *et al.*, 2015). Recent data reveals that schistosomiasis is responsible for an estimated 200,000 deaths per year, and about 700 million cases of morbidity-related case (Verjee, 2019). The *Schistosoma japonicum*, *S. haematobium*, and *S. mansoni* species are the most prevalent pathogenic agents, causing symptoms of abdominal pain, diarrhoea, blood in urine or stool, and in extreme cases, resulting in organ failure and mortality (Rollinson *et al.*, 1987). Current methods of preventing and controlling schistosomiasis rely on a combination of multifaceted strategies, including administering Praziquantel (PZQ), an anti-schistosome drug, improving sanitation, and employing health education campaigns aimed at raising awareness and minimising the risk of infections (Vale *et al.*, 2017). However, challenges remain in eliminating the disease, particularly in resource-limited regions with limited diagnostic tools, drug availability for mass drug administration, and the increase in global travel, leading to the spread of the disease across the world. Moreover, the curative effects of PZQ only apply to adult worms and not juvenile parasites (Fenwick, 2015). Hence, there exists a dire need to harness more sustainable and effective treatment and control options aimed at understanding the epidemiology, prevention,

and treatment of schistosomiasis, thereby mitigating the impact of this devastating disease on the health and well-being of individuals across the globe.

1.3 Rationale and research question

As the use of praziquantel for prevention chemotherapy continues to increase, the emergence of resistant strains to the drug becomes inescapable. This can lead to potential outbreaks and pose significant risks to controlling schistosomiasis. Therefore, it is crucial to discover new or develop existing therapeutic strategies to control schistosomiasis. The biochemistry of this infection is complex, involving multiple processes, pathways, and enzymes. One of the attractive therapeutic targets in the schistosome community is their key detoxification enzymes, known as glutathione transferases. Glutathione transferases (EC 2.5.1.18) are a specific class of enzymes responsible for detoxification through the catalytic conjugation of tripeptide glutathione to other forms of exogenous and endogenous compounds (Dixon *et al.*, 2020; Townsend *et al.*, 2003). In Schistosomiasis, these key enzymes help the worms evade the host immune system and be persistent in causing an infection (Townsend *et al.*, 2003). The two isozymes, *Sh28GST* and *Sbh26GST* are expressed during their life cycle, and while the exact reason for the production of two isozymes is not well understood, both enzymes act as defence mechanisms for the parasite against its host or other physicochemical stressors (Dixon *et al.*, 2020). By targeting glutathione transferases, researchers can develop novel and effective treatments to combat schistosomiasis, especially in light of the potential risks associated with praziquantel resistance.

The three-dimensional structure of *Sh28GST* isoform is homodimeric in nature with 211 amino acids in its sequence (Walker *et al.*, 1993; Padi *et al.*, 2021). Three distinguishable sites are found, the dimer interface, the G-site, and the H-site (Padi *et al.*, 2021). The G-site is where a GSH substrate binds, while the H-site is where the electrophilic substrate binds (Kenneth *et al.*, 2003). Each monomer in its interface is composed of the C- and N-terminal domains resulting in the canonical GST fold (Kenneth *et al.*, 2003). The position of *Sh28GST*'s active site is at the junction of each monomer's two domains, comprising a pocket for glutathione binding and another pocket for hydrophobic substrate binding. The residues from both domains form the glutathione-binding pocket, whereas the substrate-binding pocket mainly comprises of the C-terminal domain residues (Walker *et al.*, 1993; Padi *et al.*, 2021; Kenneth *et al.*, 2003). Overall, the structure of *Sh28GST* is similar to that of other GSTs, but

with some unique features that may be exploited for the development of new therapeutics for schistosomiasis. Similarly, *Sbh26GT* is also homodimeric. The structure consists of the H-site that is predominantly alpha-helical and the G-site with a thioredoxin fold (Padi *et al.*, 2021). Both enzymes belong to the mu family of GSTs (Walker *et al.*, 1993).

After analysing the size, and structure of the two Glutathione S-transferases (GSTs), it is evident that these enzymes share remarkable similarities, yet it remains puzzling why the parasite encodes two highly identical mu-class GSTs. It is plausible that the stability and overall functions of the enzymes are linked to their redundancy, but the underlying mechanism remains unclear. Notably, the two GSTs exhibit variable differences in their tryptophan and tyrosine content, suggesting that one enzyme may be more stable than the other.

Given the urgent need for effective treatment and vaccines against Schistosomes, revealing the stable nature of these two enzymes could provide invaluable insights into what the significance of each enzyme is in its genome, thus serving as a drug target for the new generation of anti-*Schistosoma* treatments. The aim of this study is to comprehensively investigate and reveal the conformational stability and thermodynamic variations of the 28-kDa and pseudo-26-kDa glutathione transferases from *Schistosoma haematobium*. This approach aims to elucidate important clues towards understanding what the functional roles of these two GSTs are and the underlying mechanisms that drive their redundancy.

1.4 Aims and Objectives

The aim of this study is to comprehensively investigate and reveal the conformational stability and thermodynamic variations of the 28-kDa and a pseudo-26-kDa glutathione transferases from *Schistosoma haematobium* using urea and heat as denaturing agents.

To achieve this broader aim, the following objectives were set:

- To overexpress the recombinant *Sh28GST* and *Sbh26GST* using pET-11a and pET-28a vector constructs, respectively, in an *Escherichia coli* (*E. coli*) T7 expression system.
- To purify the recombinantly overexpressed *Sh28GST* and *Sbh26GST* using immobilized metal affinity chromatography (IMAC).

- To carry out functional characterization using GST/1-Chloro-2,4-dinitrobenzene (CDNB) conjugation assay to detect the specific activity of each enzyme.
- To detect the secondary structural content of *Sh28GST* and *Sbh26GST* using Far-UV (Ultraviolet) CD (Circular Dichroism) spectroscopy.
- To determine the tertiary structural content of *Sh28GST* and *Sbh26GST* using intrinsic (tryptophan) and extrinsic [8-anilino-1-naphthalene sulfonate (ANS)] fluorescence emission spectra respectively.
- To conduct conformational stability studies of *Sh28GST* and *Sbh26GST* using urea-induced unfolding coupled with far-UV CD and Differential Scanning Calorimetry (DSC) based on heat-induced changes.

Chapter 2

Literature Review

2.1 The History of Schistosomiasis

Dating back to 1851, a *Schistosoma* discovery was made in Egypt by a German physician, Theodor Maximilian Bilharz where he described the existence of worms in the urinary tract of patients who were carriers of the disease (Di Bela *et al.*, 2018). His identification of the worms belonging to the genus *Schistosoma* led to the disease being named "Bilharzia," after him (Bilharz *et al.*, 1852). Schistosomiasis is an acute and parasitic disease, ranked second to Malaria and is caused by the genus *Schistosoma* trematodes (WHO, 2017). Schistosomiasis is also known to be one of the neglected tropical diseases (NTD) that particularly affects low- and middle-income regions due to limited access to clean water, and lack of proper sanitation. Over 240 million people account for cases of infection, with an estimate of over 280,000 deaths per year, and about 779 million cases of morbidity-related cases (Verjee, 2019). The parasite is zoonotic in its nature, infecting both marine, freshwater snails, which are known to be intermediate hosts for the parasite, as well as humans (Standley *et al.*, 2012). Depending on the geographical location and the *Schistosoma* species involved, the adult worms cause a wide range of symptoms while living and replicating in the blood vessels of their human hosts (Gryeels *et al.*, 2012). Thus far, six Schistosome species were identified to infect humans globally. These include *Schistosoma haematobium*, *S. mansoni*, *S. guineensis* and *S. intercalatum* in Africa, and *S. mekongi* and *S. japonicum* in Asia (Colley *et al.*, 2014). In animals, over 19 species are responsible for the infection, however, the severity of infection is observed in those caused by *S. curassoni*, *S. bovis*, *S. mekongi*, *S. mattheei* and *S. japonicum* (Sturrock, 2001; Lawson *et al.*, 1980). Different *Schistosoma* species have different geographic distribution, and depending on the type of species present, the management methods vary.

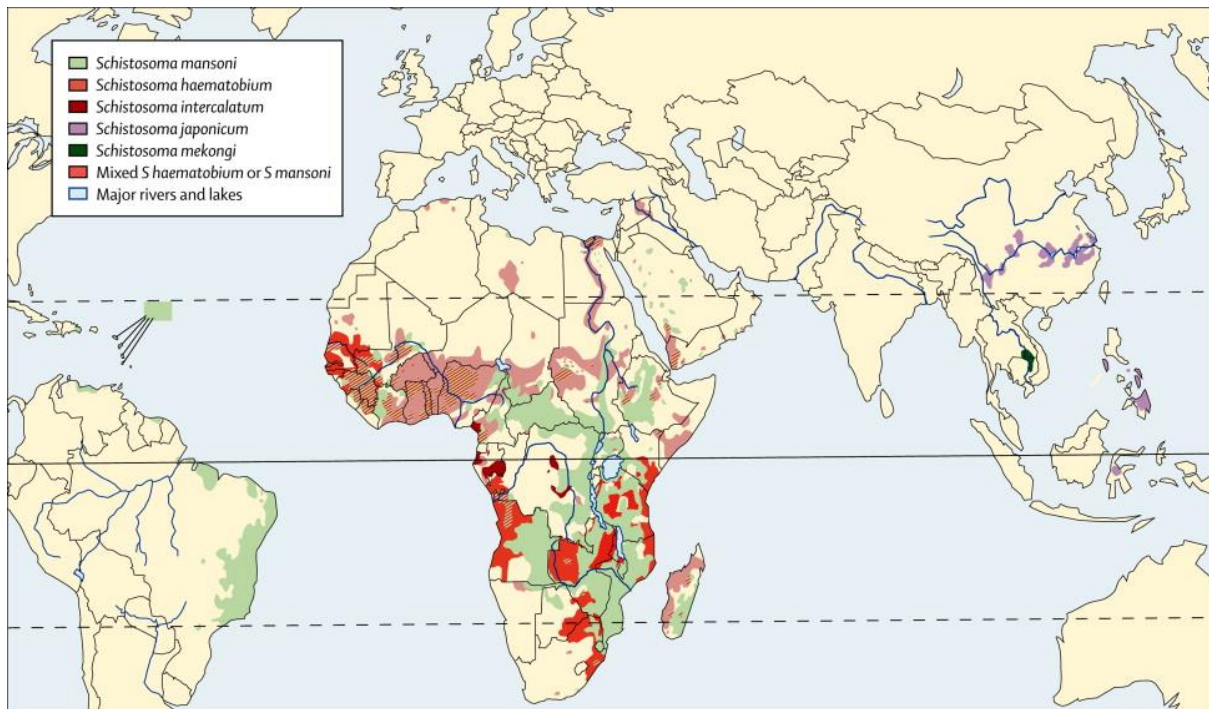


Figure 2.1. Geographical distribution of different types of *Schistosoma* species spread across the sub-tropical regions of the world. Human beings can be infected by three primary types of schistosomes, *Schistosoma mansoni*, *Schistosoma haematobium* and *Schistosoma japonicum*. Infections caused by these species spread throughout the Middle East, Africa and America, while the remaining species are limited to other parts of the world, including China, the Philippines, and Asia (Adapted from Gryseels *et al.*, 2016).

There are three main species that are responsible for most schistosomiasis cases worldwide. These include *Schistosoma japonicum*, *Schistosoma mansoni*, and *Schistosoma haematobium* (Sturrock, 2001; Lawson *et al.*, 1980). *Schistosoma mansoni*, primarily responsible for intestinal schistosomiasis dominates Africa, the Caribbean, and parts of South America (Tianfang *et al.*, 2016). *Schistosoma haematobium* is responsible for urinary schistosomiasis and it is primarily found in the Middle East and African countries. *Schistosoma japonicum* can result in both intestinal and urinary schistosomiasis and is mostly found in Indonesia, China, and the Philippines (Tianfang *et al.*, 2016). *Schistosoma mekongi* is responsible for causing intestinal schistosomiasis and is found in South East of Asia, specifically in Laos, Cambodia, and Vietnam (Sturrock, 2001; Tianfang *et al.*, 2016). The least common specie types include *Schistosoma intercalatum* which causes intestinal and genital forms of schistosomiasis, found in Central Africa and *Schistosoma guineensis*, found in Central and West Africa and is responsible for intestinal schistosomiasis (Sturrock, 2001; Tianfang *et al.*, 2016; Lawson *et al.*, 1980). In essence, the disease is most prevalent in sub-tropical and tropical regions of the Sub-Saharan Africa with greatest morbidity and mortality cases thus far.

In certain parts of South Africa, such as the provinces of Mpumalanga and Limpopo, the eastern and northern regions of Gauteng, KwaZulu-Natal and Port Elizabeth, schistosomiasis is a concern (NICD, 2018). The majority of those at risk are children, totaling approximately four million individuals (NICD, 2018). The prevalence of the disease in children in some endemic regions of South Africa is as high as 95% (NICD, 2018). Nonetheless, the actual number of infected individuals in South Africa remains unknown (NICD, 2018).

2.2 The life cycle of Schistosomiasis

The life cycle of the parasite *Schistosoma* entails a complex series of stages that involve the intermediate host blood flukes releasing larval cercariae into freshwater, and their subsequent penetration of the host cell (Charles, 2003). The infection of all *Schistosoma* species occurs through direct exposure to fresh water, which serves as a reservoir for the free-swimming cercariae. Upon invasion of the human host skin cell, the cercariae shed their bifurcated tails and metamorphose into schistosomula, which then navigate the capillaries and lymphatic vessels and into the lungs (Charles, 2003). Few days later, the worms travel to the portal blood in the liver, eventually maturing into female and male adult worms. Paired worms will move to the superior mesenteric veins (in the instance of *S. mansoni*), the inferior mesenteric and superior hemorrhoidal veins (in the instance of *S. japonicum*), or the ureter-draining veins (in the instance of *S. haematobium*) (Charles, 2003; Waine *et al.*, 1997). Roughly four weeks after infection, the egg-laying process commences, continuing for the lifespan of the trematode, which can extend up to five years. The eggs transverse from blood vessels into adjacent tissues, while the other eggs progress through the bladder or intestinal mucosa, and ultimately resulting to excretion in the faeces (in the instance of *S. japonicum* and *S. mansoni*) or urine (in the instance of *S. haematobium*). The culmination of the life cycle is achieved when the eggs hatch and release miracidia, that in turn will target and infect freshwater trematodes as their harbour (Charles, 2003). The parasitic trematode *Schistosoma haematobium* exhibits a proclivity for infecting members of the *Bulinus* genus, while *S. mansoni* and *S. japonicum* infect *biomphalaria* species and *oncomelania* species, respectively (Waine *et al.*, 1997).

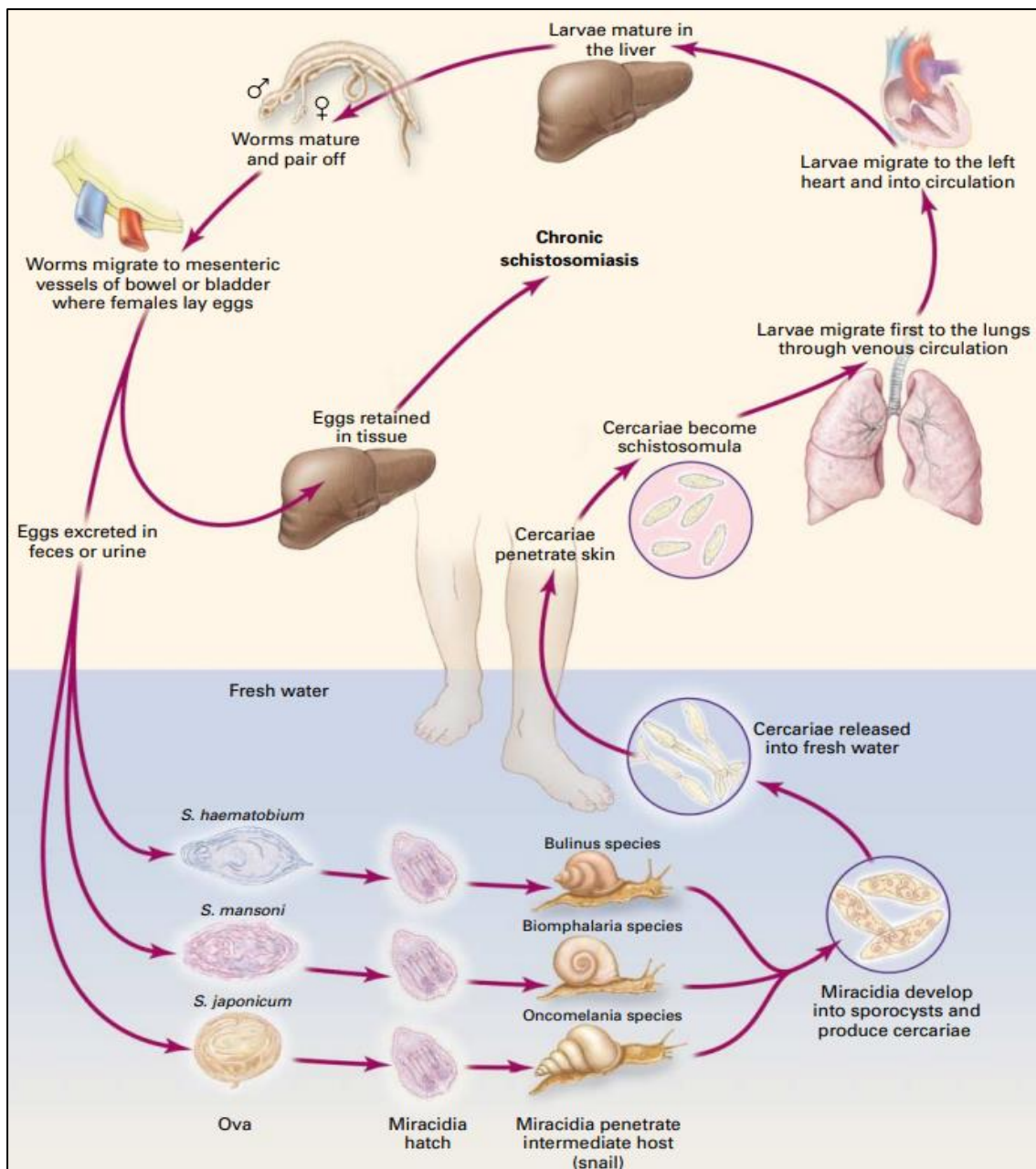


Figure 2.2. The Life Cycle of the Schistosome. Upon skin penetration, the snails gain entry into human host cells and transform into schistosomula. The fully developed cells then navigate through the venous system, traversing through the lungs and blood vessels and into the liver. Subsequently, the schistosomes mature into sexually dimorphic adult worms, which join forces and venture to the mesenteric vessels of the bowel. In this location, the female worm deposits eggs that can be excreted through urine or feces, thus entering freshwater where they have the potential to infect additional host cells. Failure to eliminate these eggs may result in their retention within liver tissues, thereby leading to the chronic form of schistosomiasis (Adapted from Charles, 2003).

2.3 The clinical manifestation of Schistosomiasis

The clinical manifestations of Schistosomiasis are a complex interplay between the type of *Schistosoma* involved, the severity of infection, and the immune response of the host. This

dynamic disease can present in either an acute or chronic phase, with the acute phase, also known as Katayama fever, occurring within the first few weeks of infection (Gobbi *et al.*, 2020). During this phase, the immune response from the host to antigens from the *Schistosoma* trematodes leads to the production of granulomas around the worms and their eggs, resulting in a range of symptoms (Visser *et al.*, 1995). These symptoms, including fever, muscle pain, fatigue, and nausea, may initially be mistaken for common viral infections, making diagnosis challenging, especially in regions with limited access to diagnostic testing (Visser *et al.*, 1995). Despite this, early detection is critical as Schistosomiasis can progress to its chronic phase, persisting for years or even decades if left untreated (Lingscheid *et al.*, 2020). The chronic phase of the disease can lead to severe complications, including damage to internal organs such as the spleen, liver, and kidneys, resulting in chronic abdominal pain, bloody urine, and even bladder cancer (Gobbi *et al.*, 2017). It is therefore of utmost importance for healthcare facilities to provide early diagnostic testing and treatment methods. By doing so, we can effectively combat Schistosomiasis and mitigate its impact on affected communities.

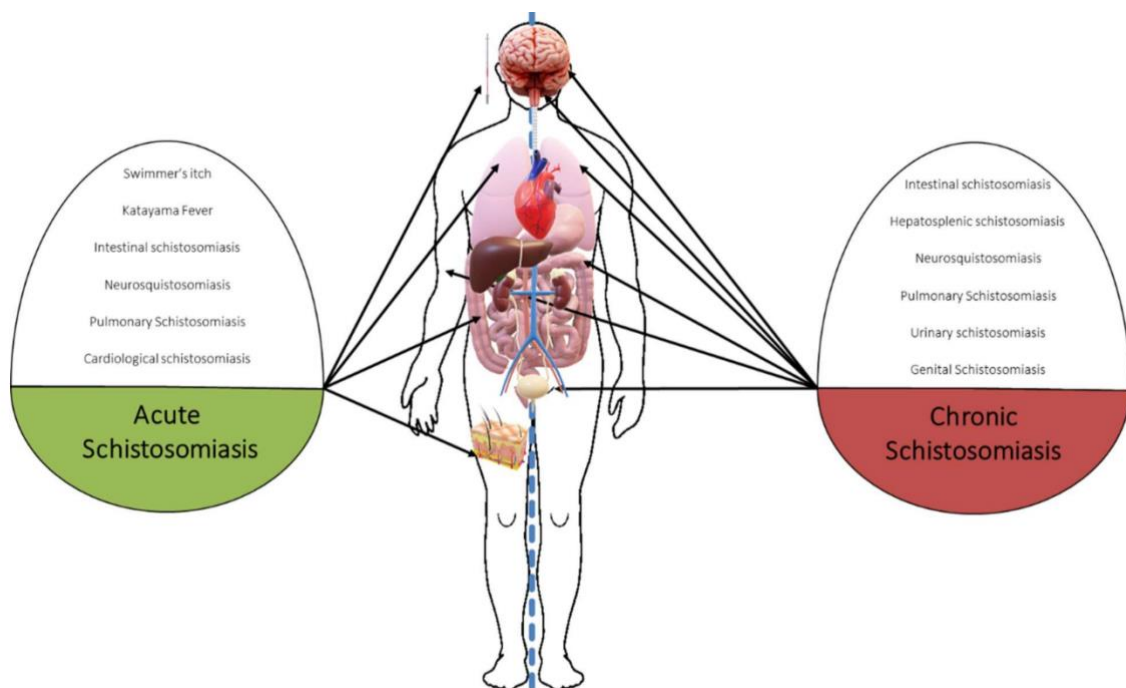


Figure 2.3. Main clinical manifestations of acute versus chronic schistosomiasis. The host's immune system responds to antigens from *Schistosoma* trematodes during the acute phase, which triggers the formation of granulomas around the parasites and their eggs. This immune response can result in a variety of symptoms. If acute phase treatment is unsuccessful, the infection can progress to the chronic phase, which has the potential to cause organ damage or failure (Adapted from Lingscheid *et al.*, 2020).

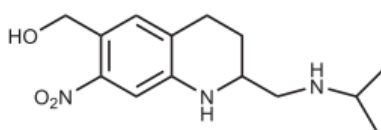
2.4 Recent advances in anthelmintic drug discovery

Diagnosis of Schistosomiasis

The conventional approach for detecting schistosomiasis involves the microscopic examination of urine or stool specimens to identify eggs of *S. japonicum* or *S. mansoni* (Bosompem *et al.*, 2004). For epidemiological purposes, serological tests such as enzyme-linked immunosorbent assay (ELISA) are employed due to their high sensitivity and reliability (Danso *et al.*, 2008). However, the ELISA method cannot distinguish between ongoing and past infections, and some of its antigens may cross-react with antigens from other helminths such as Ancylostomides and *Ascaris lumbricoides* (Carvalho *et al.*, 2011). To overcome this limitation, an optimal selection of antigens for use in the serological diagnosis of schistosomiasis is necessary (Kato *et al.*, 2010).

Treatment options of Schistosomiasis

Disease control strategies include the employment of health education, efficient supply of accessible clean drinking water, proper access to sanitation, and adequate supply of effective medication and healthcare facilities (Sow *et al.*, 2003). Schistosomiasis medical treatment strategies includes the use of chemotherapy treatment and vaccines.



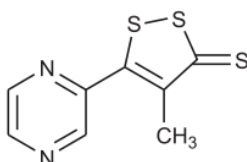
Oxamniquine (Vansil®)

1,2,3,4-Tetrahydro-2-((isopropylamino)methyl)-7-nitroquinolin-6-yl)methanol

(2.1)

Oxamniquine (2.1) is a weakly toxic drug that is rapidly absorbed from the intestine with a 2 h plasma half-life (Doenhoff *et al.*, 2008). The drug has shown effectiveness against *S. mansoni* infections. However, epileptic episodes have been documented in patients with a history of cerebral lesions, and drowsiness leading to subcomatose states has been reported in children (Pica *et al.*, 2006). These adverse effects may be attributed to the death of adult worms, including those in the lungs, which can produce temporary infiltrates and respiratory symptoms (Pica *et al.*, 2006). While widely used in Latin America, particularly in Brazil, its use in Africa

is less recommended, given the frequent coexistence of *S. mansoni* with *S. haematobium* in many regions (Southgate *et al.*, 1997). Oxamniquine may be considered if there is insufficient response to praziquantel.

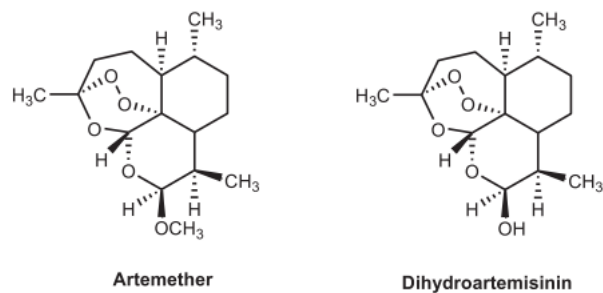
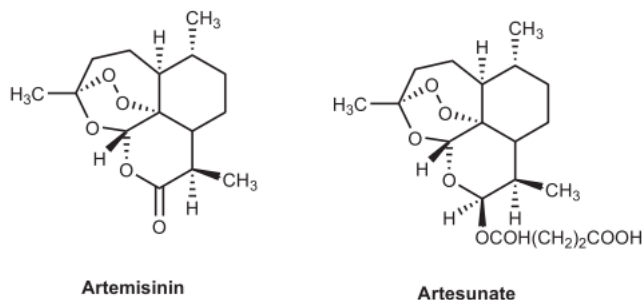


Oltipraz

4-Methyl-5-(pyrazin-2-yl)-3H-1,2-dithiole-3-thione (2.2)

Oltipraz (2.2), a pharmacological agent, has been registered for the therapeutic management of schistosomiasis (Ruggeri *et al.*, 2002). This medication exerts its therapeutic effect through the induction of glutathione S-transferase (GST) activity, which serves a pivotal role in the detoxification of carcinogens (Ruggeri *et al.*, 2002). Currently, Oltipraz is being extensively studied as a promising chemoprotective agent with potential applications in cancer prevention (Aboul *et al.*, 1989).

In the 1980s, the anti-*Schistosomal* properties of artemisinin namely artesunate, artemether, and artemisinin (2.3) were identified (Le *et al.*, 1982). These compounds exhibit efficacy against the immature, liver-stage schistosomes, while the adult worms and their invasive stages display relatively lower susceptibility to these drugs (Le *et al.*, 1982). Moreover, the associated adverse effects are negligible and transient, lasting for less than 24 hours. Monotherapy with artemisinins may not confer optimal clinical outcomes due to their stage-specific activity, but their combination with other drugs effective against different stages, such as praziquantel, may enhance the therapeutic potential of the regimen (Le *et al.*, 1982).

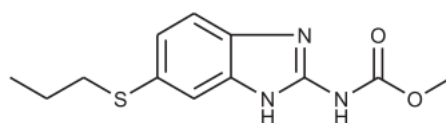


Artemisinins

(2.3)

Recently, there have been reports indicating that dihydroartemisinin, artesunate, and artemether and can be employed as an effective strategy to prevent *S. japonicum* infection. These drugs, when administered in combination treatment, result in toxicity to both adult and juvenile *S. japonicum* (Li *et al.*, 2011).

Albendazole (2.4) is a drug recommended for the treatment of various worm infestations. In recent years, it has frequently been co-administered with praziquantel to manage schistosomiasis (Friis *et al.*, 2003). However, there have been studies that reported side effects such as headaches, and gastrointestinal upsets (Zhang *et al.*, 2007).



Albendazole

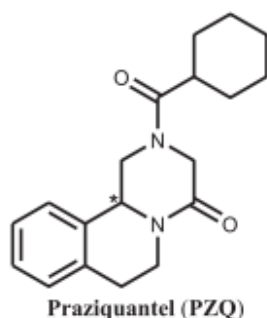
Methyl [6-(propylthio)-1H-benzimidazol-2-yl]carbamate

(2.4)

Mirazid (not shown) is an oleo gum resin extract that can be harvested from the stem of a myrrh tree, *Commiphora molmol* (syn. *Commiphora myrrha*) (Soliman *et al.*, 2004; Barakat *et al.*, 2005). A solution made from the plant using alcohol, and then distilled with steam, produces resin and volatile oil. In Egypt, it is authorized and sold for medical purposes

to treat infections caused by *Fasciola hepatica* and schistosomes (Botros *et al.*, 2005). However, its precise role in therapy is not well understood, and its effectiveness in clinical use is disputed (Fenwich *et al.*, 2006). Myrrh extracts also have the ability to kill snails that serve as intermediate hosts, particularly their eggs (Soliman *et al.*, 2004).

Praziquantel (2.5) is the present drug of choice known to result in toxicity against all schistosomiasis.



Praziquantel (PZQ)
(*RS*) 2-(Cyclohexylcarbonyl)-2,3,6,7,11b-tetrahydro-1*H*-pyrazino-[2,1-*a*]isoquinolin-4(11*bH*)-one (2.5)

Praziquantel is described as a white to near crystalline white powder that melts at 136–140 °C with decomposition (Andrews *et al.*, 1983). The drug has good stability under normal conditions. It also shows insolubility in water, some solubility in ethanol and complete solubility in dimethylsulfoxide and chloroform (Liu *et al.*, 1986). The commercial formulation comprises a racemic mixture with equimolar amounts of both S (+) and R (–) isomers. Studies have demonstrated that solely the (–) enantiomer exhibits anti-*Schistosomal* activity (Shu *et al.*, 1989). Nevertheless, both isomers demonstrate nearly identical effects in combating infections. Notably, administering 20 mg/kg of the (–) enantiomer resulted in similar cure rates with fewer adverse effects compared to administering 40 mg/kg of the racemic mixture in treated patients (Shu *et al.*, 1989; Andrews *et al.*, 1983). However, there have been reports of treatment failure and the emergence of drug-resistant strains of the parasite, particularly in areas with high rates of infection and frequent exposure to the drug (Liu *et al.*, 1986). Several factors can contribute to the development of resistance to praziquantel and other anti-*Schistosomal* drugs. One being the overuse and misuse of these drugs, which can lead to the selection of the parasite's resistant strains. In some cases, the resistance may be due to genetic changes in the parasite, which enable it to tolerate or even evade the action of the drug (Shu *et*

al., 1989). Other factors that can contribute to resistance include poor adherence to treatment regimes, incomplete treatment courses, and co-infection with other pathogens that may interfere with drug efficacy (Liu *et al.*, 1986). In addition, environmental factors such as pollution, climate change, and alterations in freshwater ecosystems can affect the transmission and survival of the parasite, making it more difficult to control (Andrews *et al.*, 1983). Thus, there is a need for continued research into the development of new drugs and treatment regimens that can overcome the challenges posed for by drug-resistant parasites.

Mode of action

The precise molecular mechanism underlying the action of praziquantel remains incompletely understood (Shu *et al.*, 1989); however, several phenomena associated with its effects are widely recognized. One of the most apparent and immediate changes observed in schistosomes exposed to the drug is the contraction of the worm musculature resulting in spastic paralysis (Andrews *et al.*, 1983). The muscle contraction is associated with a swift influx of Ca^{2+} inside the parasite. The worm tegument also undergoes modifications shortly after exposure to praziquantel, as demonstrated by vacuolization at the base of the tegumental syncytium and surface blebbing (Liu *et al.*, 1986). These morphological alterations expose schistosome antigens more prominently on the parasite's surface. (Shu *et al.*, 1989).

Vaccines

Despite considerable chemotherapeutic progress, schistosomiasis still poses as an increasing threat to the healthcare system with its rapid spread to new areas. The emergence of resistant strains is inevitable and other alternatives such as vaccine development are key areas of research to consider.

Sm28/Sh28-GST: *Sm28-GST* has GST properties (detoxification) and is observed in subtegumental tissues of most developmental stages of the schistosome (Porchet *et al.*, 1994). Vaccination administered to permissive hamsters and semipermissive rats with recombinant *Sm28-GST* led to insignificant reductions in trematodes (Xu *et al.*, 1993). Primate trials were carried out and this resulted in anti-fecundity effects, and the same effect resulted in an anti-*Sm28* monoclonal antibody (Xu *et al.*, 1993). This led to potential clinical manifestations of *Sh28-GST* in humans. Unfortunately, no data is available discussing the vaccine's efficacy.

2.5 Redox and detoxification pathways of the *Schistosoma* parasite

Redox and detoxification pathways play a crucial role in the survival and pathogenesis of *Schistosoma* parasites.

Schistosoma parasites depend on a complex network of redox pathways to maintain their metabolism and to cope with the host's immune response. *Schistosoma*'s redox mechanism encompasses a set of enzymes, which comprises glutathione peroxidase, superoxide dismutase (SOD), peroxidase, and catalase. These enzymes act as antioxidants that help counteract the harmful effects of reactive oxygen species (ROS) and reactive nitrogen species (RNS) produced by the immune cells of the host (Tracy *et al.*, 1983).

Schistosoma parasites also have a well-developed thioredoxin (Trx) system, which consists of thioredoxin reductase (TGR), thioredoxin peroxidase (TPx), and thioredoxin-like proteins (TLPs) (Valko *et al.*, 2007). The maintenance of the parasite's redox equilibrium is crucially dependent on the Trx system, as it regulates the activity of many proteins involved in essential cellular processes such as DNA synthesis, protein folding, and signal transduction (Valko *et al.*, 2007). TGR is a unique enzyme that has both Trx reductase and glutathione reductase activities, which makes it essential for the detoxification of both ROS and RNS.

The parasites face several challenges in the host's bloodstream, such as nutrient deprivation, oxidative stress, and immune attack. Therefore, these parasites have evolved an array of detoxification pathways to cope with these challenges. One of the most important detoxification pathways in *Schistosoma* is the multidrug resistance (MDR) system (Thannickal *et al.*, 2000). This system includes a family of ATP-binding cassette (ABC) transporters that can efflux a wide range of xenobiotic compounds, including drugs, toxins, and metabolic wastes (Nordberg *et al.*, 2001). *Schistosoma* parasites also have a well-developed phase I and phase II detoxification system, similar to that found in mammals. Phase I detoxification involves the activation of xenobiotic compounds by cytochrome P450 enzymes (CYPs), followed by the production of reactive metabolites that can be detoxified by phase II enzymes such as glutathione S-transferases (GSTs) and UDP-glucuronosyltransferases (UGTs) (Valko *et al.*, 2004). GSTs play a vital role in detoxifying ROS and RNS produced by the host's immune cells, while UGTs are involved in the conjugation of hydrophobic xenobiotics with polar compounds to facilitate their excretion (Valko *et al.*, 2004).

2.6 *Schistosoma* glutathione transferases

As previously discussed, *Schistosoma* relies on glutathione transferases (GSTs) as the main enzymes for detoxifying xenobiotics and reactive oxygen species (ROS). These enzymes belong to a family that facilitates cellular detoxification by catalyzing the conjugation of electrophilic substrates with glutathione (GSH), ultimately producing a less reactive, water-soluble, and easily excreted conjugate (Hayes *et al.*, 2005). There are various classes of GSTs, such as pi, zeta, mu, sigma, alpha, and theta (Precious *et al.*, 1989; Cvilink *et al.*, 2009).

The *Schistosoma* genome encodes for several GST isoforms that belong to the mu and sigma classes. These enzymes have been found to be vital in the detoxification of xenobiotics, including drugs, pesticides, and carcinogens, as well as endogenous compounds such as lipid peroxidation products and ROS (Torres *et al.*, 2008). They are also involved in the metabolism of artemisinin, a key drug used in the treatment of schistosomiasis.

The crystal structure of *Schistosoma* GSTs has been discovered, revealing a typical GST fold with two domains: a larger N-terminal domain containing the GSH-binding site and a smaller C-terminal domain containing the hydrophobic substrate-binding site (Schuller *et al.*, 2005). The active site of *Schistosoma* GSTs is highly conserved and consists of several key residues that are involved in catalysis and substrate binding.

In addition to their role in detoxification, *Schistosoma* GSTs have been found to play a role in host-parasite interactions. For example, they have been shown to modulate the host immune response by binding to and inhibiting host cytokines and chemokines (Sheehan *et al.*, 2001). They have also been implicated in the formation of egg granulomas, which are characteristic of schistosomiasis and contribute to the pathogenesis of the disease (Precious *et al.*, 1989).

Targeting *Schistosoma* GSTs with specific inhibitors has been proposed as a potential therapeutic strategy for the treatment of schistosomiasis. Several studies have shown that inhibition of *Schistosoma* GSTs can lead to increased susceptibility of the parasite to oxidative stress and artemisinin, as well as reduced viability and motility of adult worms (Brophy *et al.*, 1990).

2.7 Protein stability and protein folding studies

The basic hierarchy of describing protein structure includes the primary, secondary, tertiary, and quaternary structure.

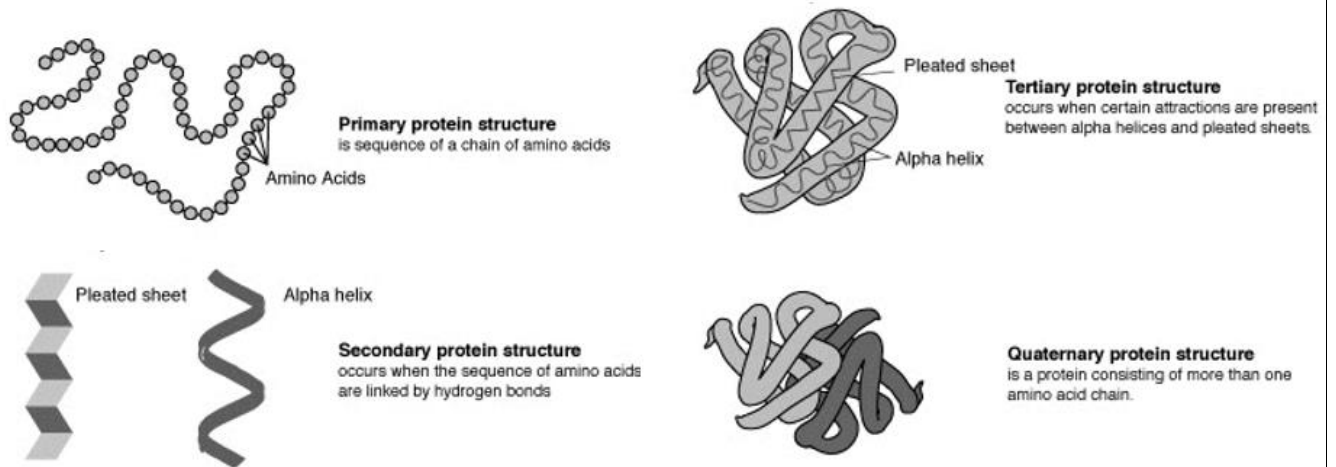


Figure 2.4. Four prominent structures of proteins. A sequence of amino acids forms the primary protein structure. Linkage by hydrogen bonds will give rise to the secondary structure of the protein containing alpha helices and/or beta sheets. The tertiary structure forms between the interactions that result from the forces of attraction between helices and sheets. The quaternary structure arises when a protein is composed of multiple amino acid chains (Adapted from <https://9xbp.short.gy/OYGQjp/>).

The primary structure is the most basic, yet most significant of all as the unique chain of amino acid determine the way in which a protein will fold, and any change in this sequence can cause changes in the shape that a protein will take thus probably also altering its function (Anfinsen, 1973). The secondary structure describes two critical conformations the protein is less or more likely to inherit. These are called alpha helices and beta pleated sheets conformations. An amino acid strand that conforms into a coiled DNA like structure held together by hydrogen bonds that are made from carbonyl oxygen and the amide group (Brandts, 1964). In contrast, beta sheets are amino acid strands that align next to each other creating a trail of parallel and anti-parallel beta sheets, containing carbonyl oxygen and amide group (Lumry *et al.*, 1966).

The tertiary structure is how the secondary structures interact with each other and with unstructured regions to give a distinct compact shape held together by other interactions such as electrostatic and hydrophobic interactions and disulfide bonds (Privalov, 1990). Electrostatic interactions tend to arise between molecules or atoms based on charge. Amino acid side chains, or R groups, either inherit a positive, negative, or neutral charge. Positively charged amino acids form attractions with negatively charged amino acids (Privalov, 1990). With hydrophobic

interactions, non-polar residues of the protein tend to have less interactions with water than their more hydrophilic (polar) counterparts (Robertson *et al.*, 1997). Amino acids with no charge, and are otherwise nonpolar tend to “bunch up,” thus allowing hydrophilic residues more exposed to interact with water and other hydrophilic substances. Lastly, however not limited to, are the disulfide bonds which are covalent bonds that form between sulfur atoms (usually found in cysteine) and are responsible for forming linkages between amino acids in the protein to aid with protein folding (Robertson *et al.*, 1997). The last prominent structure is the quaternary structure formation. This conformation occurs between two proteins, or two amino acids strands. The same interactions used to stabilise and hold the tertiary structure also aid with stabilising the quaternary structure. With all the specific interactions that contribute to the structure of a protein, it makes sense to elucidate that proteins are only stable under specific conditions. Change in conditions such as salinity, pH, exposure to denaturants may result in a protein losing its shape and as a result, loss in function as well (Kauzmann, 1959).

Proteins are involved in essential chemical processes that occur in living cells. These processes rely not only on the ability of the protein to function as a catalyst, but also in their role as structural molecules and molecular transporters or carriers (Kauzmann, 1959). All these mechanisms rely on the nascent amino acid sequence that uniquely folds into a three-dimensional structure that is biologically active and can perform a unique function in its correctly folded state. A misfolded or incorrectly folded protein leads to diverse implications such as protein aggregation, often leading to life-threatening diseases such as Alzheimer and Huntington’s diseases (Dill, 1990). The requirements for correct folding include these: (1) In order for proteins to naturally adopt their three-dimensional shape, their native configuration must have a Gibbs energy value that is lower than the unfolded structure. This proposition was put forward by American biochemist, Anfinsen, who went on to explain that (2) there is a balance between the native and unfolded states, and that the native state represents the lowest point in the Gibbs energy landscape that can be reached without any covalent bonds being broken (Herzfeld, 1991). This concept is referred to as the thermodynamic theory, which suggests that the protein folding process is primarily influenced by thermodynamic, rather than kinetic factors (Dill, 1990; Herzfeld, 1991). The first claim cannot be experimentally proven, while the second claim can using conformational stability studies. If the native state of a protein is not the global Gibbs energy minimum, it indicates the presence of a significant energy barrier between the native state and the global-minimum structure (Chothia, 1984). In such cases, a thermodynamic analysis of protein stability is justifiable and necessary to understand the

protein's behavior and stability under different conditions. If the native state of a protein is in equilibrium with the unfolded state, then no additional factors are needed for the folding of the nascent chain (Harpaz *et al.*, 1994). However, it is not always necessary for protein folding to occur co-translationally. In general, it is not accurate to claim that proteins always fold as soon as the chain emerges from the ribosome, because some proteins require additional factors or post-translational modifications for proper folding to occur (Alber *et al.*, 1987). Several studies have indicated that certain proteins' N-terminal domain lacks stability when the C-terminal domain is absent, resulting in incomplete functionality (Alber *et al.*, 1987). Therefore, the N-terminal domain cannot fold independently and may require chaperones or other factors to assist in the folding process (Alber *et al.*, 1987). Furthermore, molecules involved in protein folding, including chaperones, do not catalyze the folding process per se, but rather play a role in preventing off-pathway processes such as aggregation, misfolding, and degradation (Alber *et al.*, 1987). Chaperones and other folding factors can help guide the folding process along the correct pathway, preventing misfolding and ensuring that the protein reaches its functional native state.

In a nutshell, the stability of proteins is influenced by various factors, such as the hydrophobic effect and hydrogen bonding. However, the stabilizing effect of these factors is counteracted by the destabilizing influence of configurational entropy (Alber *et al.*, 1987). At low temperatures, the hydrophobic effect may even become destabilizing. Figure 2.5 illustrates the contribution of different interactions to the stability of a "typical" protein. Since protein stability is a delicate balance of opposing forces, slight environmental changes, such as temperature, pH, or the presence of ligands, denaturants, or stabilizing agents, can easily tip it in one direction or the other (Alber *et al.*, 1987). This allows for convenient investigation of the folding reaction.

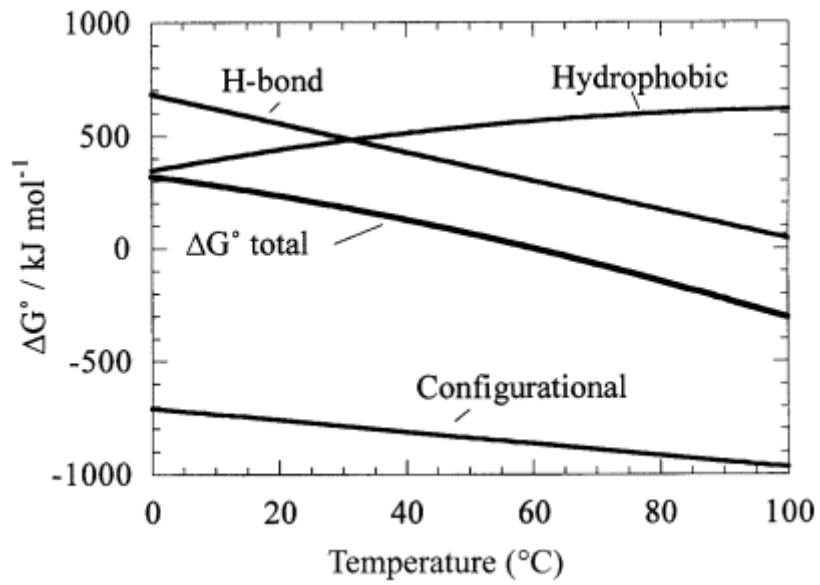


Figure 2.5. Globular protein stability under the influence of various interactions. The overall ΔG° is positively impacted by the hydrophobic effect and hydrogen bonding, which are both significant and favorable contributors. However, the configurational entropy makes a large and unfavorable contribution, leading to a modest characteristic of globular protein stability.

Chapter 3

Recombinant *Sh28GST* and *Sbh26GST* overexpression and purification studies

3.1 Introduction

Escherichia coli (*E. coli*) was chosen as an expression system of choice to produce the two recombinant proteins, *Schistosoma haematobium* 28 kDa glutathione transferase (*Sh28GST*) and pseudo-*Schistosoma bovis/haematobium* 26 kDa glutathione transferase (*Sbh26GST*). The ensuing information was obtained using ExPasy ProtParam tool (Gasteiger *et al.*, 2005). The recombinant proteins *Sh28GST* and *Sbh26GST*, inclusive of the N-terminal His-tag, are comprised of 219 and 230 amino acids, respectively. *Sh28GST* has a theoretical molecular weight of 25 kDa and an isoelectric point (pI) of 6.76, while *Sbh26GST* has a theoretical molecular weight of 26.6 kDa and a pI of 7.16. Moreover, the extinction coefficient of *Sh28GST* and *Sbh26GST* are $22920 \text{ M}^{-1} \text{ cm}^{-1}$ and $40005 \text{ M}^{-1} \text{ cm}^{-1}$, respectively (ExPasy ProtParam tool). This chapter focuses on how these recombinant proteins were overexpressed in an *E. coli* expression system, purified for the high yield of soluble protein, as well as the analysis of the results acquired from both techniques.

3.2 Materials

The pET-11a and pET-28a expression vectors were supplied by GenScript, USA. *E. coli* T7 Express competent cells were supplied by New England Biolabs, Ipswich, MA, USA. The following reagents were all acquired from Sigma-Aldrich, MO, USA: sodium chloride (NaCl), kanamycin, 2xYT media, ampicillin, Isopropyl β -d-1-thiogalactopyranoside (IPTG), Tris, nickel sulfate (NiSO_4) salt, Tween-20, glacial acetic acid, glycine, imidazole, sodium phosphate (NaH_2PO_4), sodium azide (NaN_3), dithiothreitol (DTT), ethylenediaminetetraacetic acid (EDTA) salt, N,N,N',N'-tetramethyl ethylenediamine (TEMED), acrylamide, bis-acrylamide, sodium dodecyl sulfate (SDS), β -mercaptoethanol, Coomassie brilliant blue G-250. The PageRuler prestained protein ladder was obtained from Thermo Fisher Scientific, US. The IMAC Sepharose 6 Fast Flow was obtained from GE Healthcare Bio-Sciences, Uppsala, Sweden. The Snakeskin dialysis tubing (10K MWCO, 22 mm) were supplied by Thermo Fisher Scientific, SA. The electrophoresis apparatus used, including glass slides, combs, gel tanks, electrodes with lid, and power supply box, were supplied by Bio-Rad, Hercules, California.

The rest of the chemicals used were obtained from Sigma Aldrich, MO, USA, and were all of analytical grade.

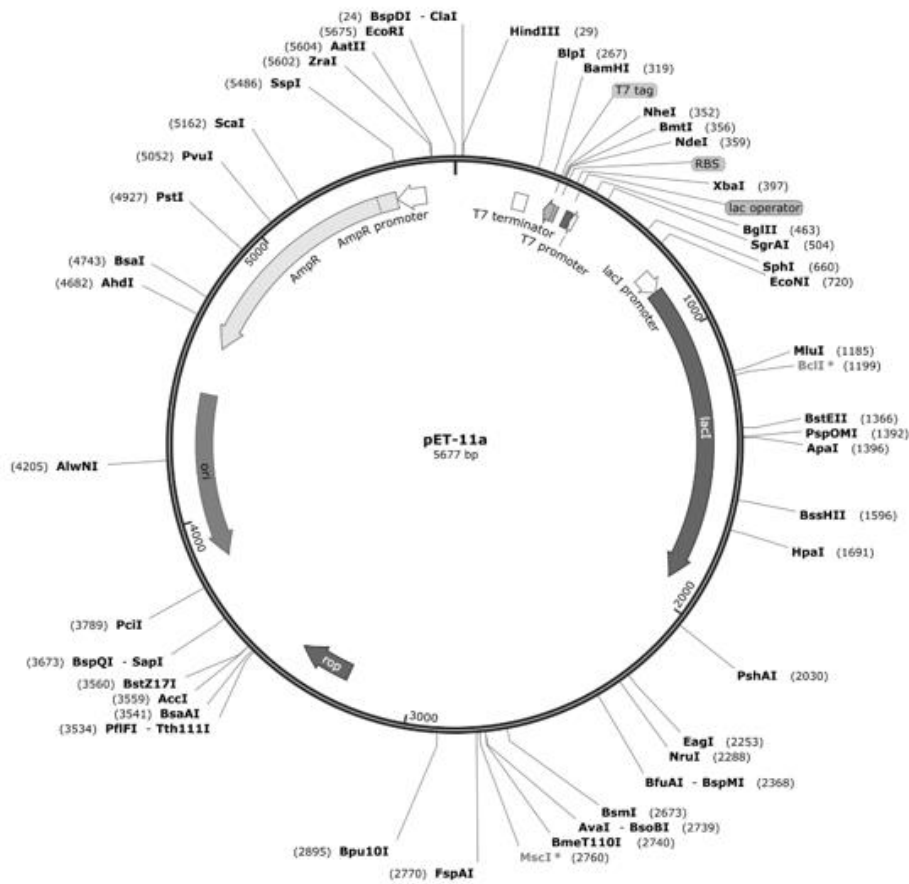
3.3 Methods

3.3.1 The reconstruction of the missing regions in the gene sequence of *Sbh26GST*.

Initially, the gene sequence of *Sbh26GST* was incomplete. To address this issue, the present research adopted a recently published study by Padi *et al* from the same laboratory, which aimed to construct a pseudo-*Sbh26GST* by utilizing various sequence analysis tools to generate the unknown region in its open reading frame (ORF). This study involved the alignment of the *Schistosoma bovis* 26 kDa glutathione transferase (*Sb26GST*) with the *Schistosoma haematobium* 26 kDa glutathione transferase (*Sbh26GST*), resulting in a sequence identity match of 99.9% similarity. Additionally, the BLAST tool was utilized to identify evolutionary sequences in the database that would match the sequence under study. The consensus sequence was then predicted and generated using the computer software CLC bio bioinformatics, resulting in the creation of a newly constructed gene called *Schistosoma bovis/haematobium* 26 kDa glutathione transferase (pseudo-*Sbh26GST*). The name "pseudo-*Sbh26GST*" was attributed due to its generation from the utilization of proteins from two species, namely *haematobium* and *bovine*.

3.3.2 Vector construction of *Sh28GST* and *Sbh26GST*

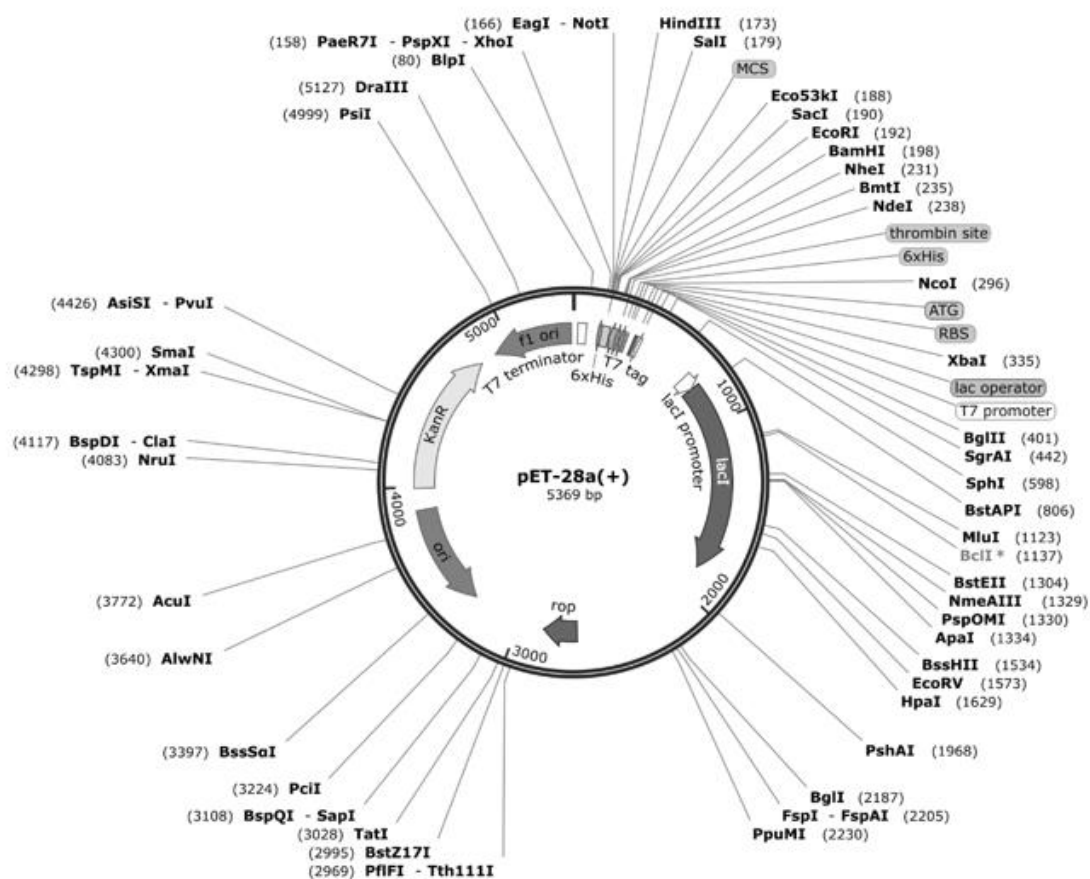
The pET-11a and pET-28a expression vectors were designed specifically for the expression of *Sh28GST* and *Sbh26GST*, respectively, in *E. coli* T7 cells. To facilitate the purification of these proteins using immobilized metal ion affinity chromatography (IMAC), *Sh28GST* was modified to include poly-histidine (His) tags at its N-termini site before insertion into pET-11a. Moreover, these vectors were equipped with an origin of replication and protein synthesis was regulated by a T7 promoter. Genes that confer resistance to antibiotics ampicillin (pET-11a) and kanamycin (pET-28a) were used to allow for the selection of cells carrying the target vectors, as well as a multiple cloning site to facilitate cleavage by restriction enzymes and insertion of the target gene fragment thereby allowing for the synthesis of *Sh28GST* (Genebank, P30114) and *Sbh26GST* (Genebank, AAA29892) by GenScript, USA.



Sh28GST amino acid sequence

MSSHHHHHHTGDHIKVIYFNGRGRAESIRMTLVAAGVNYEDERISFQDWPKIKPTIPGGRLPAVKITDN
 HGHVKWMLLESIAIARYMAKKHHMMGETDEEYYNVEKLIGQVEDLEHEYHKTLMKPEEEKQKITKEILN
 GKVPVLLDIICESLKASTGKLAVGDKVTLADLVLIAVIDHVTDLDKEFLTGKYPEIHKHRENLLASSPRLAKYL
 SDRAATPF

Figure 3.1. Schematic representation of pET-11a vector (Adapted from SnapGene, 2023) that was engineered to incorporate recombinant *Sh28GST*. The genetic sequence of *Sh28GST* (extracted from Genbank, P30114) was modified by adding a 6x histidine (His)-tag to the N-terminus of the protein (highlighted in blue). The resulting modified sequence was subsequently incorporated into the pET-11a expression vector using the *Bam*HI and *Nde*I restriction enzyme sites located within the vector's multiple cloning site and synthesized by GenScript, USA.



Sbh26GST amino acid sequence

MLVPRGSHHHHHHAPILGYWKIKGLVQPTRLLLEYVGEVYEERLYDRNDGDVWRNEKFNGLGFNPYPY
 YIDGDVKLTQSMAILRYIADKHNMLGGCPKERAISMLEGAILDIRLGVSR IAYNKEFETLKVGFLNQLPG
 MLKMFENRLSHKIYLNVDNFVDFMLYDALDVLVLYMDPKCLDAFPKLISFKQRIENLPPIKNYLNSDRH
 IKWPLQGWSAIFGGGDAPPK

Figure 3.2. Schematic representation of pET-28a vector (Adapted from SnapGene, 2023) that was engineered to incorporate recombinant *Sbh26GST*. The genetic sequence of *Sbh26GST* (extracted from Genbank, AAA29892) was incorporated into the pET-28a vector at the *Bam*HI and *Nco*I restriction sites. This resulted in the generation of the recombinant *Sbh26GST* protein with a 6x His-tag sequence fused to the N-terminus of the protein (highlighted in blue), located immediately after the thrombin cleavage site and this was synthesized by GenScript, USA.

3.3.3 Competent *E. coli* T7 cells transformation with designed constructs of *Sh28GST* and *Sbh26GST*

Competent *E. coli* T7 cells were transformed using the heat shock method, which utilizes heat to enhance the permeability of the bacterial cell membrane and facilitate uptake of

the designed constructs, pET-11a and pET-28a (Bergmans *et al.*, 1981). The competent cells were thawed on ice, while simultaneously preparing the vectors. Lyophilized pET-11a and pET-28a vectors were reconstituted by adding 100 μL of filtered MilliQ water to achieve a final concentration of 40 ng/ μL . The solution was spun down at $16,000 \times g$ for 2 *min*, and 200 ng of the vector was added to the thawed competent cells and swirled to mix. The cells were then chilled on ice for 30 min and exposed to heat (42°C) for 30 s. The cells were immediately chilled on ice for 5 min, followed by the addition of a 950 μL volume of super optimal broth (SOC) media, and this mixture was incubated at 37°C for 1 h at a speed of 230 rpm. Afterward, the cells were placed onto LB agar plates that had been enriched with 50 $\mu\text{g}/\text{mL}$ ampicillin for pET-11a-*Sh28GST* and 30 $\mu\text{g}/\text{mL}$ kanamycin for pET-28a-*Sbh26GST*. The plates were incubated overnight at 37°C.

3.3.4 Overexpression of *Sh28GST* and *Sbh26GST*

After successful transformation, a colony was selected from each agar and added to 50 mL of 2-YT media enriched with 50 $\mu\text{g}/\text{mL}$ ampicillin for T7-pET-11a-*Sh28GST* and 30 $\mu\text{g}/\text{mL}$ kanamycin for pET-28a-*Sbh26GST*. The flasks were then incubated for 16 h at 37°C while being rotated at a speed of 230 rpm. A 1/50 dilution was performed by transferring an appropriate amount of the overnight culture to freshly prepared 2 \times YT media enriched with appropriate antibiotics, and the flasks were incubated at 37°C and 230 rpm until the optical density ($\text{OD}_{600\text{nm}}$) reached approximately 0.65. After incubation, the flasks were placed on ice for 20 *min*, and protein expression was induced by adding 0.5 mM of isopropyl β -D-thiogalactopyranoside (IPTG). The expression conditions for both proteins were maintained at 30°C, at a speed of 230 rpm for 6 hours. The cells were spun down at $5000 \times g$, at 4°C for 15 min for harvesting. The supernatant was discarded, and each pellet was resuspended in 30 mL of resuspension buffer buffers (25 mM NaH_2PO_4 , 0.01% (w/v) NaN_3 , 0.5 NaCl, 0.04 M imidazole, pH 7.5). Lysozyme (0.1 mg/mL) was added to facilitate overnight lysis while the cells were stored at -20°C. The frozen cells were then thawed in ice water, sonicated (using 55-65 μm amplitude for 10 cycles) and centrifuged at 4°C and $18000 \times g$ for 20 *min* to separate the soluble fraction from the insoluble fraction. The extracts obtained from the insoluble (pellet), lysate, and soluble (supernatant) fractions were aliquoted, and protein expression was analysed using sodium dodecyl-sulfate polyacrylamide gel electrophoresis (SDS-PAGE), as outlined in Section 3.3.5. The soluble fraction, which contained the protein of interest, was filtered and was now ready for purification.

3.3.5 Purification of *Sh28GST* and *Sbh26GST*

The technique selected for purifying the proteins of interest, *Sh28GST* and *Sbh26GST*, from non-targeted proteins was immobilized metal affinity chromatography (IMAC). It was first developed in the 1980s and has been used for decades by scientists due to its effectiveness and high level of specificity (Sulkowski, 1985). During the IMAC process, common metals such as nickel, iron, and cobalt are immobilized onto an insoluble matrix by chelation (Kielkopf *et al.*, 2020). The target enzyme then binds specifically to the matrix via the specific interaction with the immobilized metal (Kielkopf *et al.*, 2020). Following removal of non-targeted molecules using buffer containing non-harsh detergent such as Tween-20, the binding interaction is reversed to elute the protein of interest.

Approximately 9 mL of the IMAC Sepharose resin was added to a column and 10 column volumes of double-distilled ddH₂O was passed through the column to lay the resin. The resin was charged with Ni²⁺ ions by adding 5 column volumes of a 0.1 M solution of nickel sulfate (NiSO₄) and then washed with 20 column volumes of ddH₂O. The charged column was then ready for use. The flow rate was set to 4.5 mL/min and 10 column volumes of resuspension buffer (25 mM NaH₂PO₄, 0.01% (w/v) NaN₃, 0.5 NaCl, 0.04 M imidazole, pH 7.5) were added to the column for equilibration. The soluble fraction was loaded and the flow through was collected. Then, 10 column volumes of the same resuspension buffer (25 mM NaH₂PO₄, 0.01% (w/v) NaN₃, 0.5 NaCl, 0.04 M imidazole, pH 7.5) were passed through the column to wash off any unbound proteins. This was followed by 10 column volume washes with the wash buffer (25 mM NaH₂PO₄, 0.01% (w/v) NaN₃, 0.5 M NaCl, 0.04 M imidazole, 0.1% (v/v) Tween-20, pH 7.5) to remove any impurities. Finally, the column was washed with 10 column volumes of the resuspension buffer, followed by elution of the protein of interest at a flow rate of 1.5 mL/min using the elution buffer (25 mM NaH₂PO₄, 0.01% (w/v) NaN₃, 0.5 NaCl, 0.5 M imidazole, pH 7.5). The higher concentration of imidazole in the elution buffer served as a competitive agent, dislodging the His-tagged protein of interest from the Nickel metal in the column. The pure protein fractions were collected, stored on packed ice, and analysed using sodium dodecyl-sulfate polyacrylamide gel electrophoresis (SDS-PAGE) as described in Section 3.3.6. Downstream applications were then carried out.

3.3.6 Qualitative analysis of *Sh28GST* and *Sbh26GST* using SDS-PAGE and UV-vis spectroscopy

Sodium dodecyl-sulfate polyacrylamide gel electrophoresis (SDS-PAGE) of Sh28GST and Sbh26GST

SDS-PAGE is a powerful, high-resolution electrophoretic technique used to separate a complex mixture of proteins according to their molecular weight. It was developed in the 1970s by Laemmli and has been used for decades by researchers (Laemmli, 1970). In SDS-PAGE, the proteins are initially denatured by an anionic detergent such as SDS, which imparts a negative charge and linearizes the proteins (Smith, 1984). The sample is then subjected to electrophoresis through a porous gel matrix, which provides high-resolution separation of the proteins based on their size (Kielkopf *et al.*, 2021). This powerful technique has become a fundamental tool in protein biochemistry and is widely used for the identification and analysis of complex protein mixtures.

The technique of SDS-PAGE was employed to analyze the results of overexpression and purification. The samples of interest were mixed with the reducing sample buffer, composed of 25% (v/v) Tris-HCl, 4% (w/v) SDS, 10% (v/v) β -mercaptoethanol, 20% (v/v) glycerol, pH 6.8, in a 1:1 ratio. The samples were then heated to above 90°C for 1 min and loaded onto the wells of a pre-filled (with tank buffer) SDS-PAGE gel, as prepared according to the protocol provided in Table 3.1. A molecular weight marker was also loaded onto the gel as a reference, and the gel was run for approximately 1 hour at a voltage of 120 volts (V). The gel was stained with Coomassie blue dye solution, composed of 0.1% (w/v) Coomassie brilliant blue G-250 in a 1:5:4 ((v/v/v) acetic acid-methanol-water solution) ratio for 20 min, and destained overnight using a destain solution (1:5:4 (v/v/v) acetic acid-methanol-water).

The distances traversed by the proteins on the gel, relative to the dye front and denoted as the retention factor, were employed to estimate the molecular weight of *Sbh26GST* and *Sh28GST*. This was achieved by utilizing a calibration curve, which relates the logarithm of molecular weight against the distance traveled by standard proteins converted into the retention factor. The results were accumulated and analysed using the gel doc system.

Table 3.1. Glycine gel protocol for producing a high-resolution gel

Reagents	12.5% separating gel	4% stacking gel
Monomer solution ^{1*}	6.25 mL	940 µL
Separating gel buffer ^{2*}	3.75 mL	-
Stacking gel buffer ^{3*}	-	1.75 mL
Distilled water	4.75 mL	4.3 mL
10% SDS	150 µL	70 µL
TEMED	15 µL	15 µL
10% (w/v) ammonium persulfate	75 µL	35 µL
Electrophoretic tank buffer ^{4*}	-	-

¹ 30% (w/v) acrylamide, 2.7% (w/v) acrylamide; ² 1.5 M Tris-HCl, pH 8.8; ³ 0.5 M Tris-HCl, pH 6.8; 250 mM Tris-HCl, 1.92 M glycine, 0.1% (w/v) SDS, pH 8.3

Ultraviolet-visible (UV-vis) spectroscopy for qualitative analysis of Sh28GST and Sbh26GST

UV-vis spectroscopy is a technique used for both qualitative and quantitative analysis of a sample in solution by measuring the absorbance spectra of electromagnetic radiation. The absorbance of the radiation excites electrons from the ground state to the first singlet excited state of the compound. A spectrophotometer is used, which includes a light source (commonly a tungsten or deuterium lamp), a sample holder, and a detector, with a filter that allows for selecting one wavelength at a time. In this experiment, the wavelength of interest is 280 nm since *Sh28GST* and *Sbh26GST* have tryptophan and tyrosine residues that will absorb maximally at this wavelength.

To prepare the sample, each pooled fraction of the target protein was dialyzed at 4°C overnight against 2 L of dialysis buffer (100 mM NaH₂PO₄, 0.01% (w/v) NaN₃, 2 mM dithiothreitol (DTT), 2 mM EDTA, pH 7.5) to remove salts. The dialysate was filtered, and the dialyzed samples were then centrifuged (12000 × g, 12 min, 4°C) and stored in packed ice. The quality of each sample was monitored by preparing a 1/20 dilution of protein and dialysate. A blank buffer (dialysate) was also measured to correct for interferences. The sample and buffer were added to a 100 mm micro-QS quartz cuvette and measured (200 nm/min scan speed, 0.5 nm data interval, 1.5 nm bandwidth, 3 accumulations) between a range of 245 nm – 365 nm at 20°C in triplicates. The averaged data were then used to construct an absorption spectrum.

UV-vis spectroscopy for quantitative analysis of Sh28GST and Sbh26GST

The concentrations of the recombinant *Sh28GST* and *Sbh26GST* proteins were determined using an ultraviolet-visible (UV-vis) spectrophotometer (Jasco V-630 spectrophotometer, Tokyo, Japan). The absorbance spectroscopy method utilized the Beer-Lambert Law equation, as follows:

$$\mathbf{A} = \boldsymbol{\varepsilon c \ell} \quad (3.1)$$

where A is the measured absorbance (unitless, denoted as arbitrary units), ε is the molar extinction coefficient (measured in units of $\text{M}^{-1} \text{cm}^{-1}$ at 280 nm for each protein), c is the protein concentration (measured in units of M), and L is the path length of the sample (usually 1 cm). This law is based on the principle that the amount of light absorbed by a sample is proportional to its concentration, and thereby allows for the quantification of protein concentrations in solution.

To prepare the samples for quantification, a series of five dilutions were prepared (1/10, 1/20, 1/40, 1/80, 1/160) with 1 blank sample (dialysate). The concentration was measured spectrophotometrically at 280 nm and 340 nm, under the same conditions as the UV-vis absorbance spectra. The results were acquired and analysed.

3.4 Results

3.4.1 Overexpression of Sh28GST and Sbh26GST

Recombinant *Sbh26GST* and *Sh28GST* were overexpressed by inducing their expression at $\text{OD}_{600\text{nm}}$ of 0.65 for 6 h at 30°C with 0.5 mM IPTG. The control, which was uninduced, exhibited no overexpression of proteins, as evident from the SDS-PAGE results (Figure 3.3). The induced cultures, however, yielded significant amounts of target proteins, with experimental molecular weights found to be approximately 27 kDa and 25 kDa for *Sh28GST* and *Sbh26GST*, respectively. The wet cell pellet yield per liter of culture was determined to be approximately 7.3 g for *Sh28GST* and 4.8 g for *Sbh26GST*.

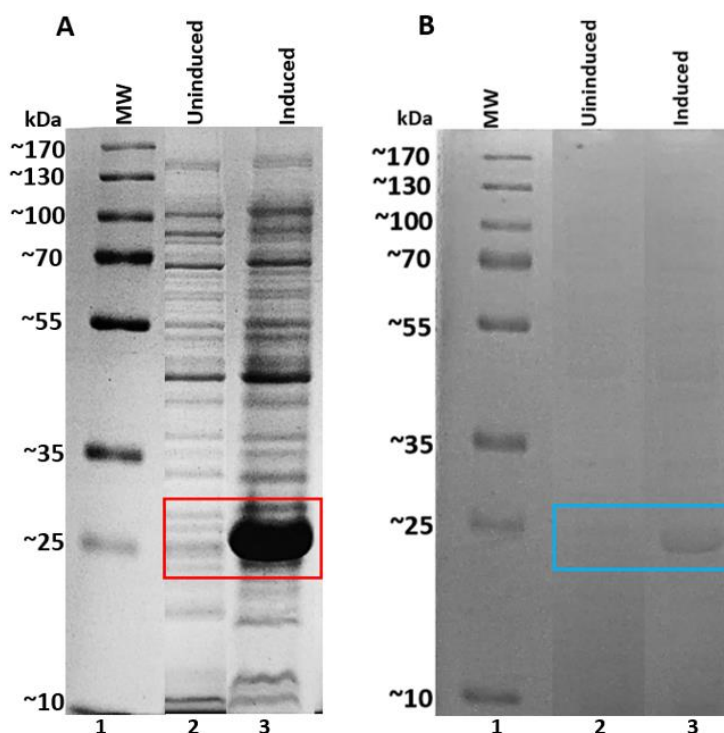


Figure 3.3. SDS-PAGE overexpression results of recombinant *Sh28GST* and *Sbh26GST* for induced versus uninduced culture. (A) *Sh28GST*, (B) *Sbh26GST*, (MW) molecular weight marker, (1) 0 mM IPTG and (2) 0.5 mM IPTG induction. Protein overexpression was induced with 0.5 mM IPTG (6 h, 30°C, 230 rpm) at $OD_{600nm}=0.65$. The analysis of overexpression per litre of culture was carried out on a 12% glycine gel and visualized with Coomassie brilliant blue G stain. Zero IPTG concentration resulted in no expression of target proteins. A concentration of 0.5 mM of isopropyl β -D-1-thiogalactopyranoside (IPTG) proved sufficient to elicit overexpression and facilitate large-scale production, a phenomenon readily observable on the gels (lanes 2) where the targeted proteins are depicted as bold bands, neatly demarcated with red and green annotation boxes for respective proteins.

3.4.2 Purification of recombinant *Sh28GST* and *Sbh26GST* from contaminants and unwanted substances

The soluble fractions of histidine-tagged proteins that were successfully overexpressed were subjected to immobilized metal affinity chromatography (IMAC) for purification, with nickel being the chelator of choice. After removal of all impurities, imidazole in high concentrations was employed to elute the proteins of interest. At every stage of the procedure, a sample was retrieved and mixed with a reducing sample buffer for subsequent analysis on an SDS-PAGE 12% glycine gel, enabling us to establish a purification profile and monitor the progress of the process. The results disclosed that neither gel's lanes 5 nor 6 (Figure 3.4) presented any detectable target protein, implying the successful capturing of the proteins of interest by the resin, with no protein loss during the wash steps. The target proteins were eluted with a high level of purity, as is evident from the presence of solitary, well-defined bands in

lanes 7 (Figure 3.4). These bands have been demarcated with a red and a blue box for *Sh28GST* and *Sbh26GST*, respectively. The soluble fractions yielded significant amounts of target proteins. The retention factor against logarithmic molecular weight standards were plotted and the experimental molecular weights were found to be approximately 27 kDa and 25 kDa for *Sh28GST* and *Sbh26GST*, respectively, which also agreed with earlier studies (Padi *et al.*, 2021).

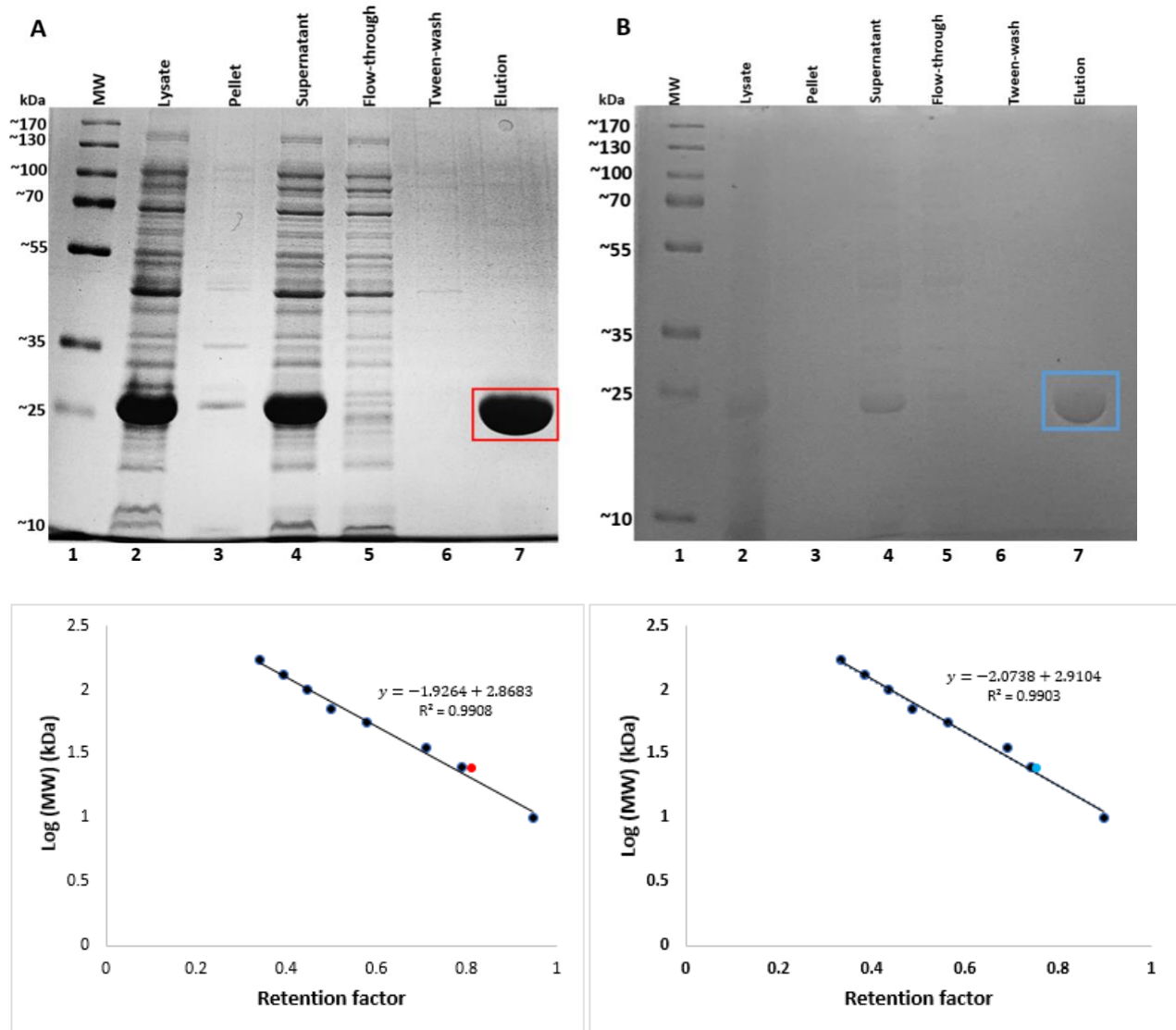


Figure 3.4. SDS-PAGE analysis showing the purification profiles of *Sh28GST* and *Sbh26GST* from *Schistosoma haematobium*. Protein purification was performed using affinity chromatography. (A) *Sh28GST*, (B) *Sbh26GST*, (MW) molecular weight marker, Lane 2 = cell lysate composed of both pellet and supernatant; Lane 3 = Pellet after centrifugation; Lane 4 = Soluble fraction containing the target protein; Lane 5 = Flow through after the supernatant was passed through the column; Lane 6 = wash step using equilibration buffer and tween-20 to get rid of unwanted proteins and impurities; Lane 7 = Eluent containing the pure protein of interest demarcated by red box for *Sh28GST* (~27 kDa size) and blue box for *Sbh26GST* (~25 kDa size) on a 12% glycine gel. The approximate sizes were determined using respective standard curves of retention factor as a function of log molecular weight.

3.4.3 Quantitative and qualitative analysis of *Sh28GST* and *Sbh26GST*

UV-Vis spectroscopy was employed as the preferred analytical method for comprehensive evaluation of the quality and quantity of the *Sh28GST* and *Sbh26GST*. Analysis of the proteins within the wavelength range of 245 nm - 365 nm demonstrated a prominent absorption peak at 280 nm and a pronounced dip at 260 nm (Figure 3.5), which served as confirmation of their high degree of purity and absence of contamination, aggregation, and light-scattering interfering particles. The protein concentrations of *Sh28GST* and *Sbh26GST* were estimated using the gradient generated from the absorbance versus wavelength plot displayed in Figure 3.6 and using the Beer-Lambert's law equation. The absorbance values acquired were corrected for baseline contributions and plotted against the dilution factor, resulting in the generation of a linear regression line for each protein with equations $y = 9.4246x - 0.004$, $R^2=1$ for *Sh28GST* and $y = 6.8587x - 0.00003$, $R^2=1$ for *Sbh26GST*. The slopes of each linear regression line were utilized in conjunction with the Beer-Lambert law to estimate the protein concentrations. Based on these calculations, the concentration of *Sh28GST* was determined to be approximately 6 mg/mL, while *Sbh26GST* was found to have a concentration of approximately 3 mg/mL.

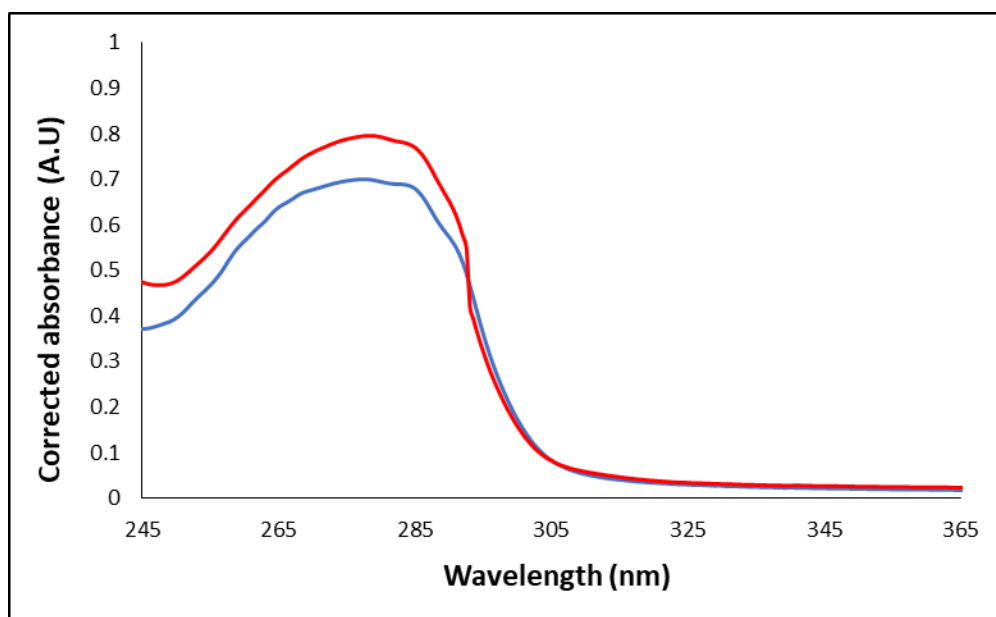


Figure 3.5. UV absorption spectra *Sh28GST* and *Sbh26GST*. The spectra of *Sh28GST* (red) and *Sbh26GST* (blue) was determined by measuring the absorbance across a 245 nm – 365 nm range with equilibration buffer (25 mM NaH_2PO_4 , 0.01% (w/v) NaN_3 , 0.5 NaCl, 0.04 M imidazole, pH 7.5) as the selected buffer for the protein samples. Prominent absorption peaks at 280 nm are observed indicating presence of protein. A pronounced dip at 260 nm and a flat baseline was observed at 340 nm from both curves thus confirming that the proteins were highly pure without any significant nucleic acid contamination or aggregation.

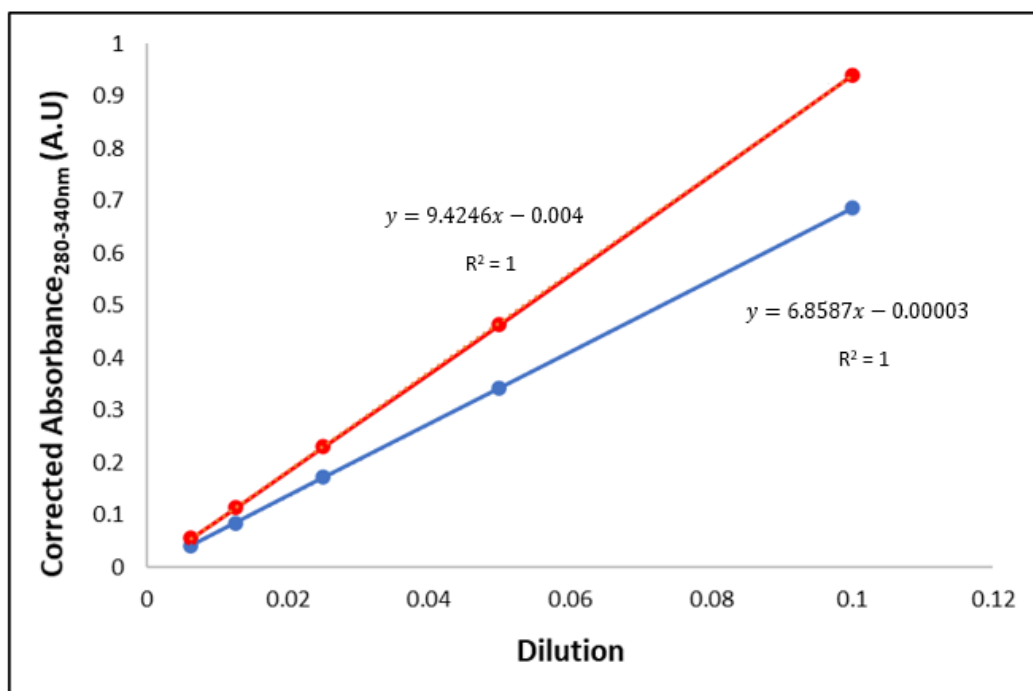


Figure 3.6. Absorbance against dilution plot for concentration determination of *Sh28GST* and *Sbh26GST*. A series of dilutions were conducted using spectrophotometry for two distinct proteins. The protein solutions were diluted with equilibration buffer (25 mM NaH₂PO₄, 0.01% (w/v) NaN₃, 0.5 NaCl, 0.04 M imidazole, and pH 7.5). To quantify the concentration of the proteins, their presence was monitored at two distinct wavelengths: 280 nm to detect the presence of the protein and 340 nm to detect protein aggregation.

3.5 Discussion

The pET-11a and pET-28a expression vectors are frequently used to express recombinant proteins in *E. coli*. These vectors incorporate numerous features that facilitate efficient transcription and translation, for successful protein expression and purification studies. The pET-11a vector, which was used to produce *Sh28GST*, contained the β -lactamase gene, which conferred ampicillin resistance to *E. coli* (Shilling *et al.*, 2020). In addition, pET-28a vector used for *Sbh26GST* conferred resistance to the antibiotic kanamycin, which allowed for selection of transformed cells during cloning and maintenance of the vector (Shilling *et al.*, 2020). Both vectors contain a strong T7 promoter that promoted high transcription levels of each recombinant gene (Tabor, 2001). They also possess a ribosome binding site (RBS) to ensure optimal translation initiation and inducibility by isopropyl β -D-1-thiogalactopyranoside (IPTG) for precise control over the timing and level of expression (Tabor, 2001). This led to successful expression of *Sh28GST* and *Sbh26GST*, as evidenced by the appearance of a thick dark band on the predicted molecular weight of the target sequence in the induced lane of the

SDS-PAGE results (Figure 3.3 A and B, lanes 3) compared to the faint expression observed in the uninduced lane (Figure 3.3 A and B, lanes 2).

The purification profiles of both proteins, shown in Figure 3.4, illustrate the steps taken to achieve highly pure proteins. The proteins were extracted in their soluble form after separating the pellet from the supernatant via centrifugation. Lanes 5 and 6 in Figure 3.4 resulted in a null presence of the target proteins, suggesting that the N-terminal his-tagged *Sh28GST* and *Sbh26GST* were successfully captured by the nickel resin, while all other contaminants were washed away. Moreover, the addition of highly concentrated imidazole competed with the covalent binding between the imidazole ring of the polyhistidine tag and the nickel ions in the resin, causing the target proteins to be released from the column with a >95% purity yield ratio. This was indicated by the appearance of a single thick band corresponding to the 28 kDa and 26 kDa sizes for *Sh28GST* and *Sbh26GST*, respectively (Figure 3.4, lane 7 in A and B). The soluble protein fractions were free of aggregation and nucleic acid contamination. The soluble fraction of *Sh28GST* and *Sbh26GST* amounted to approximately 6 mg/mL and 3 mg/mL, respectively. These results led to the conclusion of successful overexpression and purification studies of *Sh28GST* and *Sbh26GST* from *Schistosoma haematobium*. The choice of a purification tag depended on several factors, including the nature of GSTs tagged with a poly His-tag and the downstream applications for which it will be used. Purifying the poly His-tagged proteins using immobilized metal affinity chromatography (IMAC) was a fair choice. This technique takes advantage of the ability of the His-tag to bind to metal ions such as nickel or cobalt (Block *et al.*, 2009). IMAC purification of His-tagged proteins is efficient and selective, and it can be performed under mild conditions, making it a good option for preserving protein activity (Kielkopf *et al.*, 2020). One of the main advantages of using His-tagged purification is that it allows for high-purity protein isolation with minimal contamination from other cellular components (Riguero *et al.*, 2020). The His-tag is typically located at either the N- or C-terminus of the protein, which means it does not interfere with the protein structure or function, allowing for uninfluenced downstream applications.

Additionally, because the His-tag is only a short peptide sequence (usually 6 to 10 histidine residues), it is unlikely to induce any immune response or interfere with protein interactions. In terms of the wash buffer, Tween 20, a mild detergent was used to wash off contaminants and to reduce non-specific binding of proteins to the column. Other detergents like Triton X-100 or Tween 80 may have been too harsh and disrupted the interaction between the protein of interest and the metal ion resin (Zampieri *et al.*, 2000). Finally, because His-

tagged resin is often less expensive than other types of resin, such as glutathione sepharose resin used in GST-tagged purification (Block *et al.*, 2009), it was a cost-effective option for protein purification.

Obtaining high yields of soluble recombinant protein was significantly important because it formed as an indication of properly folded and functional GSTs. Insoluble and inclusion- body formed proteins are more complex to work with (Makrides *et al.*, 1996). Procedures involved in purifying them is costly and usually results in decreased yields of functional protein due to risk of protein aggregation and misfolding during the refolding process (Singh *et al.*, 2005). Recombinant proteins recovered from inclusion bodies could be less reliable than those obtained from soluble expression, as they may have contained misfolded or aggregated protein that could interfere with downstream applications (Singh *et al.*, 2005). Therefore, it was generally preferred to obtain soluble protein expression, and many techniques had been developed to optimize expression conditions and increase the yield of soluble protein (Singh *et al.*, 2005).

Procedures described in this chapter form a fundamental cornerstone for the research study at hand. Successful protein expression and purification are pivotal components of protein biochemistry for downstream applications, which will be introduced in the ensuing chapters.

Chapter 4

Comprehensive analysis of the functional and structural properties of *Sh28GST* and *Sbh26GST*

4.1 Introduction

An infinite number of chemical reactions occur within living organisms every second. These reactions play a vital role in ensuring that living systems function optimally and that metabolic processes occur (Robinson, 2015). Enzymes are molecules responsible for facilitating these reactions, and when fused with the correct substrate, reactions occur at physiologically significant rates (Sheehan *et al.*, 2001). Following successful overexpression and purification, this chapter focuses on assessing and analysing the function and structure of *Sh28GST* and *Sbh26GST* using various assays and structure-determining techniques.

4.2 Materials

The following reagents were supplied by Sigma Aldrich, USA: 8-anilino-1-naphthalenesulfonic acid (ANS), urea, L-glutathione reduced (GSH), 1-chloro-2,4-dinitrobenzene (CDNB), sodium phosphate (NaH₂PO₄), sodium azide (NaN₃), dithiothreitol (DTT), and ethylenediaminetetraacetic acid (EDTA) salt. The Snakeskin dialysis tubing (10K MWCO, 22 mm) was supplied by Thermo Fischer Scientific, SA. The rest of the chemicals used were obtained from Sigma Aldrich, MO, USA, and were all of analytical grade.

4.3 Methods

4.3.1 Enzyme activity studies of *Sh28GST* and *Sbh26GST*

Glutathione-S-transferases (GSTs) play a crucial role as detoxification enzymes, participating in the conjugation of the thiol group of glutathione with electrophilic xenobiotics. This process serves to protect cells from the harmful effects of carcinogens, mutagens, and toxic effects or stressors (Wilce *et al.*, 1994). The activity of these enzymes is found to be abundant in bacteria, yeast, insects, plants, and most mammalian tissues. To measure this activity, the GST assay is employed with GSH as the substrate and 1-Chloro-2,4-dinitrobenzene (CDNB). CDNB is a colourless, ultraviolet, chromogenic compound converted by GST enzymes into a yellow-coloured product, 1-glutathionyl-2,4-dinitrobenzene (GS-

DNB), which can be measured spectrophotometrically at 340 nm (Tamaki *et al.*, 1999). The rate of formation of GS-DNB is directly proportional to the activity of GST in the sample (Mannervik *et al.*, 1988). Therefore, the amount of GS-DNB formed can be used to measure the GST activity present in the sample as it becomes the amount of enzyme-producing 1 μ mol of GS-CDNB conjugate per min (Figure 4.1). This assay is useful in assessing the GST activity in cells, tissue homogenates, and in plasma and erythrocyte lysates (Mannervik *et al.*, 1988).

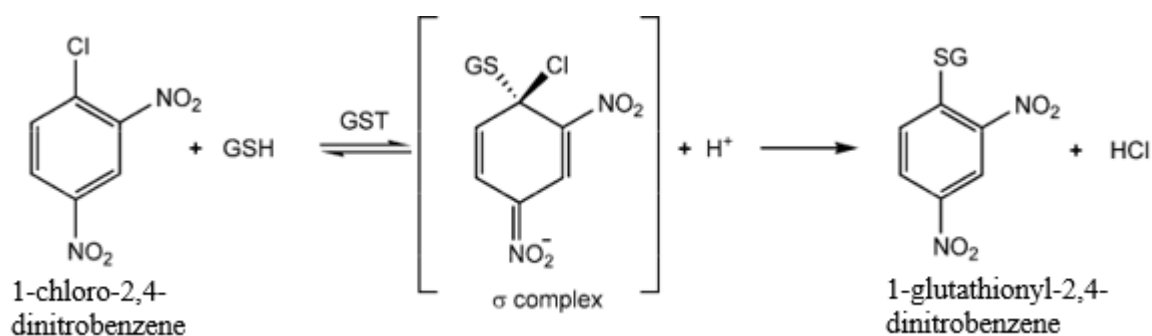


Figure 4.1. Schematic illustration of the GSH-CDNB conjugation assay. GSTs use GSH to conjugate CDNB, a colourless, ultraviolet, chromogenic compound. This process results in the conversion of CDNB into a yellow-coloured product called 1-glutathionyl-2,4-dinitrobenzene (GS-DNB). The concentration of GS-DNB can be measured spectrophotometrically at 340 nm, allowing for the quantification of GST activity. (Adapted from <https://www.mdpi.com/2072-6643/11/8/1741>).

The absorbance observed was converted to concentration using Beer-Lambert Law. Beer-Lambert law is a core principle in spectroscopy that explains the relationship between the concentration of a solution and the extent to which it absorbs light. The law states that the amount of light absorbed by a sample is directly proportional to three factors: the concentration of the solution, the distance that light travels through the sample (known as the path length), and the molar absorptivity of the substance being analysed. The molar absorptivity is a measure of how strongly the substance absorbs light at a particular wavelength. To determine the concentration of GS-DNB in a sample, Beer-Lambert's law converts the absorbance readings to concentration, using the formula provided below.

$$\text{Enzyme Activity } (\mu\text{mol}/\text{min}) = \frac{A_{340\text{nm}} \times 3000}{9600 \times 10^6} \quad (4.1)$$

The enzymatic activities of *Sh28GST* and *Sbh26GST* were evaluated by utilising GSH as the substrate and CDNB as the initiator of the reaction. Samples were prepared by varying the concentrations of each GST, while keeping the GSH substrate and CDNB concentrations constant at 1 mM, in a reaction buffer comprising 100 mM NaH₂PO₄, 0.01% (w/v) NaN₃, 2 mM EDTA, and pH 6.5, resulting in a final 3 ml volume. The rate of product formation during the conjugation process was determined by continuously monitoring the absorbance at a wavelength of 340 nm. Throughout the experiment, the instrument parameters remained unchanged, including a 1.5 nm bandwidth, a 200 nm/min scan speed, and a 0.5 sec data pitch. The reactions were conducted at a temperature of 20°C for 60 s using a UV-visible spectrophotometer (Jasco V-630 spectrophotometer, Tokyo, Japan). All measurements were performed in triplicates, and the averaged absorbance data was corrected (using blank sample) and converted to concentration using Beer-Lambert's Law. The specific activity ($\mu\text{mol}\cdot\text{min}^{-1}\cdot\text{mg}^{-1}$) of each enzyme was acquired from the velocity vs amount of enzyme (in mg) slope. Results were recorded and analysed.

4.3.2 Michaelis-Menten enzyme kinetics of *Sh28GST* and *Sbh26GST*

In every living cell, an enormous number of chemical reactions occur, and enzymes play a crucial role by participating as biocatalysts in those reactions. Michaelis-Menten kinetics is a model used to follow and explain how the rate of an enzyme-catalysed reaction depends on the enzyme concentration and substrate concentration (Cornish, 2013). Enzymes are very selective in their binding capabilities to ligands. A ligand is a substrate that undergoes a chemical reaction that is catalysed by an enzyme. Considering a reaction in 4.2, a substrate binds reversibly to the enzyme, and this results in an enzyme-substrate (ES) complex. The ES complex reacts irreversibly to produce a product thereby releasing the enzyme again.



Michaelis-Menten kinetics comprises of two most important parameters, K_m (Michaelis constant) and V_{max} (maximum velocity). K_m is the Michaelis-Menten constant, and it refers to the concentration of the substrate at which the rate of reaction is $\frac{1}{2}$ the V_{max} (Cornish, 2013). It measures the affinity an enzyme has for its substrate. The lower the K_m value, the tighter the binding, and the greater the efficiency of the enzyme at a low substrate concentration (Cornish,

2013). The other parameter is V_{max} and it denotes to the maximum rate of reaction, when the active sites of the enzyme are fully saturated with substrate. This can be formulated as,

$$v = \frac{V_{max}[S]}{K_m + [S]} \quad (4.3)$$

The initial rate of the reaction (v) is affected by the initial concentration of substrate $[S]$. It assumes that the reaction is in its steady state, where the concentration of the ES complex remains constant. When plotting a curve of substrate concentration versus rate of reaction, it is easier to see that the initial reaction rate increases rapidly in a linear format as substrate concentration increases (1st order kinetics). The rate then plateaus, indicating that all the active sites of the enzyme are fully saturated with the substrate (0 order kinetics) and the reaction velocity can no longer change (Habig *et al.*, 1974). This is demonstrated in Figure 4.2.

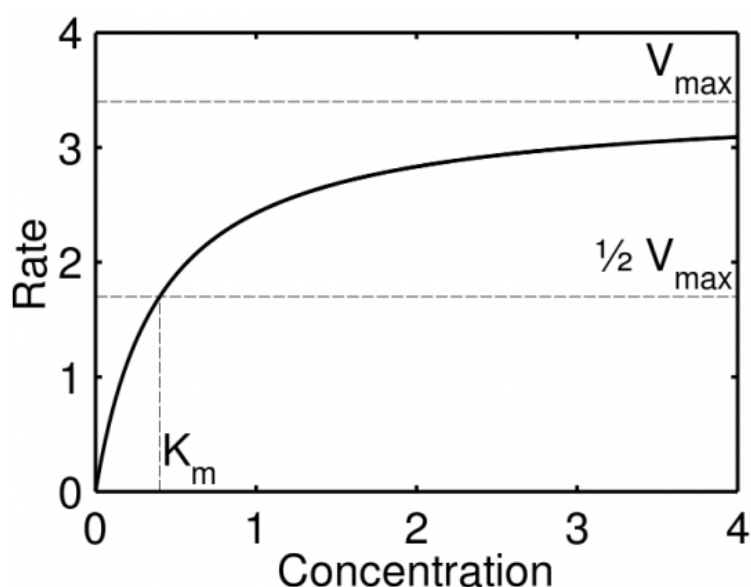


Figure 4.2. Schematic illustration of reaction rate versus substrate concentration described using Michaelis-Menten kinetics. The rate of an enzyme catalysed reaction is always examined at different substrate concentrations and the pathway follows a hyperbolic relationship. K_m is the Michaelis constant and is the substrate concentration that gives rise to 50% V_{max} . The V_{max} denotes to the reaction rate when the enzyme is fully occupied by substrate molecules and the velocity can no longer change.

The kinetics of *Sh28GST* and *Sbh26GST* enzymes were monitored using the GSH-CDNB assay previously described in Section 4.3.1. However, for enzyme kinetics, the concentration of each enzyme was kept constant at 20 nM while the concentration of GSH was varied throughout each experiment. The resulting data was used to plot Michaelis-Menten

curves, from which the K_m and V_{max} values were obtained. The turnover number of an enzyme, k_{cat} was also determined:

$$k_{cat} = \frac{V_{max}}{[E_T]} \quad (4.4)$$

Where $[E_T]$ is defined as enzyme's total concentration. The specificity constant, k_{cat}/K_m , or the ratio of the catalytic efficiency of the enzyme to its affinity for the substrate was also determined. This parameter reflects how efficiently the enzyme can convert substrate into product at low substrate concentrations (Cornish, 2013). The data acquired was fitted in GraphPad Prism and the kinetic parameters were acquired and analysed.

4.3.3 Secondary structure prediction of *Sh28GST* and *Sbh26GST* using far-UV CD

Far-UV Circular Dichroism (CD) spectroscopy is an inexpensive and useful technique for studying the secondary structure of proteins, as these biomolecules exhibit characteristic CD spectra sensitive to their conformations (Brahms *et al.*, 1980). The principle is based on the differential absorption of right- and left-handed circularly polarised light by chiral molecules. In far-UV CD, the light source emits light in the UV region of the spectrum between 200 and 260 nm (Brahms *et al.*, 1980). This range is particularly sensitive to the intrinsic protein chromophores, such as the peptide bond, and the side-chain aromatic residues, tryptophan and tyrosine (Brahms *et al.*, 1980). These chromophores provide valuable information about the overall conformation of the protein. Additionally, the secondary structural content of a protein can consist of one or a combination of beta-sheets, alpha-helices, and random coils (Corrêa *et al.*, 2009). Proteins that have a high beta-sheet content in their backbone exhibit an absorbance peak at 218 nm in negative ellipticity and 195 nm in positive ellipticity. Furthermore, alpha-helices dominate proteins with positive ellipticity at 190 nm and negative ellipticity at 208 nm and 222 nm (Brahms *et al.*, 1980).

To analyse the secondary structural content of *Sh28GST* and *Sbh26GST*, 2 μ M of each GST was dialysed against a buffer consisting of 10 mM NaH_2PO_4 , 0.01% (w/v) NaN_3 , 2 mM dithiothreitol (DTT), 1 mM GSH and 2 mM EDTA at a pH of 7.5. The prepared samples were subjected to far UV-CD spectroscopy using a 1 mm CD QS path length cuvette and a Jasco J-810 Spectropolarimeter from Tokyo, Japan. The instrument was set to constant conditions of 1 nm bandwidth, 0.5 nm data pitch, and a scanning speed of 100 nm/min. The spectra were

collected over a wavelength range of 190 – 250 nm at a temperature of 20°C. The data was expressed as mean residue molar ellipticity, $[\theta]$:

$$[\theta] = \frac{\theta}{C l n 10} \quad (4.5)$$

Where: θ is the ellipticity expressed in millidegrees, C is the protein concentration in mg/mL, l is the optical path length in cm, and n is the number of residues within each respective GST. The mean residue molar ellipticity units were expressed as mdeg.cm².dmol⁻¹. Furthermore, CONTIN-LL on Dichroweb Algorithm Server was used to estimate the secondary structural content in percentages using the obtained CD data.

4.3.4 Tertiary structure analysis of *Sh28GST* and *Sbh26GST* using fluorescence spectroscopy

Fluorescence spectroscopy is an important tool in biochemical research due to its sensitivity, non-invasiveness, and reliability (Ladokhin *et al.*, 2000). This methodology has superseded the use of radioactive tracers owing to the significant advancements in optics and electronics (Lakowicz *et al.*, 2006). The technique relies on the absorption of light by specific molecules known as fluorophores, which then emit light of a longer wavelength after a short delay. For studying biomolecules, fluorescent labelling is typically required (Sauer *et al.*, 2011). A variety of fluorophores are available, including biological fluorophores (such as tryptophan, phenylalanine, and tyrosine), organic dyes (ANS), and fluorescent nanoparticles (Ghisaidoobe *et al.*, 2014). The choice of each fluorophore depends on its photophysical properties, detection techniques, and ease of use. This section focuses on intrinsic and extrinsic fluorescence methods used to investigate the tertiary structures of GSTs in their native and denatured states.

Intrinsic tryptophan fluorescence of *Sh28GST* and *Sbh26GST*

The intrinsic fluorescence exhibited by proteins is attributed to the presence of three amino acid residues that possess aromatic side chains (Dmitry *et al.*, 2017). These are known as phenylalanine, tyrosine, and tryptophan. However, tryptophan is the most abundant of the three, found at a concentration of around 1 mol % in soluble proteins and up to 3 mol % in

membrane proteins (Ghisaidoobe *et al.*, 2014). Phenylalanine contributes negligibly to the intrinsic fluorescence of proteins due to its low absorptivity and quantum yield. Although tyrosine has a similar quantum yield to tryptophan, tryptophan's unique indole group is the primary source of UV absorbance at approximately 280 nm, with an excitation maximum at around 295 nm and emission at approximately 350 nm in proteins, thus making it an excellent fluorescence probe (Ghisaidoobe *et al.*, 2014). When excited by light at a specific wavelength, the indole ring absorbs the energy and enters an excited state. The molecule then relaxes to its ground state by emitting energy as a photon of light. This emitted light is what we observe as tryptophan fluorescence.

The tertiary structures of *Sh28GST* and *Sbh26GST* were analysed in the presence and absence of a denaturant, urea, including respective blanks. This was done by dialysing 2 μ M of each GST to a buffer consisting of 100 mM NaH₂PO₄, 0.01% (w/v) NaN₃, 2 mM dithiothreitol (DTT), 2 mM EDTA, and 1 mM GSH at a pH of 7.5. Samples used for denaturation were treated with 8 M urea, while this was omitted for native state samples. A 10 mm path-length quartz cuvette was used to hold the samples, which were then subjected to fluorescence spectroscopy using a Jasco FP-6300 Spectrofluorometer from Tokyo, Japan. The experiment was carried out at a maintained temperature of 20 °C with instrument conditions set to a bandwidth of 2.5 nm for both excitation and emission, 0.5 nm data pitch, and a scanning speed of 200 nm/min. The excitation wavelength was set at 295 nm and the spectra were collected over a wavelength range of 300 - 600 nm. The experiment was performed in triplicates and the results were collected and analysed.

Extrinsic ANS fluorescence of Sh28GST and Sbh26GST

ANS fluorescence is a widely employed biochemical technique utilised for investigating the stability, folding, and aggregation of proteins (Ota *et al.*, 2021). This method employs an external fluorescent probe, namely 8-anilino-1-naphthalenesulfonic acid (ANS), to identify and characterise protein binding sites. ANS exhibits two prominent features during this process: a blue shift of fluorescence emission maxima coupled with an increase in fluorescence intensity (Ota *et al.*, 2021). These features are typically associated with the hydrophobic nature of the binding site and the limited mobility of ANS when it binds to the hydrophobic patches of the protein.

By using both intrinsic and extrinsic probes, we acquired a more comprehensive understanding of protein conformational changes and dynamics. Tryptophan fluorescence provides information on changes in the protein core, while ANS fluorescence can detect changes in surface hydrophobicity.

The tertiary structures of *Sh28GST* and *Sbh26GST* were analysed in the presence and absence of a denaturant, urea, including respective blanks. This was done by dialysing 2 μ M of each GST to a buffer consisting of 100 mM NaH_2PO_4 , 0.01% (w/v) NaN_3 , 2 mM dithiothreitol (DTT), 2 mM EDTA, and 1 mM GSH at a pH of 7.5. Samples used for denaturation were treated with 8 M urea, while this was omitted for native state samples. A 10 mm path length quartz cuvette was used to hold the samples, which were then subjected to fluorescence spectroscopy using a Jasco FP-6300 Spectrofluorometer from Tokyo, Japan. The experiment was carried out at a constant temperature of 20 $^\circ\text{C}$ with instrument conditions set to a bandwidth of 2.5 nm for both excitation and emission, 0.5 nm data pitch, and a scanning speed of 200 nm/min. The excitation wavelength was set to 395 nm and the spectra were collected over a wavelength range of 400 - 600 nm. The experiment was performed in triplicates and the results were collected and analysed.

4.4 Results

Specific activities of Sh28GST and Sbh26GST

The enzymatic activities of two GSTs, *Sh28GST* and *Sbh26GST*, were evaluated by using GSH-CDNB assay. Samples were prepared by varying GST concentrations while keeping the GSH substrate and CDNB concentrations constant at 1 mM. The reaction was conducted in a buffer containing 100 mM NaH_2PO_4 , 0.01% (w/v) NaN_3 , and 2 mM EDTA, at pH 6.5 to a final volume of 3 ml with 1 mM of GSH and CDNB included. The rate of product formation during the conjugation process was measured by monitoring the absorbance at a wavelength of 340 nm using a UV-visible spectrophotometer (Jasco V-630 spectrophotometer, Tokyo, Japan). The reactions were conducted at 20 $^\circ\text{C}$ for 60 s, and all measurements were performed in triplicates. The averaged absorbance data was corrected using a blank sample and converted to concentration using Beer-Lambert's Law. The specific activity (Figure 4.3) of each enzyme was determined to be 40 $\mu\text{mol}/\text{min}/\text{mg}$ and 67 $\mu\text{mol}/\text{min}/\text{mg}$ for *Sbh26GST* and *Sh28GST*, respectively.

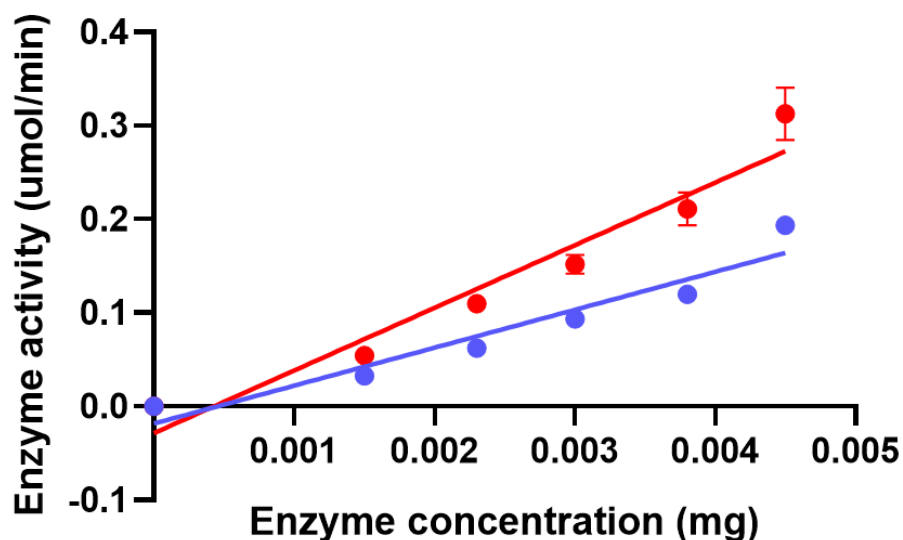


Figure 4.3. Enzyme specific activity analysis of *Sh28GST* and *Sbh26GST* using GSH-CDNB conjugation assay. An enzyme activity assay was performed with GSH used as the substrate and CDNB used as the initiator of the reaction. The reaction mixture contained fixed concentrations of 1 mM GSH and 1 mM CDNB, and the experiment was performed by varying nanomolar concentrations of each GST in a buffer containing 100 mM NaH₂PO₄, 2 mM EDTA, and 0.01% (w/v) NaN₃, at pH 6.5 The GST activity was then monitored as an increase in absorbance at 340 nm upon conjugation of the thiol group of glutathione to the CDNB substrate as a function of time in 1 min. The GST activity thus is the amount of enzyme-producing 1 μ mol of GS-CDNB conjugate per min. The standard deviation was used to account for error bars as shown in both plots and the specific activity was determined to be 40 μ mol/min/mg and 67 μ mol/min/mg for *Sbh26GST* (represented in blue) and *Sh28GST* (represented in red), respectively.

Michaelis-Menten analysis of Sh28GST and Sbh26GST

The kinetics of *Sh28GST* and *Sbh26GST* enzymes were evaluated using the GSH-CDNB assay previously described in Section 4.3.1. However, to determine enzyme kinetics, the concentration of each enzyme was maintained at 20 nM, while the concentration of GSH was varied in each experiment. The data obtained was used to generate Michaelis-Menten curves, from which the K_m and V_{max} values were calculated. The curves exhibited a hyperbolic shape, with *Sh28GST* and *Sbh26GST* displaying a shallow and steep slope before plateauing. Additionally, the turnover number (k_{cat}) and specificity constant (k_{cat}/K_m) were also determined. The obtained kinetic parameters were tabulated in Table 4.1.

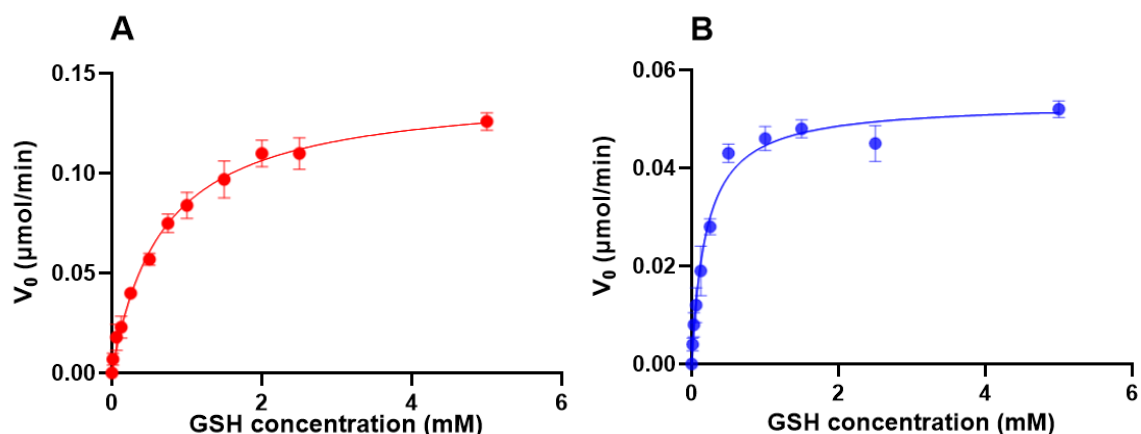


Figure 4.4. Michaelis-Menten plot of velocity versus GSH concentration for *Sh28GST* (A) and *Sbh26GST* (B). The GSH-CDNB assay was conducted by incubating 20 nM of each GST in a buffer containing 100 mM NaH_2PO_4 , 0.01% (w/v) NaN_3 , and 2 mM EDTA, at pH 6.5, with 1 mM CDNB and varying concentrations of GSH. The activity of the GST was monitored by measuring the increase in absorbance at 340 nm resulting from the conjugation of the thiol group of glutathione to CDNB over a period of 1 min. The curves exhibited a hyperbolic shape, with *Sh28GST* (represented in red) and *Sbh26GST* (represented in blue) displaying a shallow and steep slope, respectively before plateauing. Kinetic parameters, such as the K_m and V_{max} values, were obtained from the curves. The error bars in the Figure represent the standard deviation of each replicate experiment.

Table 4.1. Kinetic parameters of *Sh28GST* and *Sbh26GST* determined by Michaelis-Menten plotting using the GSH-CDNB assay with varied GSH concentrations and constant GST concentrations

Parameter	<i>Sh28GST</i>	<i>Sbh26GST</i>
K_m (mM)	0.67	0.20
V_{max} ($\mu\text{mol}/\text{min}$)	0.14	0.05
k_{cat} (min^{-1})	67	40
k_{cat}/K_m ($\text{mM}^{-1}\text{min}^{-1}$)	100	200

Far-UV CD for secondary structural content detection of Sh28GST and Sbh26GST

The secondary structural content of *Sh28GST* and *Sbh26GST* was analysed on a Jasco J-810 Spectropolarimeter from Tokyo, Japan. The samples were prepared by subjecting 2 μM of each GST against a buffer consisting of 10 mM NaH_2PO_4 , 0.01% (w/v) NaN_3 , 2 mM dithiothreitol (DTT), 1 mM GSH, and 2 mM EDTA at a pH of 7.5. The buffer blanks were also included. The spectra were collected in triplicates over a wavelength range of 190 – 250 nm at a temperature of 20°C. Both *Sh28GST* and *Sbh26GST* exhibited predominantly alpha helices with maximal intensities at troughs of ~ 222 and ~ 220 nm, respectively. Furthermore,

CONTIN-LL on Dichroweb Algorithm Server was used to estimate the secondary structural content in percentages using the obtained CD data. This data was tabulated in Table 4.2.

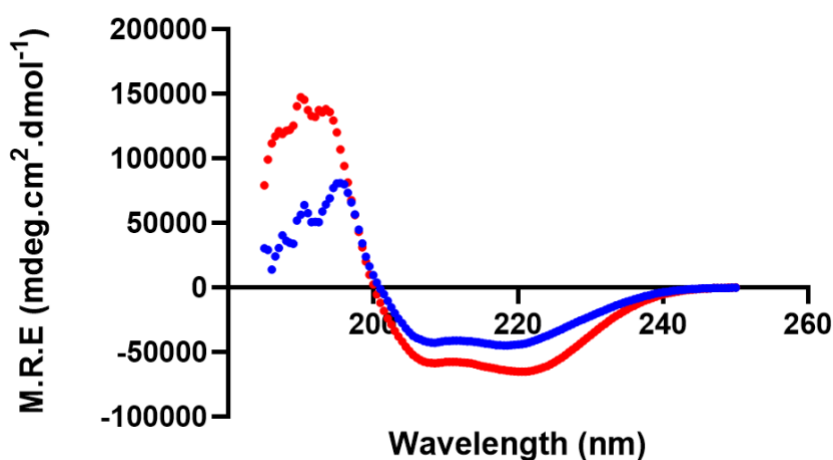


Figure 4.5. Far UV-CD spectra of *Sh28GST* and *Sbh26GST* for secondary structure prediction. The spectral measurement of both proteins was obtained from a JASCO J-810 Spectropolarimeter at 20 °C using a 1 mm CD QS path length cuvette which contained 2 μ M concentration of each protein in buffer containing 10 mM NaH₂PO₄, 0.01% (w/v) NaN₃, 2 mM dithiothreitol (DTT), and 2 mM EDTA at pH 7.5. The protein *Sh28GST* (represented in red) and *Sbh26GST* (represented in blue) both exhibited predominantly alpha helices with maximal intensity at troughs of ~222 and ~220 nm, respectively.

Table 4.2. Secondary structure prediction of *Sh28GST* and *Sbh26GST* determined using DichroWeb software. The CONTIN-L-L (Provencher and Glockner Method), reference set 7 revealed the NRMSD (Normalised Root-Mean-Square Deviation) as an indicator of how best fitted the estimated data was to the experimental data. Values below 0.1 are accepted as a good fit (Sreerama and Woody, 2000)

Type of GST	α -helix (%)	β -strand (%)	β -turn (%)	Unordered (%)	NRMSD
<i>Sbh26GST</i>	67.20	6.91	25.60	0.29	0.11
<i>Sh28GST</i>	64.01	7.60	28.29	0.10	0.19

Intrinsic and extrinsic fluorescence spectroscopy of Sh28GST and Sbh26GST

The tertiary structures of *Sh28GST* and *Sbh26GST* were analysed in the presence and absence of a denaturant, urea, including respective blanks. This was done by dialysing 2 μ M of each GST to a buffer consisting of 100 mM NaH₂PO₄, 0.01% (w/v) NaN₃, 2 mM dithiothreitol (DTT), 2 mM EDTA, and 1 mM GSH at a pH of 7.5. Denaturation was induced in some samples by adding 8 M urea while leaving others in their native state. The samples were then placed in a 10 mm path-length quartz cuvette and subjected to fluorescence

spectroscopy using a Jasco FP-6300 Spectrofluorometer. For intrinsic tryptophan fluorescence, the excitation wavelength was set at 295 nm and the spectra were collected over a wavelength range of 300 - 550 nm. The experiments were performed in triplicates and from the data collected the following observations were made: Both *Sh28GST* and *Sbh26GST* showed an increase in fluorescence intensity and a redshift as they transitioned from their native to denatured states. However, the increase in fluorescence intensity observed from the native to denatured states was greater in *Sbh26GST* compared to *Sh28GST*. For extrinsic ANS fluorescence, the same reaction conditions were used. However, ANS was excited at 395nm and an emission spectra was collected from 400 – 550 nm. *Sh28GST* exhibited an increase in fluorescence intensity from unbound ANS to ANS bound protein, resulting in a blueshift wavelength. Similarly, *Sbh26GST* showed an increase in fluorescence intensity from unbound ANS to ANS bound protein, resulting in a blueshift wavelength as well. However, the difference in fluorescence intensity observed from ANS free to ANS-bound protein was slightly higher in *Sh28GST* than in *Sbh26GST*. Treating proteins with 8 M urea resulted in a complete shutdown in fluorescence intensity of *Sh28GST*, while a little bit of intensity was left in *Sbh26GST*.

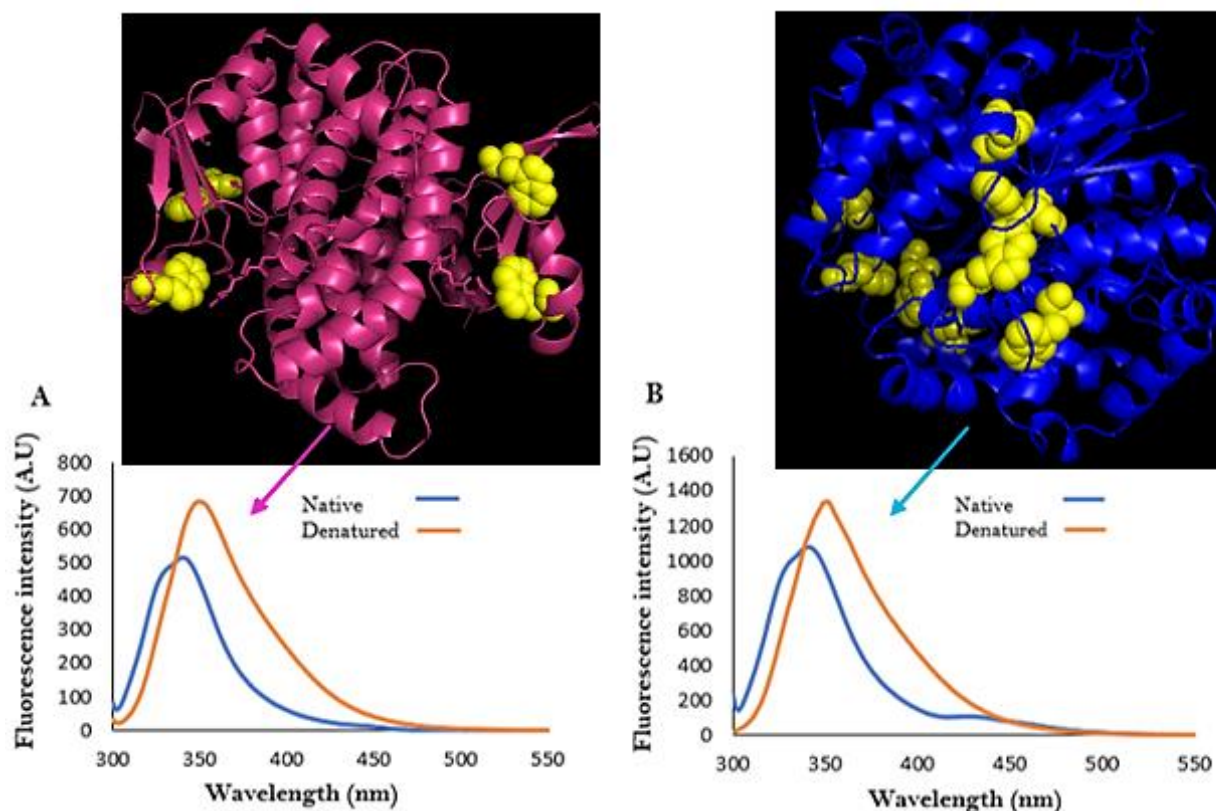


Figure 4.6. Intrinsic tryptophan fluorescence emission spectra of two glutathione S-transferase proteins, *Sh28GST* (A) and *Sbh26GST* (B), in the presence (depicted in orange) and absence (depicted in blue) of 8 M urea with a corresponding structure showing exposed tryptophan (depicted as yellow spheres) residues. Each protein was present in a concentration of 2 μM in a dialysate buffer (100 mM NaH_2PO_4 , 0.01% (w/v) NaN_3 , 2 mM dithiothreitol (DTT), 2 mM EDTA, 1 mM GSH, pH 7.5) and was excited at 295 nm to excite the tryptophan residues within the protein. The intrinsic fluorescence emission spectra were obtained for the native and denatured states, in the absence and presence of 8 M urea, respectively. *Sh28GST* exhibited an increase in fluorescence intensity from 517 to 683 A.U for native to denatured, respectively, resulting in a redshift. Similarly, *Sbh26GST* showed an increase in fluorescence intensity from 1099 A.U to 1333 A.U for native to denatured, respectively, also resulting in a redshift. However, the difference in fluorescence intensity observed from native to denatured was higher in *Sbh26GST* than in *Sh28GST*.

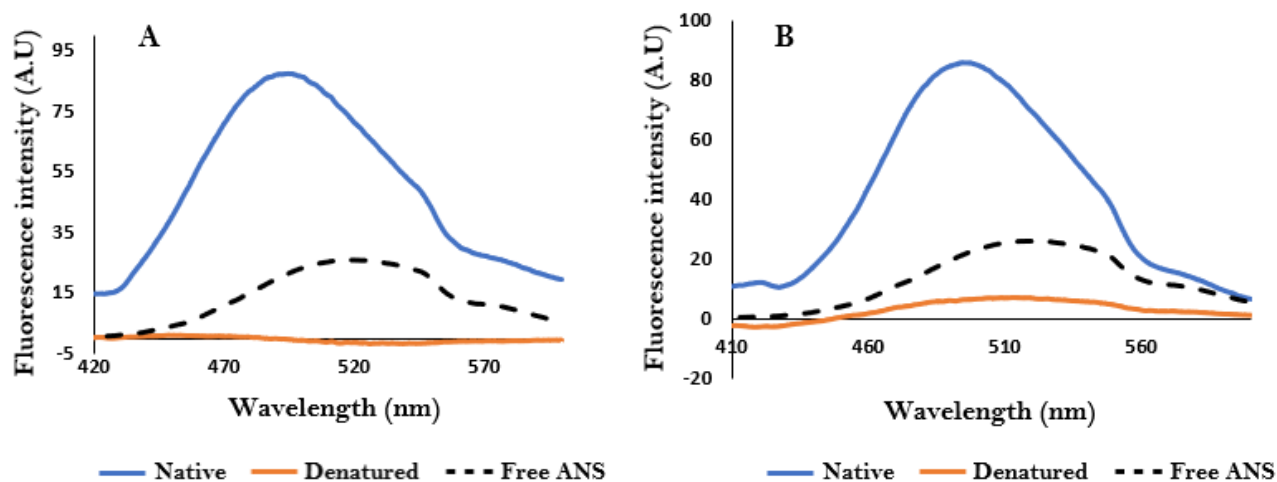


Figure 4.7. Extrinsic ANS fluorescence emission spectra of *Sh28GST* (A) and *Sbh26GST* (B), in the presence (depicted in orange) and absence (depicted in blue) of 8 M urea. Each protein was present in a concentration of 2 μ M in a dialysate buffer (100 mM NaH_2PO_4 , 0.01% (w/v) NaN_3 , 2 mM dithiothreitol (DTT), 2 mM EDTA, 1 mM GSH, pH 7.5) with 100 μ M of ANS and was excited at 395 nm. The extrinsic fluorescence emission spectra were obtained for the native and denatured states, in the absence and presence of 8 M urea, respectively, over a wavelength range of ~400 – 600 nm. The spectra of ANS in the absence of protein (depicted in black) was used as a reference. *Sh28GST* exhibited an increase in fluorescence intensity from unbound ANS to ANS bound protein, resulting in a blueshift wavelength from 519 nm to 495 nm, respectively. Similarly, *Sbh26GST* showed an increase in fluorescence intensity from unbound ANS to ANS bound protein, resulting in a blueshift wavelength from 519 nm to 495 nm. However, the difference in fluorescence intensity observed from ANS free to ANS-bound protein was slightly higher in *Sh28GST* than *Sbh26GST*. Denaturing the protein in 8 M urea resulted in a complete shutdown of fluorescence intensity of *Sh28GST*, while a little bit of intensity was left in *Sbh26GST*.

4.5 Discussion

Glutathione transferases are a group of essential enzymes that are involved in the detoxification of xenobiotic compounds. The activity of GSTs is most likely to be found in humans, insects, plants, bacteria, and yeast (Jakoby *et al.*, 1980). There are various classes of GST isozymes that differ in their specificity toward xenobiotic or endogenous substrates. The GSH-CDNB assay makes use of 1-Chloro-2,4-dinitrobenzene (CDNB) as the suitable substrate of choice thus allowing for studying the broadest range of GST isozymes (Mannervik *et al.*, 1988). In nature, GSH is present in high concentrations (1 - 10 mM) in the cells, thus being made readily available for conjugation reactions (Wilce *et al.*, 1994). Its tripeptide structure provides a reactive sulfhydryl (-SH) group that can result in an interaction with electrophilic compounds and give rise to a stable conjugate that aids in detoxifying xenobiotic compounds (Wilce *et al.*, 1994). In this study, the catalytic efficiency of two enzymes, *Sh28GST* and *Sbh26GST*, was compared. Michaelis-Menten kinetics comprises of two most important parameters, K_m (Michaelis constant) and V_{max} (maximum velocity). K_m is the Michaelis-

Menten constant, and it refers to the concentration of the substrate at which the rate of reaction is $\frac{1}{2}$ the V_{max} (Cornish, 2013). It was revealed that *Sbh26GST* had a higher catalytic efficiency than *Sh28GST*. According to literature, the V_{max} and K_m values of an enzyme follow an inversely proportional relationship, revealing that a decrease in K_m value is associated with an increase in V_{max} value (Robinson, 2015). As K_m decreases, which implies an increase in enzyme-substrate affinity, the enzyme attains half of its maximum velocity at lower substrate concentrations (Robinson, 2015). Therefore, less substrate is required to saturate the enzyme, and V_{max} is achieved at a lower substrate concentration. Additionally, k_{cat} , a significant parameter in enzyme kinetics was used to measure the efficiency of the enzyme in converting substrate to product. Higher k_{cat} values indicate faster turnover rates and greater efficiency in catalysing reactions (Robinson, 2015). Conversely, lower k_{cat} values denote slower turnover rates and reduced efficiency (Choi *et al.*, 2017). However, the reported data in this study indicated otherwise. *Sh28GST* showed a higher specific activity, a higher V_{max} value, lower K_m and a higher k_{cat} value than *Sbh26GST*. In addition, *Sbh26GST* exhibited a lower K_m value, indicating a higher affinity for its natural substrate, GSH. *Sbh26GST* can reach its maximum velocity at lower substrate concentrations, making it more efficient. In addition, a lower V_{max} value indicates that the enzyme is less efficient at converting the substrate into product (Wilce *et al.*, 1994). However, its lower V_{max} may be compensated for by the lower K_m , as the lower K_m in *Sbh26GST* implies that it can work efficiently at lower substrate concentrations, and therefore, it can reach its maximum velocity more quickly and with fewer substrate molecules. Moreover, *Sbh26GST* has a higher k_{cat}/K_m value, indicating a higher catalytic efficiency and specificity for its substrate than *Sh28GST*. Therefore, despite having a lower V_{max} value, *Sbh26GST* is more efficient and effective at catalysing the reaction than *Sh28GST*. Therefore, a higher V_{max} does not necessarily always imply higher catalytic efficiency. Especially when its K_m is also higher. In essence, *Sbh26GST* had better catalytic properties, despite possessing a lower V_{max} value.

The subsequent experiments were conducted with each GST bound to 1 mM GSH, a critical requirement to ensure the preservation of substrate specificity and facilitate meaningful comparisons with earlier investigations, while also emulating the parasite's natural physiological environment (Sheehan *et al.*, 2001). In terms of the structural integrity of *Sh28GST* and *Sbh26GST*, CD results indicate that both proteins have a predominantly alpha-helical secondary structure, confirming previous studies (Padi *et al.*, 2021). Alpha helices result from a polypeptide chain's coiling into a compact, tight, and right-handed helix (Makhatadze,

2005). These proteins have a significant content of amino acids such as leucine, alanine, methionine, and glutamate, all of which have small side chains that contribute to the alpha helix's tight packing as it is more prone to such folds (Makhatadze, 2005). Such helical content can have several effects on the proteins' properties and functions, including stability, rigidity, and binding properties (Makhatadze, 2005).

The alpha helices contribute to the protein's stability by forming a compact and robust structure. *Sbh26GST* has a higher alpha-helical content than *Sh28GST*, indicating that it is more stable with a more rigid structure, providing it with overall structural support and rigidity. Research has shown that proteins with high alpha-helical structures often involve protein-protein interactions and binding to other molecules (Errington *et al.*, 2006). Since *Sbh26GST* has a higher alpha-helical content, it may also suggest that it has a higher binding affinity for other molecules at its active site and can readily bind to them with higher affinity. GSH is a natural substrate that binds with high affinity to *Sbh26GST*, contributing to its stability. This is further supported by the Michaelis-Menten data, which revealed that *Sbh26GST* has better catalytic properties than *Sh28GST*.

The tertiary structure of *Sbh26GST* and *Sh28GST* was analysed utilising intrinsic tryptophan fluorescence emission spectra, in the presence and absence of 8 M urea, in order to uncover any differences that could potentially contribute to the proteins' functional properties. Interestingly, both proteins exhibited a red shift upon denaturation, but the intensity difference observed from native to denatured was higher for *Sbh26GST* compared to *Sh28GST*. This observation may be attributed to *Sbh26GST* possessing a higher tryptophan residue content than *Sh28GST*, and the location of those tryptophan residues plays a vital role in the intensity observed from the emission spectra. Further analysis revealed that most tryptophan residues in both proteins were exposed to the polar environment, with only a select few being partially buried in the non-polar regions (Figure 4.6 A and B). This explains the slight change in intensities observed from native to denatured and indicates that the unfolding of the proteins would not cause a significant change to their globular structure (Ghisaidoobe *et al.*, 2014). Tryptophan, with its bulky, hydrophobic side chain, also contributes to the stability of GSTs through hydrophobic interactions, hydrogen bonding, and aromatic interactions (Corrêa *et al.*, 2009). Its ring structure can participate in pi-stacking interactions with other amino acids in the protein, such as tyrosine and phenylalanine, further contributing to the protein's stability (Corrêa *et al.*, 2009; Ladokhin *et al.*, 2000). Since *Sbh26GST* has a higher tryptophan content, it would suggest that it is more stable than *Sh28GST*. However, it is important to note that

overall protein stability depends on many factors, including the overall amino acid content, shape, size, and environment, and therefore, this suggestion alone is not enough to conclusively determine which protein is more stable than the other.

The tertiary structure was further probed with hydrophobic fluorescent probe called ANS dye. ANS works by binding to the folded or partially folded hydrophobic regions of proteins (Gasymov *et al.*, 2007). Effective binding to hydrophobic patches increases fluorescent intensity (Ota *et al.*, 2021). *Sh28GST* exhibited an increase in fluorescence intensity from unbound ANS to ANS bound protein, resulting in a blueshift wavelength from 519 nm to 495 nm. Similarly, *Sbh26GST* showed an increase in fluorescence intensity from unbound ANS to ANS bound protein, resulting in a blueshift wavelength from 519 nm to 495 nm also resulting in a blueshift (Gasymov *et al.*, 2007). This occurred when both proteins were in their folded/native states. This implies that the hydrophobic core was already largely exposed in the native states of the protein, making it accessible for ANS to bind to those hydrophobic patches (Gasymov *et al.*, 2007). As a result, there was a change in the environment around the ANS, and it could bind, resulting in increased intensity. However, the difference in fluorescence intensity observed from ANS-free to ANS-bound protein was slightly higher in *Sh28GST* than *Sbh26GST*. This suggests that hydrophobic patches in *Sh28GST* were more accessible in native state of protein (Guliyeva *et al.*, 2020). In *Sbh26GST*, they tend to be more buried and less accessible to the ANS when protein is in its native state (Guliyeva *et al.*, 2020). Denaturing the proteins in 8 M urea resulted in an intense shutdown of fluorescence intensity in *Sh28GST*, with some intensity still left in *Sbh26GST* (Figure 4.7). This is because as the protein unfolds, the hydrophobic environment disappears and ANS was more exposed to a more polar environment (Guliyeva *et al.*, 2020). Such changes in the environment of ANS results in what we call quenching of its fluorescence, and a decrease in intensity. Urea is a chemical denaturant that disrupts the hydrophobic interactions and hydrogen bonds that stabilise structure of the protein, leading to protein unfolding (Wang *et al.*, 2014). The concentration of urea required to induce a complete shutdown of ANS fluorescence varies depending on the protein, with more stable proteins requiring higher urea concentrations to achieve complete shutdown. Therefore, *Sbh26GST* requires more urea concentration than *Sh28GST* to achieve complete shutdown thus it is more stable as it has higher tolerance for urea induced denaturation. Such observations were essential as they revealed the functionality of the proteins as enzymes, their secondary and tertiary structures. Both will be fundamental for exploring the conformational

stability of these enzymes using a chemical denaturant called urea, as well as the use of heat to denature the two GSTs.

Chapter 5

Stability studies of *Sbh26GST* and *Sh28GST*

5.1 Introduction

Protein stability is a complex and multifaceted phenomenon that affects numerous aspects of protein structure and function. The ability of a protein to maintain its native conformation is critical for its proper functioning and has implications for its stability in vivo and its potential for use in various applications in biochemistry and drug design studies. Changes in temperature, pH, or chemical environment can result in alterations to the structure of a protein, leading to the disruption of the protein's overall function (Khan *et al.*, 2016). Additionally, mutations or alterations to the protein's amino acid sequence or the presence of disulfide bonds can impact its stability, as can interactions between the protein and the environment its exposed to.

This chapter focuses on investigating the conformational stability of two similar GST proteins encoded by the *Schistosoma haematobium* genome, *Sh28GST*, and *Sbh26GST*. Despite sharing high sequence identity, the factors responsible for their functional divergence and evolutionary rationale for encoding highly similar proteins remain unclear. One possible explanation is that the stability of one GST is greater than the other, allowing the parasite to perform detoxification functions specific to that protein. To elucidate the precise molecular mechanisms underlying the functional differences of these homologous GSTs, this chapter employs two distinct methodologies: chemical denaturation, achieved through urea-induced unfolding and measured using far-UV CD, and thermal denaturation measured using differential scanning calorimetry (DSC) of the two enzymes were investigated. By providing insights into their conformational stability, we aim to address the research question and give possible insights into why the parasite encodes two similar GSTs in its genome.

5.2 Materials

The following reagents were purchased from Sigma Aldrich, USA: urea, L-glutathione reduced (GSH), sodium phosphate (NaH_2PO_4), sodium azide (NaN_3), dithiothreitol (DTT), Tris, NaCl, HCl, and ethylenediaminetetraacetic acid (EDTA) salt. The SYPRO Orange dye, including a full kit was purchased from Bio-Rad, SA. The Snakeskin dialysis tubing (10K

MWCO, 22 mm) was supplied by Thermo Fischer Scientific, SA. The rest of the chemicals used were obtained from Sigma Aldrich, MO, USA, and were all of analytical grade.

5.3 Methods

5.3.1 Establishing reversibility of urea-induced unfolding of *Sh28GST* and *Sbh26GST*

The folding pathway of a protein is a critical process that determines its function and stability. It is guided by the primary sequence, which provides the information for the protein to adopt a specific shape (Khan *et al.*, 2016). Proteins typically fold into their native conformation through a series of intermediate structures, driven by interactions between the amino acid side chains, such as hydrogen bonding, van der Waals forces, hydrophobic interactions, and electrostatic interactions (Khan *et al.*, 2016). The folding mechanisms of a protein refer to the specific series of steps that the protein takes to transform from its initial, unfolded polypeptide chain into its native state, where it adopts its biologically active conformation.

Equilibrium unfolding is a process in which a protein is unfolded and denatured using a chemical denaturant such as urea or guanidine hydrochloride. The process continues until the protein reaches a state of thermodynamic equilibrium between the folded and unfolded states (Pace, 1986). Spectroscopic probes, such as far-UV CD and intrinsic tryptophan fluorescence emission, are used to determine the unfolded pathway by detecting changes in secondary and tertiary structures, respectively. (Englander 2000). By plotting the fraction of unfolded protein at various denaturant conditions, the folding mechanism of a specific protein can be elucidated (Li *et al.*, 2015). Urea was the selected denaturant over guanidine hydrochloride, due to its milder denaturing properties (Rashid *et al.*, 2005) thus allowing proteins to undergo a gradual unfolding process, thereby generating a more diverse set of structural intermediates. Additionally, urea is less toxic and less expensive than guanidine hydrochloride (Li *et al.*, 2015).

Establishing reversibility and equilibrium of *Sh28GST* and *Sbh26GST*

A 10 M urea stock solution was freshly prepared prior to each experiment in the dialysate buffer (100 mM NaH₂PO₄, 0.01% (w/v) NaN₃, 2 mM dithiothreitol (DTT), 2 mM EDTA, 1 mM GSH, pH 7.5). The final concentration was determined using a refractometer to confirm the exact concentration of urea. To determine if changes in protein structure were reversible, 20 μM of *Sh28GST* and *Sbh26GST* was treated 8 M urea, with their respective

blanks prepared for background correction. The protein samples were incubated at room temperature for an hour before being transferred to a 1 mm CD QS path length cuvette and measured using a JASCO J-810 Spectropolarimeter at 20°C. The instrument was set to fixed conditions of 1 nm bandwidth, 0.5 nm data pitch, and a scanning speed of 100 nm/min. To evaluate any changes in the protein's secondary structure, the instrument measured the loss or gain of isolated helical content by recording ellipticity values at 222 nm and 220 nm for *Sh28GST* and *Sbh26GST* proteins, respectively, at incremental changes of denaturant concentration. Non-treated samples (without urea) were also prepared and measured under the same conditions.

To recover the denatured GSTs, the samples were diluted tenfold into a dialysate solution and the intensities were recorded. After acquiring the results, the highest intensity observed on the native samples and its respective wavelength were recorded. At the same wavelength, the fluorescence intensity of the recovered sample was also recorded. Recovery % test was determined by calculating the ratio of fluorescence intensity of the recovered sample to the fluorescence intensity of the native sample at the same wavelength.

$$\text{Recovery test} = \frac{f_{\lambda}(\text{recovered})}{f_{\lambda}(\text{native})} \times 100 \quad (5.1)$$

The recovery test yielded favorable results, with both proteins demonstrating a recovery rate of over 90%. This allowed us to proceed with establishing the equilibrium pathway. To do this, 2 μM of each GST was treated with concentrations of urea ranging from 0 – 8 M, with 0.5 increments throughout. The samples were incubated for an hour at room temperature and were measured using far-UV CD. To refold the proteins in the same pathway, a stock solution of 20 μM of each GST in urea was prepared and incubated at room temperature. Following a duration of 1 hour, the initial stock solution underwent a dilution process, producing a set of distinct samples with varying and appropriate concentrations of urea, with 0.5 decrements. All corresponding blanks were used to eliminate background interruptions. The resulting data was utilised to generate unfolding and refolding curves, which were subsequently analysed.

5.3.2 Urea-induced unfolding of *Sh28GST* and *Sbh26GST*

Far-UV CD was used to probe secondary structural changes during the unfolding of *Sh28GST* and *Sbh26GST*. Protein samples were prepared at a concentration of 2 μM and treated to varying concentrations of urea ranging from 0 to 8 M in 0.5 increments, before and after the transition states. The transition region was investigated at intervals of 0.25. The samples were prepared in triplicates and measured using a far-UV CD spectropolarimeter under the same conditions described in section 5.3.1.

A two-state folding mechanism can accurately describe the unfolding pathway of many globular proteins, including the ones examined in this study. In this model, the folding pathway contained only two states – folded (F) and unfolded (U), and each GST transitions between these two states during unfolding. Thus, the sum of the fractions of folded (f_F) and fractions of unfolded (f_U) GST at any given point during the unfolding process was equal to 1:

$$f_U + f_F = 1 \quad (5.2)$$

The signal contribution stems from the presence of protein concentrations in both unfolded and native conformations. As a result, any observed y-value at any given point will be defined as:

$$y = y_F f_F + y_U f_U \quad (5.3)$$

Where: y_U and y_F are y-values defining unfolded and folded states, respectively. Thus, combining equations 5.1 and 5.2 produces the equation for the fraction of the protein that is unfolded, denoted as f_U :

$$f_U = \frac{(y_F - y)}{(y_F - y_U)} \quad (5.4)$$

The equilibrium constant, K , can then be defined as,

$$K = f_U(1 - f_U) = \frac{f_U}{f_F} = \frac{(y_F - y)}{(y - y_U)} \quad (5.5)$$

The Gibbs free energy change, ΔG (in cal/mol) can be defined as,

$$\Delta G = -RT \ln(K) = -RT \ln \left(\frac{(y_F - y)}{(y - y_U)} \right) \quad (5.6)$$

Where: R is the gas constant (1.987 cal/K/mol) and T is the temperature measured in Kelvins, K. In a two-state model, ΔG is linearly dependent on the denaturant concentration thus adopting this formula (Pace, 1986):

$$\Delta G = \Delta G_{H_2O} - m[urea] \quad (5.7)$$

Where ΔG_{H_2O} (measured in kcal/mol) is the free energy change in the absence of urea, m (kcal/mol/M) is the cooperativity of the reaction which relates to solvent accessible surface area of the protein during unfolding. The C_m (measured in Molar) value is the midpoint denaturant unfolding concentration from the curve. These parameters were all accumulated and tabulated.

5.3.3 Differential scanning calorimetry *Sh28GST* and *Sbh26GST*

Differential scanning calorimetry (DSC) is a powerful tool that measures the heat flow of a sample as its temperature is increased or decreased under controlled conditions (Van Holde *et al.*, 2006). This technique is widely used to study phase transitions and biochemical reactions, including the melting points and conformational changes of molecules in various phases conditions (Van Holde *et al.*, 2006). In a typical experiment using Differential Scanning Calorimetry (DSC), a sample containing the molecule of interest and a reference cell containing only the solvent are heated simultaneously (Pooria *et al.*, 2010). The difference in energy required to match the temperature of the sample to that of the reference cell is measured and provides information about the amount of heat absorbed or released by the sample during an endothermic or exothermic process, respectively (Cooper *et al.*, 2000). The presence of the molecule being studied results in increased energy required to bring the sample and reference cell to the same temperature, which is known as heat excess (Figure 5.1). DSC is a valuable technique for studying biomolecule folding and stability by monitoring changes in heat capacity (C_p), which reveal the disruption of stabilizing forces such as hydrogen bonds and electrostatic interactions (Cooper *et al.*, 2000).

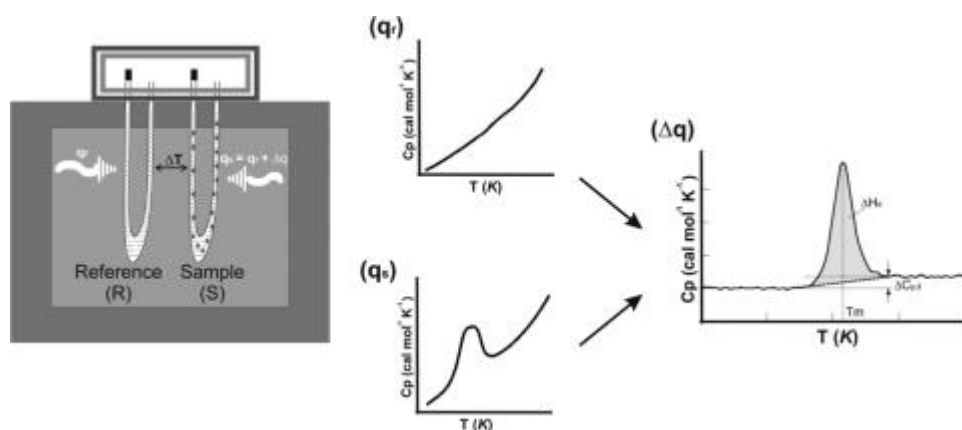


Figure 5.1. Schematic illustration of the experimental setup of a DSC experiment. During a DSC experiment, the sample cell absorbs excess heat, resulting in a higher amount of heat needed to raise its temperature compared to the reference cell. By subtracting the reference signal from the sample signal, DSC scans can show how this excess heat changes with temperature. This provides valuable information on parameters such as the change in enthalpy (ΔH_d), change in heat capacity (ΔC_p , d), and transition/melting point (T_m) (Adapted from Cooper *et al.*, 2000).

A concentration of 5 μ M of *Sh28GST* and *Sbh26GST* was subjected to dialysis against buffer consisting of 100 mM NaH₂PO₄, 0.01% (w/v) NaN₃, 2 mM dithiothreitol (DTT), 2 mM EDTA, and 1 mM GSH, at pH of 7.5. This process was carried out overnight. Subsequently, the sample and reference cells were subjected to NANO Differential Scanning Calorimetry from SA, which involved simultaneous heating in the range of 5 – 90 °C, at a rate of 1°C/min. The resulting DSC scans were analysed to obtain information on various parameters, including changes in enthalpy, heat capacity, and transition/melting points.

5.4 Results

Establishing reversibility and equilibrium of Sh28GST and Sbh26GST

A 10 M urea stock solution was freshly prepared in a sodium phosphate dialysate buffer with a pH of 7.5. To determine if changes in protein structure were reversible, 20 μ M of *Sh28GST* and *Sbh26GST* was treated 8 M urea, with their prepared respective blanks for background correction. This included the preparation of none urea-treated, native samples. The samples were incubated for 1 hour and measured using a JASCO J-810 Spectropolarimeter, which recorded ellipticity values at 222 nm and 220 nm for *Sh28GST* and *Sbh26GST*, respectively, to evaluate any changes in the protein's secondary structure. The denatured GSTs were recovered by diluting the samples tenfold into a dialysate solution and the samples were

also measured using far-UV CD. The recovery test yielded favorable results, with both proteins demonstrating a recovery rate of over 90% (Figure 5.2 A and B).

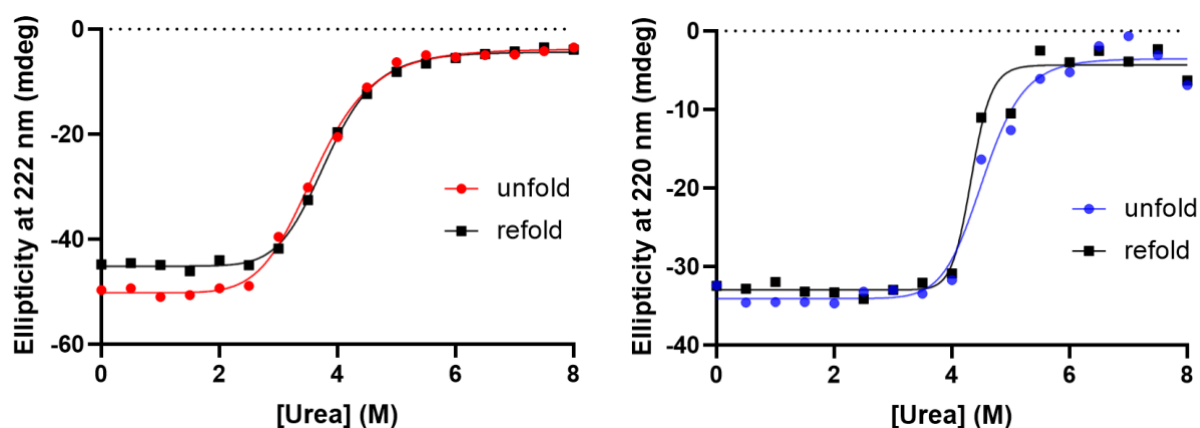


Figure 5.2. Detecting the equilibrium pathway by following unfolding and refolding curves of *Sh28GST* (A) and *Sbh26GST* (B) using far-UV CD. For unfolding, 2 μ M of *Sh28GST* and *Sbh26GST* were treated with urea concentrations ranging from 0 – 8 M using dialysate buffer (100 mM NaH_2PO_4 , 0.01% (w/v) NaN_3 , 2 mM dithiothreitol (DTT), 2 mM EDTA, 1 mM GSH, pH 7.5) with 0.5 increments throughout. The samples were incubated for an hour at room temperature and measured on a 1 mm CD QS path length cuvette using far-UV CD to monitor secondary structural changes of *Sh28GST* and *Sbh26GST* as urea concentrations gradually increase or decrease for unfolding and refolding pathways, respectively. Proteins were refolded in the same pathway, starting with stock solution of 8 M urea then following the pathway of refolding using 0.5 decrements. Both proteins demonstrate a recovery rate of over 90%.

Urea-induced unfolding of Sh28GST and Sbh26GST

Far-UV CD was used to probe secondary structural changes during the unfolding of *Sh28GST* and *Sbh26GST*. A 2 μ M of *Sh28GST* and *Sbh26GST* was treated to varying concentrations of urea ranging from 0 to 8 M in 0.5 increments before and after the transition states. The transition region was investigated at intervals of 0.25 (Figure 5.2 A and B). The samples were prepared in triplicates and measured using a far-UV CD spectropolarimeter under the same conditions described for establishing reversibility and equilibrium. A two-state model was fitted, with transitions between native and unfolded states observed. *Sbh26GST* is more stable than *Sh28GST* as it is seen resisting the change to go into the transition state at the same or lesser concentration that *Sh28GST* goes. The thermodynamic parameters were accumulated and recorded (Table 5.1).

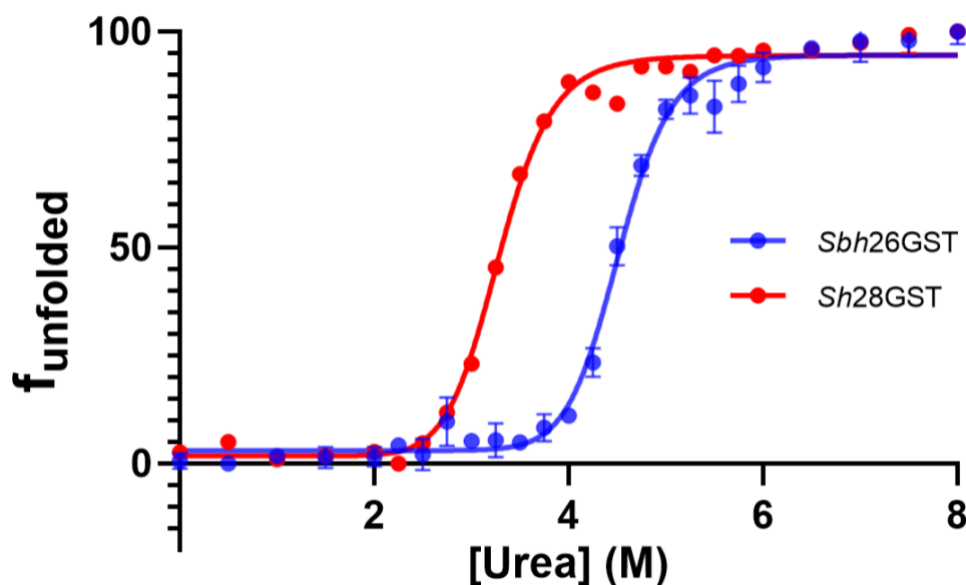


Figure 5.3. Global fitted urea unfolding curves of *Sh28GST* (red) and *Sbh26GST* (blue) using far-UV CD. A 2 μM of *Sh28GST* and *Sbh26GST* was treated to varying concentrations of urea ranging from 0 to 8 M using dialysate buffer (100 mM NaH_2PO_4 , 0.01% (w/v) NaN_3 , 2 mM dithiothreitol (DTT), 2 mM EDTA, 1 mM GSH, pH 7.5) in 0.5 increments, before and after the transition states. The transition region was investigated at intervals of 0.25. The samples were prepared in triplicates and measured using 1 mm CD QS path length cuvette and a far-UV CD spectropolarimeter. *Sbh26GST* (represented in blue) is more stable than *Sh28GST* (represented in red) as it is seen resisting the change to go into the transition state at the same or lesser concentration that *Sh28GST* goes. The data fitted in GraphPad Prism using a non-linear regression fit that resulted in $R^2 = 0.99$ for both GSTs as a goodness of fit.

Table 5.1. Thermodynamic parameters derived from urea unfolding curves of *Sh28GST* and *Sbh26GST*

Protein	$\Delta G_{\text{H}_2\text{O}}$ (kcal/mol)	m -value (kcal/mol/M)	C_m value (M)
<i>Sh28GST</i>	7.63	2.39	3.19
<i>Sbh26GST</i>	16.86	3.78	4.46

Differential scanning calorimetry of Sh28GST and Sbh26GST

A concentration of 5 μM of *Sh28GST* and *Sbh26GST* was subjected to dialysis against buffer consisting of 100 mM NaH_2PO_4 , 0.01% (w/v) NaN_3 , 2 mM dithiothreitol (DTT), 2 mM EDTA, and 1 mM GSH, at pH of 7.5. This process was carried out overnight. Subsequently, the sample and reference cells were subjected to NANO Differential Scanning Calorimetry from SA, which involved simultaneous heating in the range of 5 – 90°C, at a rate of 1°C/min. The resulting triplicate DSC scans were averaged and blank corrected. Curves of heat capacity

versus temperature (Figure 5.4 and Figure 5.5) were analysed to obtain information on various parameters, including changes in enthalpy, heat capacity, and transition/melting points.

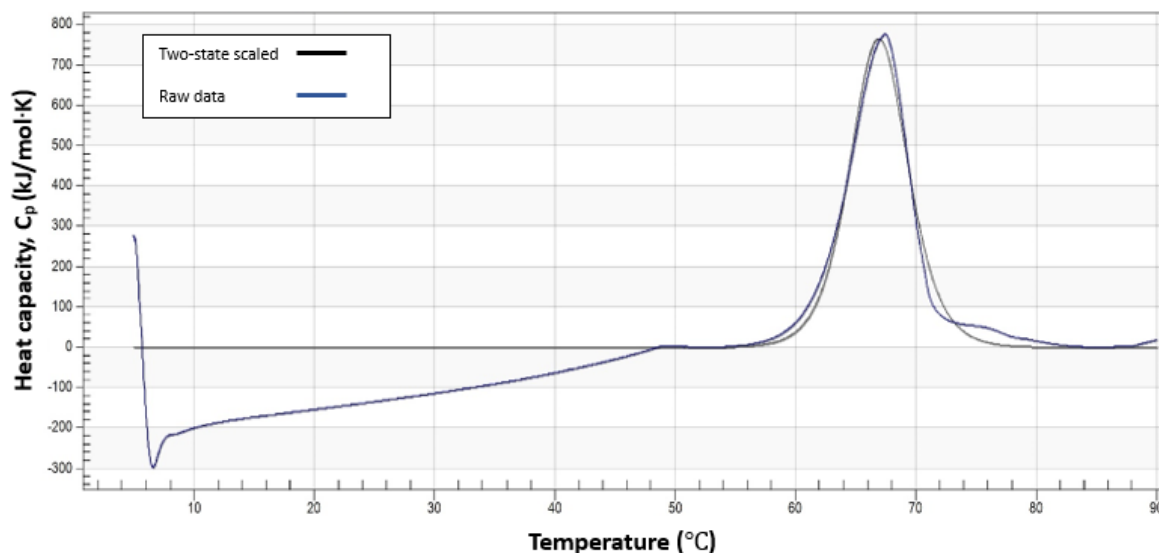


Figure 5.4. Heat capacity against temperature curve of *Sh28GST*. 5 μM of *Sh28GST* in dialysis buffer (100 mM NaH_2PO_4 , 0.01% (w/v) NaN_3 , 2 mM dithiothreitol (DTT), 2 mM EDTA, 1 mM GSH, pH of 7.5) with relevant blank was subjected to sample and reference cell in a NANO Differential Scanning Calorimetry from SA, which involved simultaneous heating in the range of 5 – 90 $^\circ\text{C}$, at a rate of 1 $^\circ\text{C}/\text{min}$. Two-state scaled implies that enthalpy change associated with the glass transition or relaxation is normalised or scaled to the enthalpy change associated with a fully crystalline material.

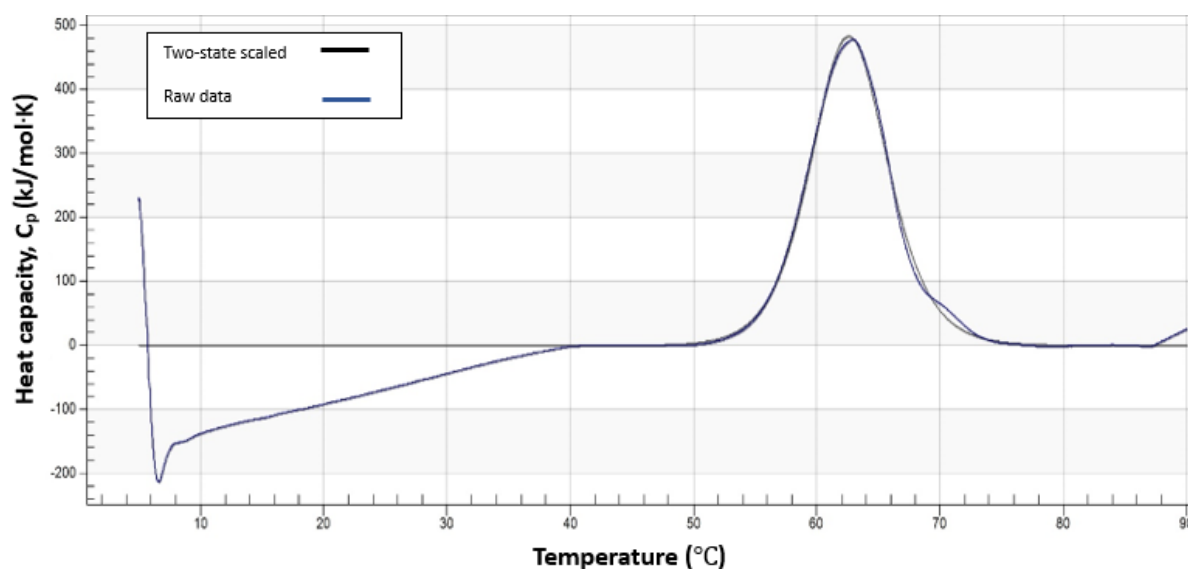


Figure 5.5. Heat capacity against temperature curve of *Sbh26GST*. 5 μM of *Sbh26GST* in dialysis buffer (100 mM NaH_2PO_4 , 0.01% (w/v) NaN_3 , 2 mM dithiothreitol (DTT), 2 mM EDTA, 1 mM GSH, pH of 7.5) with relevant blank was subjected to sample and reference cell in a NANO Differential Scanning Calorimetry from SA, which involved simultaneous heating in the range of 5 – 90 $^\circ\text{C}$, at a

rate of 1°C/min. Two-state scaled implies that enthalpy change associated with the glass transition or relaxation is normalized or scaled to the enthalpy change associated with a fully crystalline material.

Table 5.2. Thermodynamic parameters obtained from thermal heat curves of *Sh28GST* and *Sbh26GST* using Differential Scanning Calorimetry

Protein	T_m (°C)	ΔH (kJ/mol)
<i>Sh28GST</i>	66.94	599.01
<i>Sbh26GST</i>	62.64	451.60

5.5 Discussion

In this study we demonstrated that urea unfolded *Sh28GST* and *Sbh26GST* in a simple two-state (N→U) process. In Figure 5.3, it was demonstrated that *Sbh26GST* was more stable than *Sh28GST* as it required a higher concentration of urea to undergo significant unfolding, resulting in a curve that was shifted to the right. This allowed us to estimate the conformational stability parameters of each protein: *Sbh26GST* exhibited $\Delta G_{H20} = 16.86$ kcal/mol, m-value = 3.78 kcal/mol/M, C_m value = 4.46 M; *Sh28GST* exhibited $\Delta G_{H20} = 7.63$ kcal/mol, m-value = 2.39 kcal/mol/M, C_m value = 3.19 M. The experimentally determined m-values were consistent with those of most GSTs, which have m-values ranging from 2.5 to 4.9 kcal/mol/M (Kaplan *et al.*, 2008). Furthermore, the obtained ΔG_{H20} value from the unfolding curve as a measure of protein stability in an aqueous environment provided insights into the contributing factors such as hydrophobic interactions, hydrogen bonding, van der Waals forces, and electrostatic interactions (Wilson *et al.*, 2010). The differences in ΔG_{H20} values between the two proteins suggested that *Sh28GST* was less stable and more prone to unfolding than *Sbh26GST* (Glasser *et al.*, 2009). Moreover, *Sh28GST* exhibited a lower m-value, suggesting a less cooperative unfolding transition with weaker interactions (Myers *et al.*, 1995). This may imply that the protein is more prone to incremental unfolding rather than a sharp transition from the folded to the unfolded state (Johnson *et al.*, 1995). On the other hand, *Sbh26GST* displayed a higher m-value, indicating tighter packing and more cooperative unfolding (Myers *et al.*, 1995). The C_m value was measured as the denaturant concentration required to unfold half of the protein (Tischer *et al.*, 2013). A lower C_m value in *Sh28GST* suggested that it enters the transition state at a lower concentration compared to *Sbh26GST* (Tischer *et al.*, 2013). This indicates that *Sbh26GST* is more resistant to urea and requires a higher concentration to unfold the protein. Overall, *Sbh26GST* is considered more stable to chemical denaturation than *Sh28GST*, with higher ΔG_{H20} , m-value, and C_m value.

Additionally, differential scanning calorimetry (DSC) was used to probe a different aspect of protein stability, which involved the use of heat to denature the protein. Far-UV circular dichroism (CD) spectroscopy and differential scanning calorimetry (DSC) are two complementary techniques commonly used in protein unfolding studies (Consalvi *et al.*, 2000). DSC measures the heat absorbed or released by a protein as it undergoes thermal denaturation (Murali *et al.*, 2016). By using both techniques, the aim was to obtain a more complete picture of the unfolding process and the factors that contribute to protein stability and function.

In this case, the thermal stability, and thermodynamic properties of two proteins, *Sbh26GST* and *Sh28GST*, were determined using DSC data. The T_m value, which represented the temperature at which the GSTs transitioned from the folded state to an unfolded state, was used as a measure of thermal stability (Privalov *et al.*, 1986). This transition is often accompanied by a change in heat capacity, resulting in an endothermic peak in the DSC curve (Haynie, 2008). The T_m value provides an estimate of the protein's thermal stability, with more stable proteins requiring higher temperatures to undergo this transition (Haines *et al.*, 1998). *Sbh26GST* exhibited a T_m value of 62.64 °C, while *Sh28GST* had a higher T_m value of 66.94 °C, which was consistent with previous studies of GSTs as most GSTs have T_m values in the range of 45-70°C (Sharma *et al.*, 2016). In fact, it was reported that the 26 kDa GST from *Schistosoma japonicum* exhibited a T_m of 61.25 °C (Kaplan *et al.*, 1997), however no published data was available to contrast with *Sh28GST*. The difference in the experimental T_m values suggested that *Sh28GST* was more thermally stable than *Sbh26GST*, as it required a higher temperature to undergo the same unfolding transition. The ΔH value is the enthalpy change associated with the unfolding transition and is related to the amount of energy required to disrupt the protein's structure and break its intermolecular bonds (Haynie, 2008; Zucca *et al.*, 2002). This value is typically reported in units of kilojoules per mole (kJ/mol). In this case, *Sbh26GST* exhibited a ΔH value of 451.60 kJ/mol, while *Sh28GST* had a higher ΔH value of 599.01 kJ/mol. This observation implied that more energy was required to unfold *Sh28GST* than *Sbh26GST*, which is consistent with the higher T_m value observed in *Sh28GST* (Haynie, 2008) thus implying greater stability of *Sh28GST* in the presence of heat denaturation. During the heat-induced unfolding transition of GSTs, various types of intermolecular bonds are broken, including van der Waals interactions, hydrogen bonds, and hydrophobic interactions (Wang *et al.*, 2005). However, *Sh28GST* and *Sbh26GST* displayed distinct stabilities when subjected to urea and heat treatments. *Sh28GST* exhibited greater resistance to heat-induced denaturation, while being less resistant to chemical denaturation. Conversely, *Sbh26GST*

demonstrated the opposite relationship. These anomalous results can be explained by considering the 3D structure of the GSTs and the placement of tryptophan residues within them, as tryptophan plays a crucial role in stability.

The stability of a protein can be affected by a variety of factors, including the presence of specific amino acid residues, such as tryptophan, and the nature of the denaturant used to perturb the protein structure (Yao *et al.*, 2011). Tryptophan is an aromatic amino acid with a relatively large side chain. It can participate in a variety of interactions, including hydrogen bonding, π - π stacking, and hydrophobic interactions (Palego *et al.*, 2016). In both GSTs it was observed that most of the tryptophan residues were already exposed to the polar environment in the protein's native state. However, they were found to be more exposed in *Sh28GST* as compared to *Sbh26GST*, where they were slightly more buried (Figure 4.6 A and B). Tryptophan residues that are more buried within the protein interior, like in *Sbh26GST*, surrounded by other hydrophobic residues, tend to contribute significantly to the overall stability of the protein (Palego *et al.*, 2016). These residues can form stabilizing interactions such as van der Waals forces, hydrogen bonds, and pi-pi stacking interactions (Palego *et al.*, 2016; Yao *et al.*, 2011). These interactions are relatively strong and can be more resistant to disruption by chemical denaturants, such as urea in this case (Nishizuka, 1964). However, when tryptophan residues are located on the surface of the protein, they may be more exposed to the solvent and can be more susceptible to disruption by chemical denaturants (Palego *et al.*, 2016; Nishizuka, 1964; Kaper *et al.*, 1958). This is because the solvent-accessible tryptophan residues may be more likely to form weaker pi-cation interactions with positively charged residues in the solvent, which can be disrupted by chemical denaturants, and this may have been the possible case in *Sh28GST* (Palego *et al.*, 2016; Nishizuka, 1964; Kaper *et al.*, 1958). However, tryptophan is an amino acid that contains an indole side chain. When proteins are heated, the thermal energy disrupts the weak interactions, such as hydrogen bonds and hydrophobic interactions, that hold the protein in its native conformation. As a result, the protein begins to unfold and lose its functional structure. Tryptophan has a relatively large side chain and can participate in a variety of interactions, including hydrogen bonding, π - π stacking, and hydrophobic interactions (Palego *et al.*, 2016; Kaper *et al.*, 1958). When the protein is exposed to heat, the increased thermal energy can cause tryptophan residues to become destabilised, particularly if they are in regions of the protein that are critical for maintaining the protein's native conformation (Palego *et al.*, 2016). Furthermore, tryptophan residues are known to be sensitive to oxidation and can undergo photo-oxidation when exposed to light (Bellmaine *et*

al., 2020). This process can lead to the formation of tryptophan radicals, which can damage nearby amino acids and destabilize the protein structure.

Therefore, having more tryptophan residues within the protein such as in *Sbh26GST* may have made it more susceptible to heat-induced denaturation because the tryptophan residues may be in critical regions of the protein and were easily destabilised under high thermal energy conditions (Bellmaine *et al.*, 2020). In addition to the destabilising effect of tryptophan residues under high thermal energy conditions, these residues can also undergo photo-oxidation (Ronsein *et al.*, 2008). A process that occurs when tryptophan residues absorb light energy, leading to the formation of tryptophan radicals (Pileni *et al.*, 1976). These radicals can then react with molecular oxygen to produce reactive oxygen species (ROS), such as singlet oxygen and superoxide anion radicals, which can damage nearby amino acids (Savige, 1975). The formation of ROS can have several negative effects on the protein structure. For example, the ROS can cause oxidative modifications of amino acid residues, such as oxidation of methionine or cysteine residues, which can lead to cross-linking and aggregation of the protein (Savige, 1975; Pileni *et al.*, 1976; Ronsein *et al.*, 2008). These modifications can also affect the folding of the protein by disrupting hydrogen bonds and other weak interactions that hold the protein structure together (Bellmaine *et al.*, 2020). Moreover, tryptophan residues can also undergo conformational changes under certain conditions, which can lead to the exposure of hydrophobic surfaces that are normally buried within the protein core (Pileni *et al.*, 1976; Ronsein *et al.*, 2008). These exposed hydrophobic surfaces can then interact with other hydrophobic surfaces on neighboring proteins, leading to the formation of protein aggregates. Therefore, the presence of tryptophan residues in a protein can contribute to its instability under high thermal energy conditions due to the sensitivity of these residues to photo-oxidation and their predicted ability to undergo conformational changes.

Chapter 6

Conclusion and possible future prospects

Schistosomiasis, a neglected tropical disease arises from infection with parasitic flatworms belonging to the *Schistosoma* genus, poses a significant public health threat, globally. Given the disease burden associated with this infection, there is a growing interest in conducting research aimed at understanding its underlying molecular mechanisms. In this investigation, two similar enzymes, *Sh28GST* and *Sbh26GST* were studied with the aim of revealing their conformational stability and thermodynamics thereby elucidating the reason behind the parasite encoding the two similar GSTs within its genome.

The study successfully produced high yields of two recombinant proteins, *Sh28GST* and *Sbh26GST*, using specific conditions in *E. coli* and IMAC purification. Both proteins were found to be active in enzyme assays, with *Sbh26GST* exhibiting better catalytic properties than *Sh28GST*. The proteins were also characterized for their secondary and tertiary structures using fluorescence techniques and revealed to have higher alpha helical content with a few beta strands and turns. The proteins were found to have different stability properties under chemical- and heat-denaturing conditions, which could be attributed to the number and location of tryptophan residues in the proteins. Both *Sh28GST* and *Sbh26GST* had tryptophan residues that were exposed to the polar environment in their native states. However, *Sh28GST* had more exposed tryptophan residues than *Sbh26GST*, suggesting that the former may be more susceptible to chemical denaturation. On the other hand, *Sbh26GST* had more buried tryptophan residues, which may have contributed to its susceptibility to heat-induced denaturation. The location of tryptophan residues was crucial for protein stability, and the presence of more tryptophan residues within a protein may have different effects depending on their location.

Tryptophan residues located on the surface of the protein may be more exposed to the solvent and can be more susceptible to disruption by chemical denaturants. This is because the solvent-accessible tryptophan residues may be more likely to form weaker pi-cation interactions with positively charged residues in the solvent, which can be disrupted by chemical denaturants, and this may have been the possible case in *Sh28GST*. Collective findings led to the conclusion that greater chemical denaturant stability observed in a protein does not always imply that the protein will also exhibit the same nature of stability in the presence of heat.

Sbh26GST was more stable in the presence of urea, while *Sh28GST* was more stable in the presence of heat. Clearly, conformational stability of proteins involves many complex thermodynamic processes that need to be unraveled and fully comprehended before making a conclusion about the overall stability of any protein.

For future research projects, there are several other advanced techniques that could be utilized to gain deeper insights into the conformational stability of the proteins. For example, Surface plasmon resonance (SPR) can be used to measure the binding strength and kinetics of the protein-ligand interactions. Moreover, X-ray crystallography or nuclear magnetic resonance (NMR) spectroscopy can be utilized to obtain high-resolution structural information about the proteins. Molecular dynamics simulations can also be employed to study the stability of the proteins at the atomic level and predict their conformational changes under different conditions.

REFERENCES

- Aboul, A.M., Hassan, Z.A. (1989). Oltipraz treatment in experimental schistosomiasis mansoni. II. Effect of high dose oral therapy on worm load and process of copulation in infected mice. *J. Egypt. Soc. Parasitol.* 19, 427–436.
- Adenowo, A.F., Oyinloye, B.E., Ogunyinka, B.I., Kappo, A.P. (2015). Impact of human schistosomiasis in sub-Saharan Africa. *Brazilian J. Infect. Dis.* 19, 196–205.
- Alber, T., Dao-pin, S., Wilson, K., Wozniak, J. A., Cook, S. P., Matthews, B. W. (1987). Contributions of hydrogen bonds of Thr 157 to the thermodynamic stability of phage T4 lysozyme. *Nat.* 330, 41–46.
- Andrews, P., Thomas, H., Pohlke, R., Seubert, J. (1983). *Praziquantel*. *Med. Res. Rev.* 3, 147–200.
- Anfinsen, C.B. (1973). Principles that govern the folding of protein chains. *Sci.* 181, 223–230.
- Arrigo, A.P. (1999). Gene expression and the thiol redox state. *Free Radic Biol Med.* 27, 936–44.
- Barakat, R., Elmorshedy, H., Fenwick, A. (2005). Efficacy of myrrh in the treatment of human Schistosomiasis mansoni. *Am J Trop Med Hyg.* 73, 365–367.
- Bender, D.A. (1983). Biochemistry of tryptophan in health and disease. *Mol. Asp. of Med.* 6, 101-197.
- Bergmans, H. E., Van Die, I. M., Hoekstra, W. P. (1981). Transformation in *Escherichia coli*: stages in the process. *J Bacteriol.* 146, 564-570.
- Botros, S., Sayed, H.E., Dusoki, H., Sabry, H., Rabie, I., Ghannam, M. (2005). Efficacy of mirazid in comparison with praziquantel in Egyptian Schistosoma mansoni-infected school children and households. *Am J Trop Med Hyg.* 72, 119–123.
- Brahms, S., Brahms, J. (1980). Determination of protein secondary structure in solution by vacuum ultraviolet circular dichroism. *J. Mol. Biol.* 138, 149–178.
- Brandts, J. F. (1964). The thermodynamics of protein denaturation.I. The denaturation of chymotrypsinogen. *J. Am. Chem. Soc.* 86, 4291–4301.
- Centers for Disease Control and Prevention (CDC). (2019). Parasites – Schistosomiasis. Biology. Available from <https://www.cdc.gov/parasites/schistosomiasis/biology.html>.
- Charles, H.K. (2003). Toward the Elimination of Schistosomiasis. *N Engl J Med.* 360, 106-109.
- Chothia, C. (1984). Principles that determine the structure of proteins. *Annu. Rev. Biochem.* 53, 537–572.
- Cornish, A. (2013). The origins of enzyme kinetics. *FEBS Let.* 587, 10.
- Corrêa, D., Ramos, C. (2009). The use of circular dichroism spectroscopy to study protein folding, form and function. *Afr. J. Bioc. Res.* 3, 164-173.
- Danley, R.L. (2000). New heat flux DSC measurement technique. *Ther. Acta.* 95, 201–208.
- Danley, R.L. (2001). Differential Scanning Calorimeter. *Eur. Pat.* 1, 139-183.
- Dill, K.A. (1990). Dominant forces in protein folding. *Bioch.* 29, 7133–7155.
- Dixon, D.P., Robert, E. (2010). Glutathione transferases. *T. Arabi.* 8, e0131.
- Doenhoff, M.J., Cioli, D., Utzinger, J. (2008). Praziquantel: mechanisms of action, resistance, and new derivatives for schistosomiasis. *Curr Opin Infect Dis.* 21, 659–667.

- Errington, N., Iqbalsyah, T., Doig, A.J. (2006). Structure and stability of the alpha-helix: lessons for design. *Methods Mol Biol.* 340, 3-26.
- Fenwick, A. (2015). Praziquantel: do we need another antischistosoma treatment? *Future Med. Chem.* 7, 677–680.
- Fenwick, A., Rollinson, D., Southgate, V. (2006). Implementation of human schistosomiasis control: challenges and prospects. *Adv Parasitol.* 61, 567–622.
- Friedman, P.A., Kappelman, A.H., Kaufman, S. (1972). Partial purification and characterization of tryptophan hydroxylase from rabbit hindbrain. *Journ of Biol Chem.* 247, 4165-4173.
- Friis, H., Mwaniki, D., Omondi, B., Muniu, E. (2003). Effects on haemoglobin of multi-micronutrient supplementation and multi-helminth chemotherapy: a randomized, controlled trial in Kenyan school children. *Eur J Clin Nutr.* 57, 573–579.
- Fuentes-Lemus, E., Dorta, E., Escobar, E., Aspée, A., Pino, E., Abasq, M.L., Speisky, H., Silva, E., Lissi, E., Davies, M.J., López-Alarcón, C. (2016). Oxidation of free, peptide and protein tryptophan residues mediated by AAPH-derived free radicals: role of alkoxyl and peroxy radicals. *RSC Adv.* 6, 57948-57955.
- Gakamsky, D., Gakamsky, A. (2017). Intrinsic fluorescence of proteins as a medical diagnostic tool. *Spect Eur/Wo.* 29, 331.
- Gasteiger, E., Hoogland, C., Gattiker, A., Duvaud, S., Wilkins, M. R., Appel, R. D., Bairoch, A. (2005). Protein Identification and Analysis Tools on the Expasy Server. In J. M. Walker. 3, 571-607.
- Gasymov, O.K., Glasgow, B.J. (2007). ANS fluorescence: potential to augment the identification of the external binding sites of proteins. *Biochim Biophys Acta.* 1774, 403-11.
- Ghisaidoobe, A. B., Chung, S. J. (2014). Intrinsic tryptophan fluorescence in the detection and analysis of proteins: a focus on Förster resonance energy transfer techniques. *Int J Mol Sci.* 15, 22518-22538.
- Glasser, L., Jones, F. (2009). Systematic thermodynamics of hydration (and of solvation) of inorganic solids. *Inorg Chem.* 48, 1661-1665.
- Guliyeva, A. J., Gasymov, O. K. (2020). ANS fluorescence: Potential to discriminate hydrophobic sites of proteins in solid states. *Biochem Biophys Rep.* 24, 100843.
- Habig, W.H., Pabst, M.J., Jakoby, W.B. (1974). Glutathione S-transferase. The first enzymatic step in mercapturic acid formation. *J.Biol. Chem.* 249, 7130-7139.
- Harpaz, Y., Gerstein, M., Chothia, C. (1994). Volume changes on protein folding. *Struct.* 2, 641–649.
- Haynie, D.T. (2008). *Biological Thermodynamics.* Cambridge, UK: Cambridge Uni Pres. 2, 281-368.
- Herzfeld, J. (1991). Understanding hydrophobic behavior. *Sci.* 253, 88.
- Huang, C.J., Lin, H., Yang, X. (2012). Industrial production of recombinant therapeutics in *Escherichia coli* and its recent advancements. *J Ind Microbiol Biotechnol.* 39, 383-399.
- Jakoby, W.B., Habig, W.H. (1980). Glutathione transferase. *Academ. Press Enzym Bas of Deto.* 2, 63-94.
- Johnson, C.M., Fersht, A.R. (1995). Protein stability as a function of denaturant concentration: the thermal stability of barnase in the presence of urea. *Bioc.* 34, 6795–6804.
- Kaper, J. M., Veldstra, H. (1958). Metabolism of tryptophan by *Agrobacterium tumefaciens*. *Biochimica et Biophysica Acta.* 30, 401.

- Kaplan, W., Hüsler, P., Klump, H., Erhardt, J., Sluis-Cremer, N., Dirr, H. (2008). Conformational stability of pGEX-expressed *Schistosoma japonicum* glutathione S-transferase: A detoxification enzyme and fusion-protein affinity tag. *Protein Sci.* 6, 399-406.
- Kauzmann, W. (1959). Some factors in the interpretation of protein denaturation. *Adv. Protein Chem.* 14, 1–63.
- Kenneth A. J., Francesco, A., Andrea, B., Maxime H., Josette, F., Demetrious, T., André C., François Trottein, Maurizio Brunori. (2003). Crystal Structure of the 28 kDa Glutathione S-Transferase from *Schistosoma haematobium*. *Biochemistry.* 42, 10084-10094.
- Kielkopf, C. L., Bauer, W., Urbatsch, I. L. (2020). Purification of Polyhistidine-Tagged Proteins by Immobilized Metal Affinity Chromatography. *Cold Spring Harb Protoc.* 6, 102194.
- Kielkopf, C.L., Bauer, W., Urbatsch, I.L. (2021). Sodium Dodecyl Sulfate-Polyacrylamide Gel Electrophoresis of Proteins. *Cold Spring Harb Protoc.* 12, 14.
- Ladokhin, A. S., Jayasinghe, S., and White, S. H. (2000). How to measure and analyze tryptophan fluorescence in membranes properly, and why bother? *Anal. Biochem.* 285, 235–245.
- Lakowicz, J.R. (2006). Principles of Fluorescence Spectroscopy. *Springer Sci. Rev.* 3, 144.
- Lapidus, L.J., Eaton, W.A. (2017). Chemical and thermal unfolding of proteins: insights from single-molecule and ensemble experiments. *Journal of Biol. Chem.* 292, 19823-19831.
- Lawson, J.R, Wilson, R.A. (1980). The survival of the cercariae of *Schistosoma mansoni* in relation to water temperature and glycogen utilization. *Parasitol.* 81, 337-348.
- Le, W.J., You, J.Q., Mei, J.Y. (1982). Studies on the efficacy of artemether in experimental schistosomiasis (author's transl). *Yao Xue Xue Bao.* 17, 187–193.
- Le, W.J., You, J.Q., Mei, J.Y. (1983). Chemotherapeutic effect of artesunate in experimental schistosomiasis. *Yao Xue Xue Bao.* 18, 619–621.
- Leger, E., Webster, J.P. (2017). Hybridizations within the genus *Schistosoma*: implications for evolution, epidemiology and control. *Parasitol.* 144, 65–80.
- Li, H.J., Wang, W., Li, Y.Z. (2011). Effects of artemether, artesunate and dihydroartemisinin administered orally at multiple doses or combination in treatment of mice infected with *Schistosoma japonicum*. *Parasitol Res.* 109, 515–519.
- Lim, W. K., Rösgen, J., Englander, S.W. (2009). Urea, but not guanidinium, destabilizes proteins by forming hydrogen bonds to the peptide group. *Proc. Natl. Acad. Sci. U.S.A.* 106, 2595– 2600.
- Lovenberg, W., Weissbach, H., Udenfriend, S. (1962). Aromatic l-Amino Acid Decarboxylase. *Journal of Biol Chem.* 237, 89-93.
- Lumry, R., Biltonen, R., Brandts, J. F. (1966). Validity of the “two-state” hypothesis for conformational transitions of proteins. *Biopol.* 4, 917–944.
- Makhatadze, G.I. (2005). Thermodynamics Of alpha-Helix Formation. *Adv Protein Chem.* 72, 199-226.
- Makhatadze, G.I.; Privalov, P.L. (1992). Protein interactions with urea and guanidinium chloride: a calorimetric study. *J. Mol. Biol.* 226, 491–505.
- Makrides, S.C. (1996). Strategies for achieving high-level expression of genes in *Escherichia coli*. *Microbiol Rev.* 60, 512-538.
- Malpiedi, L.P., Díaz, C.A., Nerli, B.B., Pessoa, A. (2013). Single-chain antibody fragments: Purification methodologies. *Proc. Biochem.* 48, 1242-1251.

- Mannervik, B., Danielson, U.H. (1988). Glutathione transferases - structure and catalytic activity. *CRC Crit Rev Biochem.* 23, 283-337.
- Mathev, C.J., Wilce, M., Parker, W. (1994). Structure and function of GST. *Biochimica et Biophysica Acta.* 1205, 1-18.
- Murali, K.M., Srinivasan, S. (2016). Differential scanning calorimetry: applications in drug development. *Exp Opin. Drug Disc.* 11, 1371-1386.
- Myers, J.K., Pace, C.N., Scholtz, J.M. (1995). Denaturant m values and heat capacity changes: relation to changes in accessible surface areas of protein unfolding. *Protein Sci.* 4, 2138.
- National Institute for Communicable Diseases (NICD). (2018). Schistosomiasis (Bilharzia). Document FAQ. Available from https://www.nicd.ac.za/wp-content/uploads/2017/03/Schistosomiasis-Bilharzia_20181104_Final.pdf.
- Nishizuka, Y. (1964). Metabolism of the benzene ring of tryptophan and biosynthesis of nicotinamide adenine dinucleotide in mammalian tissues. In *Tanabe Amino Acid Res. Symp.* 1, 165.
- Nordberg, J., Arner, E.S. (2001). Reactive oxygen species, antioxidants, and the mammalian thioredoxin normal physiological functions and human disease. *Int J Biochem Cell Biol.* 39, 44–84.
- Ota, C., Tanaka, S.I., Takano, K. (2021). Revisiting the Rate-Limiting Step of the ANS–Protein Binding at the Protein Surface and Inside the Hydrophobic Cavity. *Mol.* 26, 420.
- Pace, C., Scholtz, J.M., Grimsley, G.R. (2014). Forces stabilizing proteins. *FEBS Lett.* 27, 2177-2184.
- Padi, N., Akumadu, B.O., Faerch, O., Aloke, C., Meyer, V., Achilonu, I. (2021). Engineering a Pseudo-26-kDa Schistosoma Glutathione Transferase from bovis/haematobium for Structure, Kinetics, and Ligandin Studies. *Biomol.* 11, 1844.
- Palego, L., Betti, L., Rossi, A., Giannaccini, G. (2016). Tryptophan biochemistry: structural, nutritional, metabolic, and medical aspects in humans. *Journ of Am. Parasitol Res.* 88, 395–397.
- Pelton, J.T., McLean, L.R. (2000). Spectroscopic methods for analysis of protein secondary structure. *Anal. Biochem.* 277, 167–176.
- Pica, M.L., Carlini, D., Guidi, A., Cimica, V., Vigorosi, F.C.D. (2006). The schistosome enzyme that activates oxamniquine has the characteristics of a sulfotransferase. *Mem Inst. Osw. Cruz.* 101, 307–312.
- Privalov, P.L. (1990). Cold denaturation of proteins. *Crit. Rev. Biochem. Mol. Biol.* 25, 281–305.
- Privalov, P.L., Potekhin, S.A. (1986). Scanning microcalorimetry in studying temperature-induced changes in proteins. *Methods Enzymol.* 131, 4–51.
- Reene, R.F., Pace, C.N. (1974). Urea and guanidine hydrochloride denaturation of ribonuclease, lysozyme, α -chymotrypsin, and β -lactoglobulin. *J. Biol. Chem.* 249, 5388– 5393.
- Riguero, V., Clifford, R., Dawley, M., Dickson, M., Gastfriend, B., Thompson, C., Wang, S. C., O'Connor, E. (2020). Immobilized metal affinity chromatography optimization for poly-histidine tagged proteins. *J Chromatogr A.* 1629, 461505.
- Robertson, A.D., Murphy, K.P. (1997). Protein Structure and the energetics of protein stability. *Chem. Rev.* 97, 1251–1267.
- Robinson, P.K. (2015). *Enzymes: Principles and biotechnological applications.* Ess Biochem. 59, 1-41.
- Robotka, H., Toldi, J., Vcsei, L. (2008). L-kynurenine, Metabolism and mechanism of neuroprotection. *Fut Neurol.* 3, 169-188.

- Rollinson, D., Simpson, A.J.G. (1987). The Biology of Schistosomes. From Genes to Latrines. *Parasitol.* 2, 354-472.
- Ronsein, G.E., Oliveira, M.C., Miyamoto, S., Medeiros, M.H., Di Mascio, P. (2008). Tryptophan oxidation by singlet molecular oxygen [$O_2(1\Delta g)$]: mechanistic studies using ^{18}O -labeled hydroperoxides, mass spectrometry, and light emission measurements. *Chem. Res. Toxi.* 21, 1271-1283.
- Rosazza, J.P., Juhl, R., Davis, P. (1973). Tryptophol formation by *Zygosaccharomyces priorianus*. *Applied Microbiol.* 26, 98-105.
- Ruggeri, B.A., Robinson, C., Angeles, T. (2002). The chemopreventive agent oltipraz possesses potent antiangiogenic activity in vitro, ex vivo and in vivo and inhibits tumor xenograft growth. *Clin Cancer Res.* 8, 267-274.
- Sauer, M., Hofkens, J., Enderlein, J. (2011). *Handbook of Fluorescence Spectroscopy and Imaging*. Wil. Vc. Verlag. 1, 265.
- Sharma, S., Chaudhary, S., Singh, S. (2016). Characterization and stability analysis of recombinant human glutathione S-transferase. *Biotec. Reports.* 12, 46-52.
- Sheehan, C.T., Hampton, T.H., Madden, D.R. (2022). Tryptophan mutations in G3BP1 tune the stability of a cellular signaling hub by weakening transient interactions with Caprin1 and USP10. *J Biol Chem.* 298, 102552.
- Sheehan, D., Meade, G., Foley, V.M., Dowd, C.A. (2001). Structure, function and evolution of glutathione transferases: implications for classification of non-mammalian members of an ancient enzyme superfamily. *Biochem J.* 360, 1-16.
- Singh, S.M., Panda, A.K. (2005). Solubilization and refolding of bacterial inclusion body proteins. *J Biosci Bioeng.* 99, 303-310.
- Smith, B.J. (1984). SDS Polyacrylamide Gel Electrophoresis of Proteins. *Methods Mol Biol.* 1, 41-55.
- SnapGene 2023. pET & Duet Vectors: pET-28a(+). Available from [https://www.snapgene.com/plasmids/pet_and_duet_vectors_\(novagen\)/pET28a%2B](https://www.snapgene.com/plasmids/pet_and_duet_vectors_(novagen)/pET28a%2B).
- SnapGene. 2023. pET & Duet Vectors: pET-11a. Available from [https://www.snapgene.com/plasmids/pet_and_duet_vectors_\(novagen\)/pET-11a](https://www.snapgene.com/plasmids/pet_and_duet_vectors_(novagen)/pET-11a).
- Soliman, O.E., Arman, M., Abdul, S.E.R., Nemr, H.I., Massoud, A. (2004). Evaluation of myrrh (Mirazid) therapy in fascioliasis and intestinal schistosomiasis in children: immunological and parasitological study. *J Egypt Soc Parasito.* 34, 941-966.
- Southgate, V.R. (1997). Schistosomiasis in the Senegal River Basin: before and after the construction of the dams at Diama, Senegal and Manantali, Mali and future prospects. *J Helminthol.* 71, 125-132.
- Sturrock, R.F. (2001). Schistosomiasis epidemiology and control: how did we get here and where should we go? *LSHTM Res. Onli.* 96, 17-27.
- Sulkowski, E. (1985). Purification of proteins by IMAC. *Trends in Biotech.* 3, 1-7.
- Takikawa, O., Yoshida, R., Kido, R., Hayaishi, O. (1986). Tryptophan degradation in mice initiated by indoleamine 2,3-dioxygenase. *Journal of Biological Chemistry.* 261, 3648. Tamaki, H. (1999). Expression of two Glutathione S-Transferase genes in the yeast *Issatchenkia orientalis* is induced by o-dinitrobenzene during cell growth arrest. *J Bacteriol.* 181, 2958-2962.
- Thannickal, V.J., Fanburg, B.L. (2000). Reactive oxygen species in cell signaling. *Am J Physiol Lung Cell.* 279, L1005-28.

- Tianfang, W., Min, Z., Bronwyn, A.R., April, S., Di, Liang., Guoying, Ni., Yanin, L., Pongrama, R., Donald, P.M., Scott, F.C. (2016). Proteomic Analysis of the *Schistosoma mansoni* Miracidium. *PLOS ONE*. 11, e0147247.
- Tischer, A., Auton, M. (2013). Urea-temperature phase diagrams capture the thermodynamics of denatured state expansion that accompany protein unfolding. *Protein Sci*. 22, 1147-1160.
- Townsend, D., Tew, K. (2003). The role of glutathione-S-transferase in anti-cancer drug resistance. *Oncog*. 22, 7369–7375.
- Tracy, J.W., Catto, B.A., Webster, L.T. (1983). Reductive metabolism of niridazole by adult *Schistosoma*. Correlation with covalent drug binding to parasite macromolecules. *Mol Pharmacol*. 24, 291-299.
- Vale, N., Gouveia, M.J., Rinaldi, G., Brindley, P.J., Gartner F., Correia da Costa J.M. (2017). Praziquantel for schistosomiasis: single-drug metabolism revisited, mode of action, and resistance. *Antimicrob. Agents Chemother*. 61, 34.
- Valerio, C., Roberta, C., Laura, G., Roberto, S., Petya, C., Andrej, K., Stefan, K., Rudolf, L. (2000). Thermal unfolding and conformational stability of the recombinant domain II of glutamate dehydrogenase from the hyperthermophile *Thermotoga maritima*. *Protein Eng, Des and Sel*. 13, 501-507.
- Valko, M., Izakovic, M., Mazur, M., Rhodes, C.J. (2004). Role of oxygen radicals in DNA damage and cancer incidence. *Mol. Cell Biochem*. 266, 37–56.
- Valko, M., Leibfritz, D., Moncol, J., Cronin, M.T., Mazur, M., Telser, J. (2007). Free radicals and antioxidants in normal physiological functions and human disease. *Int J Biochem Cell Biol*. 39, 44-84.
- Verjee, M.A. (2019). Schistosomiasis: Still a Cause of Significant Morbidity and Mortality. *Res Rep Trop Med*. 31, 153-163.
- Walker, J., Crowley, P., Moreman, A.D., Barrett, J. (1993). Biochemical properties of cloned glutathione S-transferases from *Schistosoma mansoni* and *Schistosoma japonicum*. *Mol. Biochem. Parasitol*. 61, 255–254.
- Wang, C., Chen, Z., Hong, X., Ning, F., Liu, H., Zang, J., Yan, X., Kemp, J., Musselman, C.A., Kutateladze, T.G., Zhao, R., Jiang, C., Zhang, G. (2014). The structural basis of urea-induced protein unfolding in β -catenin. *Acta Crystallogr D Biol Crystallogr*. 70, 2840-2847.
- Wang, L., Zhao, Y., Ng, E., Lid, Q. (2005). A MEMS differential calorimeter for biomolecular characterization. *Proceedings of the IEEE Int. Confer*. 39, 814–817.
- Weissbach, H., Redfield, B.G., Axelrod, J. (1960). Biosynthesis of melatonin: enzymic conversion of serotonin to N-acetylserotonin. *Biochimica Biophysica Acta*. 29, 352-353.
- Wilce, M.C.J., Parker, M.W. (1994). Structure and function of Glutathione S-Transferases. *Biochem Biophys Acta*. 1205, 1-18.
- Wilson, K., & Walker, J. (2010). *Principles of Protein Structure, Function, and Bioinformatics*. John Wiley & Sons.
- Wood, W.A., Gunsalus, I.C., Umbreit, W.W. (1947). Function of pyridoxal phosphate: resolution and purification of the tryptophanase enzyme of *Escherichia coli*. *Journal Biol Chem*. 170, 313-321.
- World Health Organization (WHO). (2022). Schistosomiasis (Bilharzia). Health topics. Available from https://www.who.int/health-topics/schistosomiasis#tab=tab_1.
- Yao, K., Fang, J., Yin, Y. L., Feng, Z. M., Tang, Z. R., Wu, G. (2011). Tryptophan metabolism in animals: important roles in nutrition and health. *Front. in Bio*. 3, 286-297.

Zampieri, S., Ghirardello, A., Doria, A., Tonello, M., Bendo, R., Rossini, K., Gambari, P.F. (2000). The use of Tween 20 in immunoblotting assays for the detection of autoantibodies in connective tissue diseases. *J Immunol Methods*. 239, 1-11.

Zhang, Y., Koukounari, A., Kabatereine, N. (2007). Parasitological impact of 2-year preventive chemotherapy on schistosomiasis and soil-transmitted helminthiasis in Uganda. *BMC Med*. 5, 27.

Zocchi, G. (1997). Proteins unfold in steps. *Proc Natl Acad Sci*. 94, 10647-10651.

Zucca, N., Erriu, G., Onnis, S., Longoni, A. (2002). An analytical expression of the output of a power-compensated DSC in a wide temperature range. *Thermochim. Acta*. 143, 117-125.

APPENDIX

SUPPLEMENTARY MATERIAL

ENA RTG84353 RTG84353.1 ENA KAF1314627 KAF1314627.1	CTTGTACAACCGACTCGTCTTCTTTTGGAAATATGTTGGCGAAGTATATGAAGAGCGTTTG CTTGTACAACCGACTCGTCTTCTTTTGGAAATATGTTGGCGAAGTATATGAAGAGCGTTTG *****	60 60
ENA RTG84353 RTG84353.1 ENA KAF1314627 KAF1314627.1	TATGATCGCAATGATGGTGATGCTGGCGAAACGAAAAGTTCAATTTAGGTCTGGAATTT TATGATCGCAATGATGGTGATGCTGGCGAAACGAAAAGTTCAATTTAGGTCTGGAATTT *****	120 120
ENA RTG84353 RTG84353.1 ENA KAF1314627 KAF1314627.1	CCTAATCTACCTTATTATATTGATGGTGATGTTAAATTAACACAGTCTATGGCTATTTTA CCTAATCTACCTTATTATATTGATGGTGATGTTAAATTAACACAGTCTATGGCTATTTTA *****	180 180
ENA RTG84353 RTG84353.1 ENA KAF1314627 KAF1314627.1	CGTTATATAGCTGATAAACACAAATATGTTGGGTGGTTGTCCCAAAGAACGTGCAGAATTT CGTTATATAGCTGATAAACACAAATATGTTGGGTGGTTGTCCCAAAGAACGTGCAGAATTT *****	240 240
ENA RTG84353 RTG84353.1 ENA KAF1314627 KAF1314627.1	TCTATGCTTGAGGGAGCCATTTTGGATATCAGACTTGGTGTTCGAAGAATTGCATATAAT TCTATGCTTGAGGGAGCCATTTTGGATATCAGACTTGGTGTTCGAAGAATTGCATATAAT *****	300 300
ENA RTG84353 RTG84353.1 ENA KAF1314627 KAF1314627.1	AAAGAATTTGAAACTCTCAAAGTTGGTTTTCTCAATCAACTCCCTGGAATGCTGAAAATG AAAGAATTTGAAACTCTCAAAGTTGGTTTTCTCAATCAACTCCCTGGAATGCTGAAAATG *****	360 360
ENA RTG84353 RTG84353.1 ENA KAF1314627 KAF1314627.1	TTTGAAAATCGTTTATCTCACAAAATATATTTGAATGGTGATAATGTGACTCATGTTGAC TTTGAAAATCGTTTATCTCAC----- *****	420 381
ENA RTG84353 RTG84353.1 ENA KAF1314627 KAF1314627.1	TTCATGCTGTACGACGCTCTTGATGTAGTTTTATACATGGACCCAAAGTGCTTGGATGCA -----	480 381
ENA RTG84353 RTG84353.1 ENA KAF1314627 KAF1314627.1	TTTCCAAAACATAATTAGTTTTCAAACAGCGTATAGAAAATTTACCACCAATCAAGAACTAC -----	540 381
ENA RTG84353 RTG84353.1 ENA KAF1314627 KAF1314627.1	CTGAATCTGACAGGCACATAAAATGGCCTCTGCAAGGCTGGTCCGCCATTTTTGGTGGT -----	600 381
ENA RTG84353 RTG84353.1 ENA KAF1314627 KAF1314627.1	GGAGATGCTCCTCCAAAATAA -----	621 381

Figure S1. Multiple sequence alignment of *Schistosoma bovis* (*Sb*) 26-kDa glutathione transferase (EBI ID RTG84353) with the *Schistosoma haematobium* (*Sh*) 26-kDa glutathione transferase (EBI ID KAF1314627) acquired from Clustal Omega Program. The analysis revealed a high level of sequence conservation, with 99.9% similarity between the gene fragments of *Sb*26GST and *Sh*26GST.